EXPLORING THE USE OF MACHINE LEARNING FOR IMPROVING THE EFFICIENCY OF COATING PERFORMANCE EVALUATION

A dissertation submitted to The University of Manchester for the degree of Master of Science in the Faculty of Science and Engineering.

2022

João Gabriel Guimarães de Farias

Student ID: 10982790

School of Natural Sciences

Corrosion Control Engineering MSc – 2021-2022

Supervisor: Dr Michele Curioni

LIST OF CONTENTS

Word count: 23993

LIST OF FIGURES

LIST OF TABLES

ABSTRACT

The use of machine learning was explored in the context of electrochemical impedance spectroscopy (EIS), with the purpose of overcoming some of its inherent complexities and increasing the efficiency in its use for coating performance evaluation . For this project, EIS and visual inspection data from marine coatings exposed to accelerated corrosion tests for approximately 2.5 years were applied to machine learning techniques to acquire a prototyped classification-type algorithm. Also, electrochemical tests – including EIS and alternative methods – were applied to coated samples immersed in 5 wt.% *NaCl* to generate data for the training, testing and validation of fitting-type machine learning algorithms, “prepared as a proof of concept”. An experimental setup using automatable components was adopted, which surpassed the necessity of preparing and performing each electrochemical test one-by-one. Overall, the results have shown that machine learning approaches have the potential to overcome several complexities related to EIS, and this combination of knowledges should be further exploited.

DECLARATION

This dissertation represents the student's original work unless referenced cleary on the contrary, and no portion of the work referred to in this dissertation has been submitted in support of an application for another degree or qualification of this or any other university or other institute of learning.

The Author

COPYRIGHT STATEMENT

i. The author of this dissertation (including any appendices and/or schedules to this dissertation) owns certain copyright or related rights in it (the “Copyright”) and s/he has given The University of Manchester certain rights to use such Copyright, including for administrative purposes.

ii. Copies of this dissertation, either in full or in extracts and whether in hard or electronic copy, may be made only in accordance with the Copyright, Designs and Patents Act 1988 (as amended) and regulations issued under it or, where appropriate, in accordance with licensing agreements which the University has entered into. This page must form part of any such copies made.

iii. The ownership of certain Copyright, patents, designs, trademarks and other intellectual property (the “Intellectual Property”) and any reproductions of copyright works in the dissertation, for example graphs and tables (“Reproductions”), which may be described in this dissertation, may not be owned by the author and may be owned by third parties. Such Intellectual Property and Reproductions cannot and must not be made available for use without the prior written permission of the owner(s) of the relevant Intellectual Property and/or Reproductions.

iv. Further information on the conditions under which disclosure, publication and commercialisation of this dissertation, the Copyright, and any Intellectual Property and/or Reproductions described in it may take place is available in the University IP Policy, in any relevant Dissertation restriction declarations deposited in the University Library, and The University Library’s regulations.

ACKNOWLEDGEMENTS

Firstly, I would like to thank my family for all their support through the different stages of my academic and professional life. I would not be here without them.

I would like show gratitude on being selected for the Corrosion Control Engineering MSc course by the Brazilian Navy (*Marinha do Brasil*) and reaffirm the commitment to apply and to disseminate the knowledge acquired this experience, not only in the fields of corrosion science and corrosion engineering but also in many others.

I am very grateful to the Directorate of Naval Engineering and all the people involved in the process that made it possible for me to attend this course abroad. And to the esteemed Materials Division, big thanks for this journey thus far!

To be part of the University of Manchester during this course was an unbelievable reality, that will always be cheerfully remembered. I am profoundly grateful for all the incredible teaching experiences I had here. Many thanks to all the staff and lecturers of the Corrosion and Protection Centre, who shared their skills and dedication. I wish also to thank all my colleagues from the different postgraduate courses of the Department of Materials for their mutual support and priceless share of experiences.

Special thanks to my academic supervisor, Dr Michele Curioni for his teaching, guidance, and encouragement, and for Vincenzo Bongiorno, who dedicated much of this time and talent to help me in countless aspects of this Dissertation. *Grazie mille!*

I would also like to thank the industrial partner AkzoNobel for the data and samples that were provided. I am also very grateful for the discussion and exchange of information about electrochemical testing in coatings.

To be here writing this Dissertation simply would not be true without the help of many people, including: Marcia Valeria Guimaraes de Farias, Joao Manuel Lima de Farias, Hozana Reis, Joao Batista, RAdm Ximenes, Capt Waldeque, Capt Feris, Capt Anderson Costa, Manoel França, Professor Dr Renata Antoun Simão, Capt Dauton, Cdr André Ricardo, Lt Cdr André Barbosa, Lt Cdr Idalba, Lt Cdr Gisele, Lt Felipe

Teixeira, Lt Lorenzo Bastos, Audrey, Dora, Vida, Jane, and many others. I am forever grateful. Thanks for everything!

Finally, I would like to thank my wife Maria Carolina Reis for her love and courage in taking this year's journey with me. It was not easy, but it was incredible!

Dedicated to Antonio Juarez Farias. My mentor, friend, and Grandpa. Avôhai!

1. GENERAL INTRODUCTION

1.1. IMPACTS OF CORROSION

When the American mathematical physicist Josiah Willard Gibbs (1839 – 1903) published his remarkable paper, “On the Equilibrium of Heterogeneous Substances” (1878), his focus was to define the total energy of a thermodynamic system for non-uniform substances (Scaliger, 2014). Among its achievements, his work has led to the definition of the thermodynamic state function now known as Gibbs free energy and, more importantly, to a powerful tool to analyse the spontaneity of a given chemical reaction (at least, from the thermodynamical aspect).

When a chemical reaction results in a negative variation in the Gibbs free energy (ΔG) of a system, the process is understood as thermodynamically spontaneous, which has a profound meaning for metallic materials. In nature, many of them are not found as metals, but as ores (such as oxides and sulphides). Therefore, energy must be expended to transform these materials into the several important metals and alloys used in countless structural and industrial applications, which means that these materials remain at higher thermodynamic energy levels. When exposed to specific combinations of environments and conditions, reactions that could reduce the free energy state of metals would be then thermodynamically favourable (Elayaperumal and Raja, 2015).

This point creates a fundamental question – for example: how to safely utilize metals and alloys, and benefit from their mechanical, thermal, electrical and many other vital properties for many engineering applications, if they could be chemically triggered to transform themselves to something other than metallic materials (in order to return to their low energy state), losing much of the design properties on which these applications depend? Therein lies the importance of studying the corrosion mechanisms and its characteristics (corrosion science), which provides the

necessary knowledge for developing methods to provide corrosion protection (corrosion engineering) to the materials that surround our everyday life.

As an example, Figure 1.1 illustrate the thermodynamic cycle related to the production of iron from iron ore (Fe_2O_3), which requires a large amount of energy. At high temperatures, and with the presence of coke (carbon) and limestone ($CaCO_3$), a chemical reaction transforms the ore into iron (metallic). Since this reaction is non-spontaneous, it requires an energy input (in this case, thermal). This raw material can be later transformed into steel to serve in many engineering applications. However, if exposed to the environment in specific conditions, another chemical reaction would happen, transforming steel into rust. This later reaction is an example of corrosion, a phenomenon that could be seen as the thermodynamic process by which a material reacting to its environment can achieve a lower energy state by reverting to its natural form, consequently resulting in the degradation of the material's original properties (McCafferty, 2010).

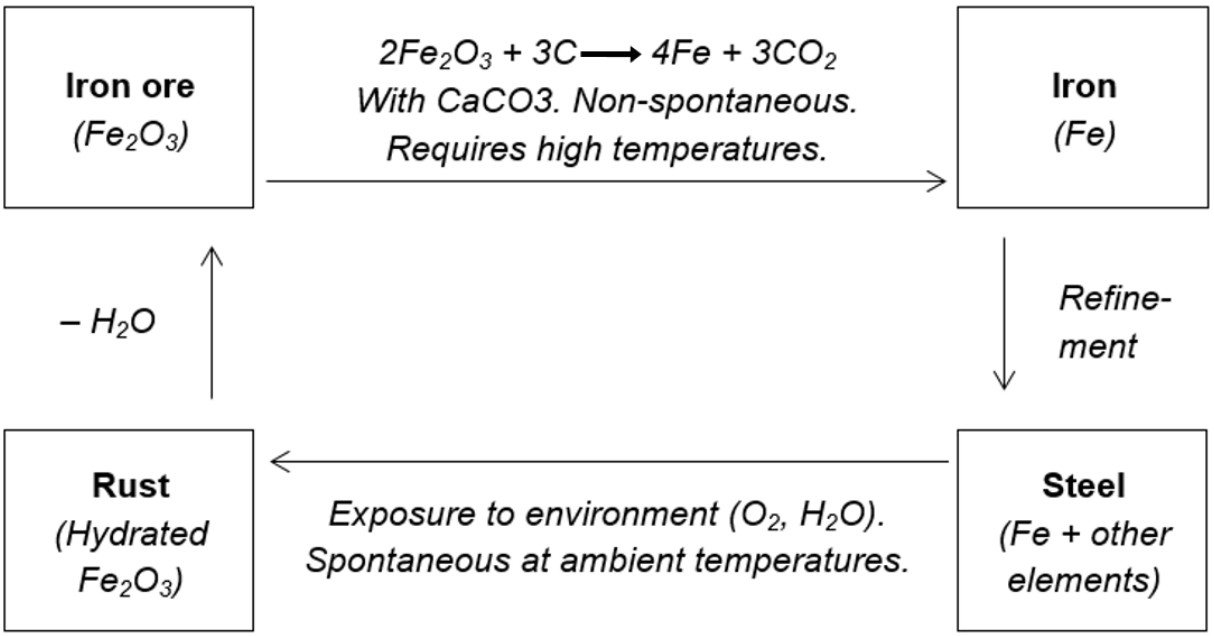

Figure 1.1 – Thermodynamic cycle for iron ore. Adapted from Elayaperumal and Raja (2015); McCafferty (2010).

An important relation for the study of corrosion involves the free energy change associated with a chemical reaction and the electrochemical potential, established by the German chemist Walther Nernst (1864 – 1941). His equation (which will be discussed later in Section 2), makes it possible to describe an electrochemical reaction by measurable parameters, enabling the prediction of the corrosion tendency on metallic materials. However, it is relevant to point out that the thermodynamical aspect is not the only factor governing chemical reactions such as corrosion. It does enable the verification whether a corrosion phenomenon is possible or not in any given scenario. However, corrosion, as every other chemical reaction, is also dependent on the aspect of kinetics, which is not a state function as ΔG and depends on the interaction between different electrochemical factors (Elayaperumal and Raja, 2015).

According to McCafferty (2010), the study of corrosion is relevant for social reasons regarding human health and safety, for the aspect of conservation of materials and for the economic cost of corrosion. The first topic is majorly related to the effect of corrosion on the functional integrity of engineering components in service, which can result in a catastrophic failure of an entire mechanical ensemble (for example, a bridge, a prosthetic implant, or an industrial plant), consequently affecting the lives of individuals. Koch et al. (2005) pointed that corrosion was one of the primally reasons for the structural deficiency of about 15% of the United States highway bridges (Koch et al.), which certainly gives a dimension of the problem.

The issue of the conservation of materials accrues from the need of replacing corroded and degraded structures, consuming a portion of the world's materials supply, which definitely is not infinite. It has been reported that close to 40% of the steel produced is destinated for replacing corroded steel. (Pedeferri, 2018) Also, the supply of certain ores and metals – for example, the chromium used in the composition of corrosion resistant alloys – is geographically restricted, impacting the importation strategies of raw materials among the nations (Koch et al., 2005).

Finally, the economic impact of corrosion has been often reported as a percentage between 3–5% of a nation's Gross National Product (Elayaperumal and Raja, 2015; Koch et al., 2005; McCafferty, 2010). Some authors have organized the costs associated with corrosion into different groups, many of them which can be taken as indirect expenditures (Elayaperumal and Raja, 2015): the costs associated with the selection of a corrosion preventative measure, the loss in production due to shutdowns, the loss of product (if stored), product contamination, maintenance costs and the costs of applying overprotective measures. Doshvarpassand, Wu and Wang (2019) estimated a corrosion management cost of 2 trillion dollars per year across different industries. For example, Masunaga (2020) article states that 3 billion US-dollars were expended in corrosion-related maintenance by the US Navy in 2014. Figure 1.2 shows US Navy warships under maintenance at a dry dock. The underwater hull area has been treated, removing some previous coating layers. A cathodic protection anode, used for corrosion prevention, can be seen on the right part of the image, surrounded by the remaining of a reddish coating.

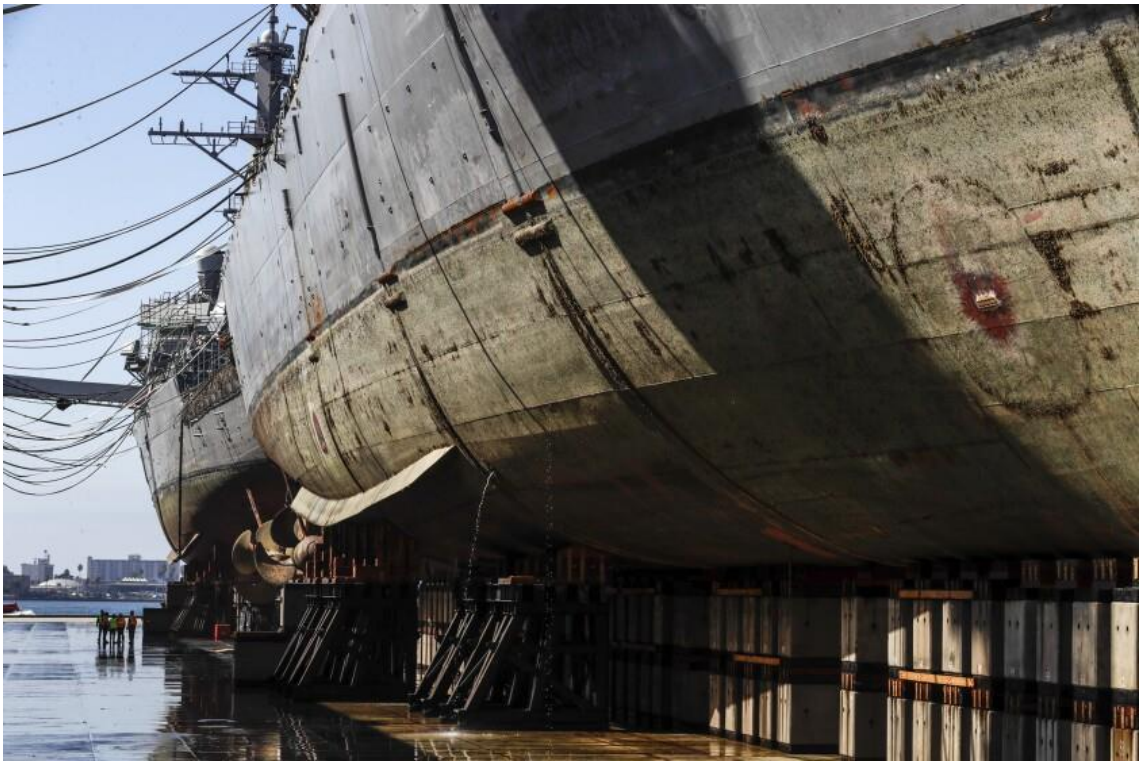

Figure 1.2 – Ships under maintenance – credits to Irfan Khan (Masunaga, 2020).

1.2. CORROSION PREVENTION

In this context, the use of suitable corrosion control methods has a major importance in our contemporary society. Unfortunately, there is not a unique tool to deal with the problem, which will depend on the corrosion mechanisms taking place, the reactions, and the characteristics of the system being studied. Also, the selection of the corrosion control method must be economically favourable. In order words, the total maintenance costs after the introduction of a corrosion control method should be reduced. Gentil (1996) organizes the corrosion control methods in the following groups:

- Methods that modify the environment – e.g.: de-aeration of water;
- Methods that modify the metallic material – e.g.: changing the composition;
- Methods that modify the process – e.g.: cathodic protection; and
- Using protective coatings – e.g.: the use of anticorrosive paints.

One practical example of the last above-mentioned group became very important for the naval shipbuilding sector. As the Industrial Revolution boosted the production of iron and steel, a slow and agitated transition from wooden ship hulls towards metallic ones began. In the end of the 19th century, steel would be adopted for warships and commercial ships construction, due to its higher strength-to-weight ratio and more predictable properties. However, this material is not corrosion resistant to seawater. Also, the previous common solution to the issue of hull fouling in wooden ships which was to use sheets of copper, could not be used directly on steel, otherwise galvanic corrosion would occur. It is said that, in the beginning of the transition from wood to metals (close to the middle of that century), some warships suffered severe corrosion and had to be taken off service after just a few years. The subsequential development of anti-corrosion and anti-fouling paints has mitigated the issue of corrosion (allied with the development of cathodic protection systems for ships), allowing for more widespread adoption of firstly iron and, later, steel as the ship hull material (Ferreiro, 2020). Figure 1.3 shows two passenger steamships designed by

Isambard Kingdom Brunel (1806 – 1859) for transatlantic services which illustrates this transition: the first, SS Great Western, was a wooden-hulled paddle-wheel vessel from 1838; in Figure 1.4, the 98-metres long screw-propelled SS Great Britain, an iron-hulled ship, which made her maiden voyage about 7 years later, in 1845 (Brunel, 2011).

1.3. PERFORMANCE EVALUATION

Paints, also known as organic coatings, are widely used for the protection of metallic structures that are exposed to aggressive environments, such as marine atmospheric sites or immersion conditions in seawater (ISO, 2017b). Ships and offshore installations are subjected to both these situations during their lifespans, which increases the performance demands for paint systems used in these applications.

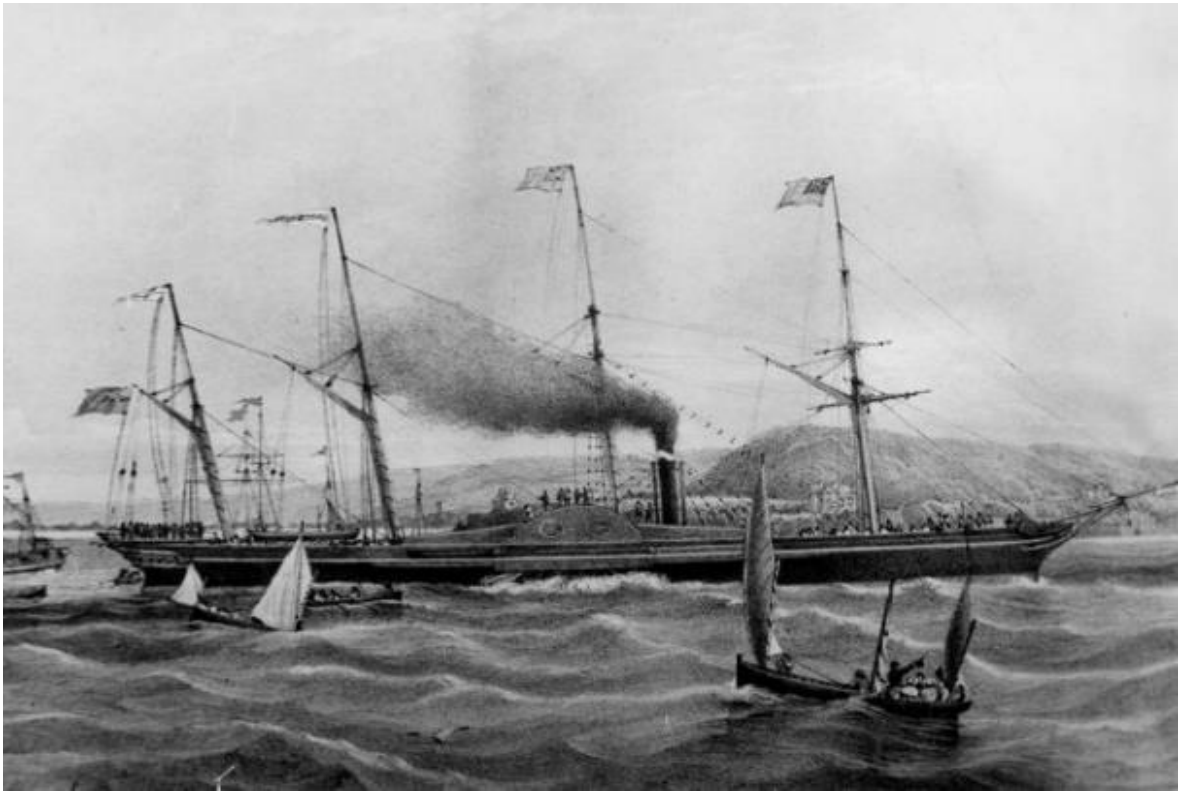

Figure 1.3 – The *SS Great Western*, a wooden-hulled steamship (Ljungström, 2018).

Figure 1.4 – The SS Great Britain, with a hull made of metallic material (Hope, 2022).

To express in practical terms the importance of corrosion protection measures in structures such as ships, the effect of corrosion on the steel plating can be assessed. Even though their thickness includes a designed corrosion allowance, and despite the application of protection methods by paint systems and cathodic protection systems, continuous maintenance is essential during ships lifetime, in order to prevent corrosion. However, although critical, economic factors may affect the regularity and quality of ships maintenance. Therewith, the effective load capacity of ships plating is affected by thickness loss, which is caused by unmanaged corrosion, compromising their safe operating life and implying in expensive repair costs and delays (Gudze and Melchers, 2008).

Not only the external underwater metallic parts of ships are under great threat of corrosion. Ballast tanks (Figure 1.5), which are used to provide manoeuvrability and to regulate ships' stability, draft and stress by controlling the volume of water

(generally seawater) in its interior (De Baere et al., 2013) are also worthy of mention. In this case, two aggressive environments are developed – an immersion and an atmospheric corrosion environment. Therefore, the structural material of these tanks is often subjected to repeated wet-and-dry cycles, as the compartments are filled and emptied as necessary for ship navigation. This results in high rates of corrosion in a critical and hard-to-access area, making maintenance very difficult (Gudze and Melchers, 2008).

In this regard, the evaluation of the corrosion resistance performance of coatings becomes an important aspect for product design for the marine sector (LeBozec et al., 2015). Coatings with better performance can reduce the degradation of properties in materials used for shipbuilding – mainly steel and aluminium alloys (Eyres, 2006) – reducing maintenance costs and increase the lifespan of components and equipment. However, an interesting question follows this argument: how could a coating be classified in good or bad? Also, how could the quality of a coating be measured?

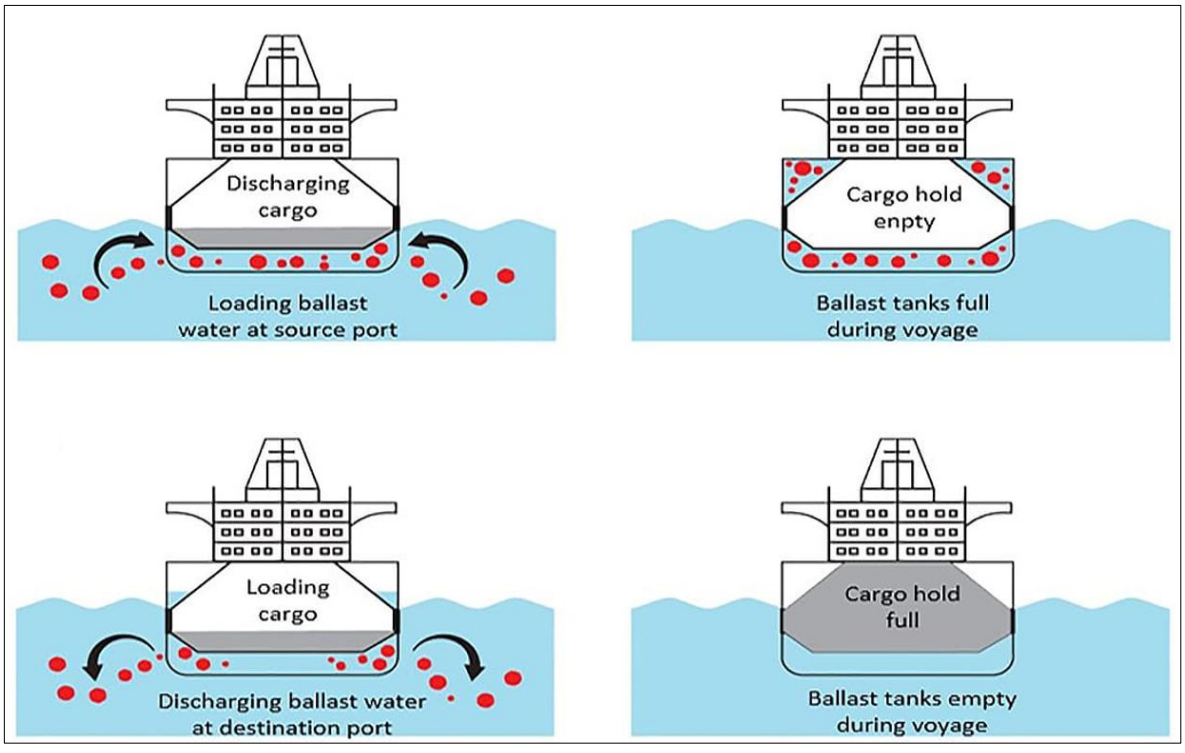

Figure 1.5 – Schematic showing how ballast tanks work (Danfoss, 2018).

Over the different techniques in which organic coatings may be evaluated – which will be further discussed in Section 2 – methods that can provide quantitative information about the corrosion protection performance of these products are of great interest. For example, the behaviour of coatings as they are exposed to degradation processes in aggressive electrolytes in laboratorial experiments can be translated into measurements and analysed over time, enabling the evaluation of the changes in the properties of the coatings, or even comparison with other formulations.

A powerful technique for evaluating the corrosion protection provided by coatings applied on metals subjected to aggressive environments is the electrochemical impedance spectroscopy (EIS), which have been broadly used by researchers as a tool to characterize the evolution of corrosion processes on coated samples (Lasia, 2014; Mansfeld and Kendig, 1985; Mouanga, Puiggali and Devos, 2013). The method is also covered on International Organization for Standardization (ISO) norms for testing on paints (Lasia, 2014).

However, despite its advantages, EIS imposes several challenges, from the specific hardware and software requirements to the necessity of expertise and a set of skills concerning the translation of the acquired data into relevant information (Mansfeld, 1995). This may be a significant drawback in using EIS as an assessment tool in contexts such as product development, for evaluating new coating products for the marine sector, for example.

In a movement to overcome those difficulties, the use of machine learning approaches has been considered, in pursuance of a more efficient tool for evaluating the performance of organic coatings. In theory, the utilization of machine learning techniques may acutely subdue the challenges and the amount of time to interpret the data. Ultimately, this could have an important economic impact in the development of newer anticorrosive paints.

1.4. PROJECT AIM AND OBJECTIVES

In this sense, this study will focus on the application of machine learning techniques for evaluating electrochemical impedance spectroscopy experimental results of coated samples. In this context, the aim of this project will be to obtain an effective analysis from EIS measurements on coated samples using ML techniques. Following that, this work will try to verify if machine learning methods can reduce not only the time needed to perform a correct interpretation of the data, but also the dependency of experts' evaluation, which can lead to cost reductions.

Therefore, the aim of the project described in this dissertation was to explore the application of machine learning techniques for evaluating data from electrochemical impedance spectroscopy experiments made on coated samples, in order to achieve reasonable interpretation of the results, accurate information about the properties of the system and an improvement in efficiency in using EIS for the evaluation of coatings performance.

In this direction, this project will intend to conclude the following objectives:

- Obtain electrochemical impedance spectroscopy data from laboratory experiments on coated samples;
- Define suitable machine learning methods and parameters for the acquired data;
- Develop machine learning "*proof of concepts*" algorithms that can process data from EIS measurements on coatings into classification evaluations and quantitative analysis; and
- Investigate the correlation between machine learning predictions and the visual aspects of the coated samples after testing.

Also, another line of investigation was purposed. Since EIS testing requires certain apparatus that could be relatively expensive, as mentioned by Gong et al. (2019), an attempt of using different types of input signals was performed. The objective in this case was to verify if these results – that in theory could be acquired by less expensive equipment – would be able to provide information about the coating conditions if a machine learning algorithm was trained combining this raw data with the results values obtained with electrochemical impedance spectroscopy. It is worth mentioning that the ML algorithms were developed as *proof of concept*, i.e., as prototypes which purpose was to test the formulated idea.

In the following sections, an overview of the key concepts related to the project was given (Section 2), together with relevant work of the related fields of study and identified knowledge gaps. In Section 3, The inputs, the experimental design and the methodologies used to investigate the aims and objectives established for the project were presented. Section 4 exhibits the obtained results and their critical analysis and interpretation, comparing them with the academic literature previously studied (where pertinent). A summary of the project and suggestions to further investigations on the theme are presented in Section 5 , followed by the references that were used (Section 6).

Appendices A and B present the visual aspects of the marine and model coatings after their corresponded tests, respectively.

2. LITERATURE REVIEW

2.1. PRINCIPLES OF CORROSION

Corrosion reactions that happen in metallic materials when exposed to environments such as immersion in aggressive aqueous solutions (wet corrosion) or even exposed to the atmosphere (atmospheric corrosion) are examples of electrochemical processes. Their mechanism is different from the ones related to other kinds of corrosion conditions found, for example, in molten salt corrosion or high-temperature oxidation processes, which will not be focused on this thesis.

The electrochemical corrosion mechanism consists of two basic reactions involving the transfer of electrons: an anodic process, related to reactions that cause the loss of metal (oxidation), therefore resulting in loss of electrons, and a cathodic process, where a reduction reaction consumes the electrons derive from the anodic reactions. Figure 2.1, adapted from McCafferty (2010), demonstrates an example of these two processes being developed on the surface of iron, when immersed in an acid solution. In this case, the anodic reaction is the *dissolution of iron* (or *metal dissolution*), supported by a cathodic reaction known as *hydrogen evolution*. It is important to note that, in the anodic process, for the *Fe* element, its oxidation number increase (from *0* to *+2*), while in the cathodic process, the oxidation number of the *H* element decreases (from *+1* to *0*). Together with the concept of accepting and donating electrons, the characterization of the anode and cathode in a corrosion system by means of the variation in the oxidation number of the species is also used. The anodic and cathodic electrochemical half-cell reactions (which shows electrons on the reactants or on the products side) are also given in the image.

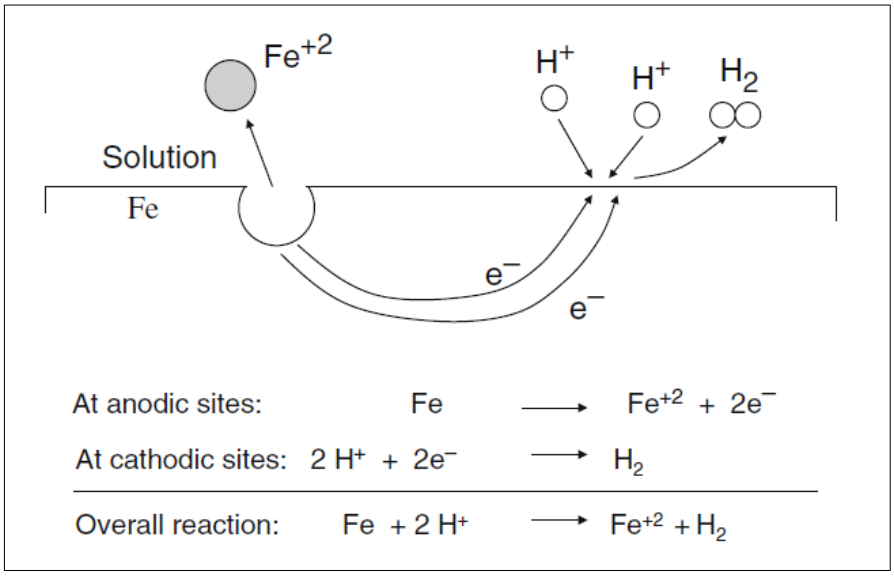

Figure 2.1 – Schematic representation of anodic and cathodic reactions taken place on the surface of iron immersed in an acid solution.

As mentioned above, the anodic and cathodic reactions are supported by the transfer of electrons between the anodic and cathodic sites, i.e., the region where each reaction occurs. However, that will imply the existence of: *(i)* an electron flow, through the metal, from the anodic area towards the cathodic area, where the electrons will be consumed – which means that the conventional current direction will be from the cathode towards the anode region; and *(ii)* a current flow in the solution (electrolyte), by means of ion transportation, from the anode to the cathode zone.

Figure 2.2 shows the four elements that must be present in an electrochemical corrosion mechanism, and the current flux among them. In the image, I_a stands for the anodic current (in other words, the number of electrons coming from the anodic process); I_{el} represents the current circulating within the electrolyte; I_c is the cathodic current; and I_m is the current flowing through the metal, from the cathode towards the anode region. All these four processes have the same rate, which can also be identified as I_{corr} (Pedeferri, 2018).

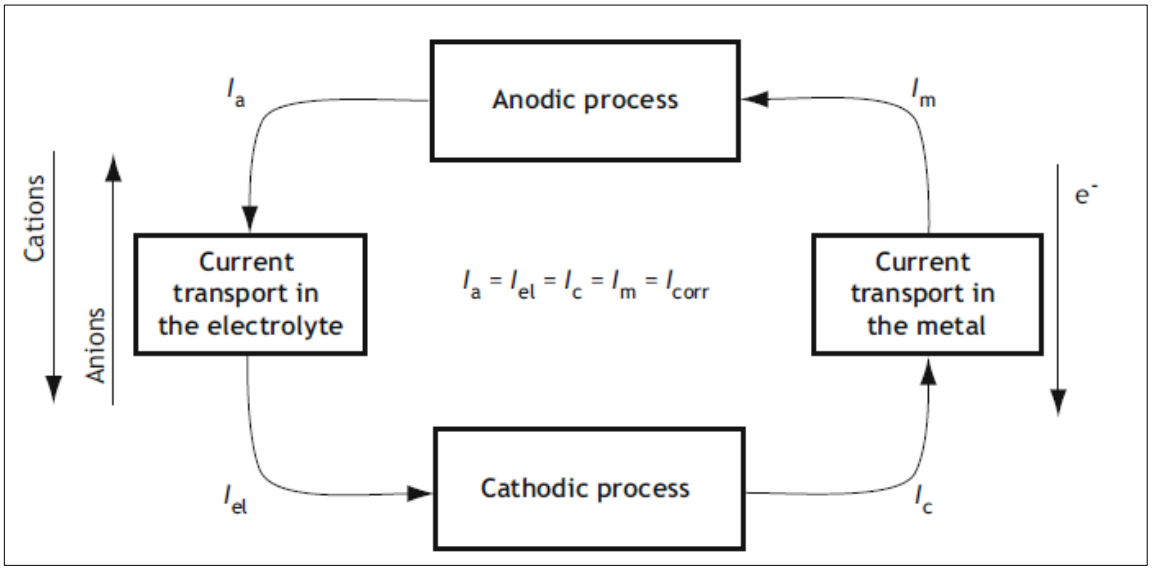

Figure 2.2 – Current flux in an electrochemical mechanism of corrosion (Pedeferri, 2018).

Regarding the subject of corrosion, the study of charged interfaces has a major importance, especially in the case of the metal/solution interface. In an electrolyte, the conduction of a current is due to the presence of dissolved ions. However, there is no net charge as the ions are in constant random motion, hydrated by water molecules (ionic hydration), and an equal amount of positive and negative charges will be present in any volume element of the electrolyte. On the other hand, at the interface between an electrolyte and metal (immersed in this solution), a local reorganization of charged species takes place, depending on the charge condition of the metallic surface. More importantly, as a corrosion process happens, the metal/solution interface may not remain stable (McCafferty, 2010).

When a metal is immersed in an electrolyte, an electrochemical potential difference between the metal and the solution is stablished (Gentil, 1996). To illustrate this, the motion of a metallic ion from the metal lattice to the solution, as happens in corrosion, can be considered. In the lattice, the ions are stabilized by metallic bonds, characterized by delocalized electrons. Once in the solution, the ions will now be stabilized by water molecules, creating a region with an array of “stacked” charged species, called “double layer” (McCafferty, 2010). As the double layer stabilizes the

charged metal surface (which will depend on the whether it accepts or donates electrons), the solution will now have a local net charge. The bulk solution, however, remain neutral. From this inequality accrues the potential difference.

As listed by McCafferty (2010), there are several models dedicated to describing the behaviour of the double layer on the metal/solution interface. The approach used in the previous paragraph is known as the *Gouy–Chapman model*. Furthermore, the *Stern model* considers the layer of charged species proposed by Gouy–Chapman and the adsorption of anions and cations at metal surface. A more recent model is known as the *Bockris–Devanathan–Müller model*, which adds to the previous model the aspect that the water molecules and ions compete for adsorption sites at the interface, therefore water molecules and anions can also be absorbed.

Finally, the consequence of the electric double layer on the metal/solution interface is the local difference in the potential. As corrosion happens, cations and anions move across the double layer, making the properties of this layer pivotal for the whole process. This scenario can be modelled by the simple equivalent electric circuit shown in Figure 2.3. The capacitive parameter C_{dl} is related to the disposal of the charged species at a metal surface, which is similar to a parallel plate capacitor as exemplified in Figure 2.4. In parallel, the resistive parameter R_P (also referred as R_{ct}) is related to the charge transfer resistance across the double layer. The ohmic resistance of the solution is modelled by R_S, which is inversely proportional to the solution conductivity.

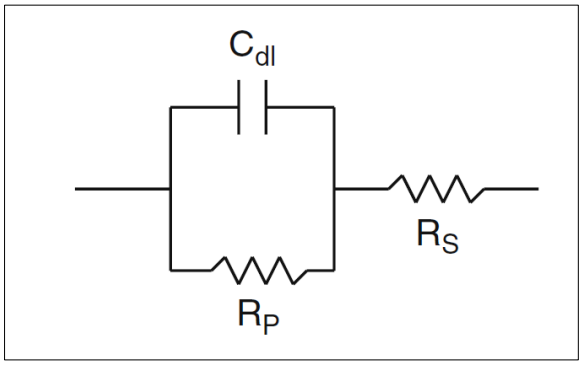

Figure 2.3 – Equivalent electric circuit (EEC) model.

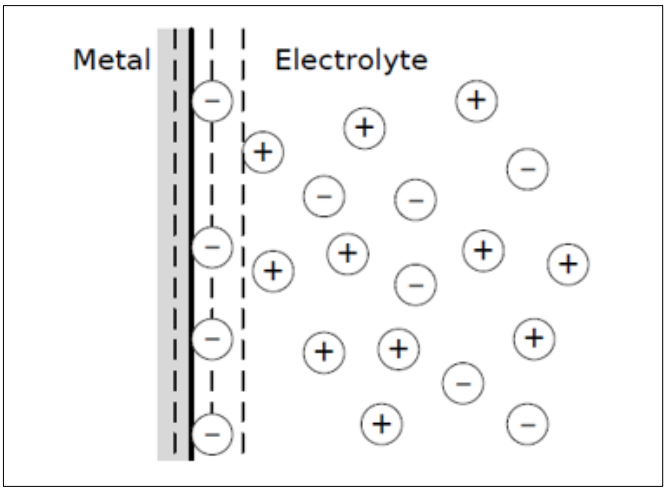

Figure 2.4 – Schematic example of the electrical double layer. Adapted from Orazem and Tribollet (2017).

It is not possible to measure the potential difference across a metal/solution interface in absolute terms because a potential-measuring device would constitute a new interface in the system, and the measured potential difference would be related to both interfaces. Nonetheless, a relative potential difference can be measured, which is conveniently measured against a reference. To this, the term *electrode potential* is given, which represents the potential difference across the interface of a given metal relative to a reference electrode. The *standard hydrogen electrode* (SHE) is related to chemical equilibrium between the ion H^+ in solution and H_2 gas in standard states, and is arbitrarily defined as having the electrode potential of 0.000 *V*, making potential measurements possible for metals (McCafferty, 2010).

In laboratory or industrial activities, however, other types of reference electrodes are used, since the SHE is not practical since it requires a constant supply of H_2 gas. Some examples are: copper/copper sulphate electrode, silver/silver chloride (saturated), and saturated calomel electrode (Pedeferri, 2018).

The Gibbs free energy can be described as a function of the entropy and the enthalpy associated with a given chemical reaction. The relation these two entities with the free energy change is given in Equation (2.1). From differential equations,

ΔG can be also expressed as given in Equation (2.2), as a function of the standard free energy change and (*ΔG*) the reaction's equilibrium constant (*K*), where *R* is the universal gas constant and *T* is the absolute temperature (McCafferty, 2010).

$$\Delta \quad = \Delta \quad - \quad \Delta \tag{2.1}$$

$$\Delta \quad = \Delta \ ° + RT \ln \tag{2.2}$$

Considering a metal/solution interface, the electrochemical potential relates to the Gibbs free energy change by Equation (2.3), where *n* is to the number of electrons involved in electrochemical reaction, *F* is the Faraday constant and *E*, the electrochemical potential.

$$\Delta \quad = - \quad \cdot \quad \cdot \Delta E \tag{2.3}$$

The electrode potential represents a measure on the tendency of metal atoms to lose or receive electrons (Gentil, 1996), and therefore has a great importance for the studies of corrosion. Combining Equations (2.2) and (2.3), it is possible to calculate the electrode potential for non-standard situations. This result in the equation known as the Nernst Equation, presented in (2.4). It is important to emphasize that the term "standard" in standard electrode potentials was used to describe potential measurements that are taken when a metal is immersed in a 1 *M* solution of its ions, which is a specific condition not always found in corrosion systems (McCafferty, 2010). However, with the Nernst equation, the corrosion tendency of a metal in other conditions can be assessing by electrochemical equilibrium potentials of the relevant reactions (Elayaperumal and Raja, 2015).

$$= \quad ° - \frac{RT}{nF} \ln \tag{2.4}$$

By calculating the potentials by the Nernst equation for the generic half-cell reactions for the anodic and cathodic processes, *ΔE* can be expressed as the difference between the equilibrium potential of the cathodic reaction (E_c) and the potential of the anodic reaction (E_a). Therefore, taking the Equation (2.3(2.3) into account, this reaction will only fulfil the thermodynamic condition for a spontaneous process if $\Delta E > 0$, which provides the conclusion given in Equation (2.5). In other words, in order to a corrosion process be thermodynamically possible, the equilibrium potential of the cathodic reaction must be more positive than the potential of the anodic process. The *ΔE* term is referred as the *driving voltage* or *potential difference* of a chemical reaction. It is a powerful tool to understand the likability of a corrosion process by evaluating the equilibrium potential of the electrode reactions happening on the surface being studied (Pedeferri, 2018).

$$\Delta \quad > 0 \Rightarrow \quad - \quad > 0 \Rightarrow \quad > \qquad (2.5)$$

The Belgian chemist Marcel Pourbaix (1904 – 1998) explored the field by studying the equilibrium potentials related to metal dissolution and typical cathodic processes in the presence of water, involving hydrogen and oxygen (Pourbaix, 1974). This gave origin to the very important *Pourbaix diagrams,* which are potential-pH charts showing thermodynamic stability areas for the chemical species of a given metallic material (i.e., not only the atomic metal but also its ions, oxides, and hydroxides). Most notably, three areas – immunity, passivation, and corrosion – are presented for every studied metal as a function of the potential and pH (in some cases, also concentration and temperature). These diagrams can graphically present the conditions where the occurrence of corrosion in a thermodynamical basis are expected and are very significant for corrosion studies (Elayaperumal and Raja, 2015; McCafferty, 2010; Pedeferri, 2018). Figure 2.5 shows a simplified Pourbaix diagram for iron, which is of most interest of this Dissertation.

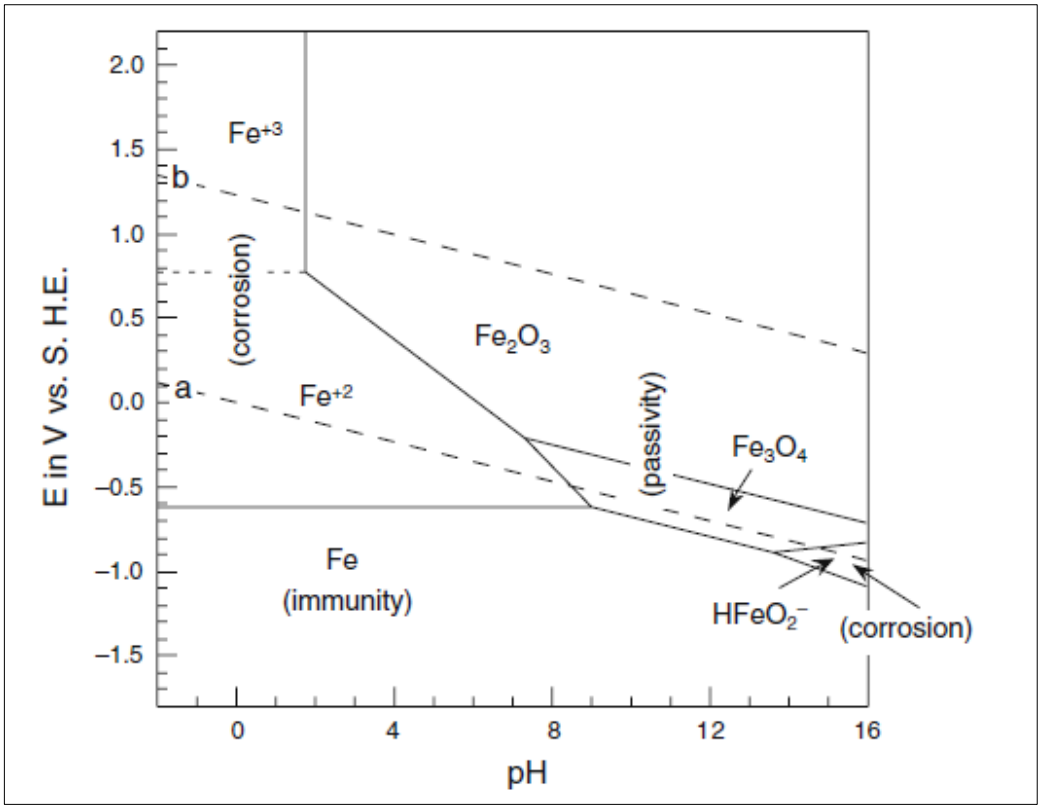

Figure 2.5 – Simplified Pourbaix diagram for iron at 25°C. The immunity, passivity and corrosion stability areas are shown (McCafferty, 2010).

2.2. CORROSION CONTROL METHODS

Having discussed the basic elements of a corrosion system, the focus in the following Sections will be on how it can be monitored and prevented in industrial and engineering applications.

As stated earlier, corrosion control methods can be divided into different groups, depending on which aspect of the corrosion system is explored (Gentil, 1996). It is not the intention of this thesis to describe every technique from each one of these groups, but actually to compare some of them with the corrosion control method by the use of coatings, which will be further examined.

Corrosion prevention should be considered from the design stages of an engineering process or component, in the regarding of achieving the desired functionality when exposed to the expected operating conditions, which must be critically evaluated in terms of its aggressiveness. Physical and chemical parameters influence how

aggressive the environment is, such as the temperature, pH, flow regime, and oxygen content for aqueous solutions, for example (Pedeferri, 2018).

Hence, one way of controlling corrosion is to modify the application surroundings. One example of this may be understanded by analysing the diagram shown in Figure 2.5. As it is known by common sense, corrosion is likely to occur if steel (basically made of iron) is exposed to aqueous solutions at acidic or neutral pH. However, if the environment is slightly alkaline solutions, with higher pH (between about 9.5 to 12.5), than the iron will reach the stability zone of an iron oxides, therefore leaving the corrosion zone. Other methods that could be used to modify the corrosiveness of an aqueous solution are removing the oxygen content (de-aeration) or adding corrosion inhibitors (Gentil, 1996).

Attention must also be given to the mechanical design of the components. Arrangements that could promote crevices, galvanic couplings, turbulence, local condensation, or local mechanical stress should be avoided in the design stage. Welding procedures should also be carefully inspected, as they may not only create crevices but also affect the local microstructure of the material, promoting heterogeneities. Finally, some applications include a corrosion allowance in the total thickness, what should be done only with adequate knowledge about the corrosion behaviour of the component in service conditions (Gentil, 1996; Pedeferri, 2018).

When selecting a material for a given application, it is fair to say that the mechanical requisites are used first for screening the potential candidates. However, the corrosion aspect should also be considered at the material selection stage. According to Pedeferri (2018), two criteria are used for this: one basic criteria, based on the knowledge of corrosion principles about thermodynamic and kinetics, and a technological criteria, which it is based on engineering standards. Certainly, the economical evaluation must also be present at the material selection. Finally, materials can also be altered by means of heat treatments and changing their composition (Gentil, 1996).

An important corrosion control technique for immersed conditions is the use of cathodic protection. It aims to bring the potential of the structure to be protected to lower values (in other words, by cathodic polarisation). This can be done in two ways: one, by using materials that are more likely to corrode than the structure to be protected (which are called *sacrificial anodes*) or through the use of *impressed current systems*, where a source of direct current is used (McCafferty, 2010). Their basic mechanisms are shown in Figure 2.6, where the cathodic reaction is the oxygen reduction.

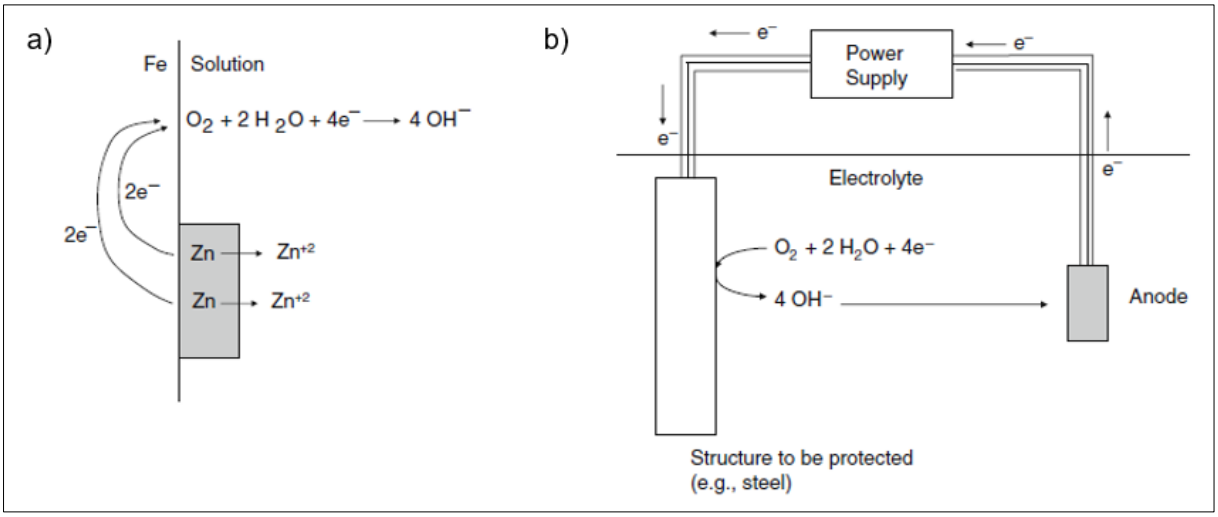

Figure 2.6 – Cathodic protection mechanism: (a) by sacrificial anodes; (b) by impressed current systems.

In the other way, If the material to be protected can be passivated by oxide films, an anodic polarisation could instead be used. This technique, known as anodic polarisation, aims to maintain the material in the passive region, where the corrosion rate is very low. This method, together with the cathodic protection and the increase of pH can be graphically understood by the simplified Pourbaix diagram presented in Figure 2.7 (McCafferty, 2010).

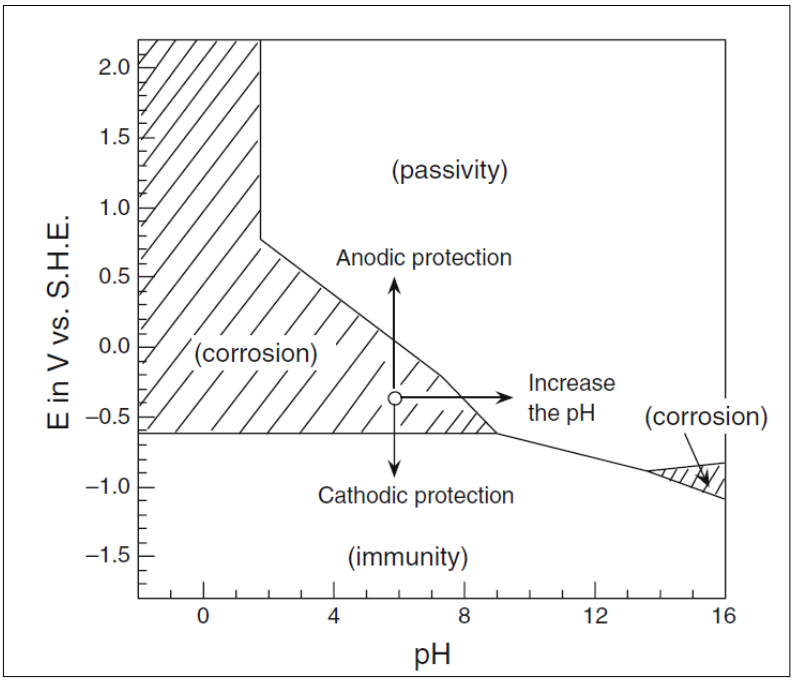

Figure 2.7 – Simplified Pourbaix diagram (iron at 25°C) showing the basic concept of anodic protection, cathodic protection and controlling pH (McCafferty, 2010).

Finally, corrosion processes may be prevented by means of applying a physical barrier separating the environment and the metal surface. Some materials develop natural protective layers in conventional conditions by chemical transformations, like in the case of stainless steel and aluminium, which have chromium and aluminium oxides on their surfaces, respectively. They are insoluble, continuous, impermeable, and well-adhered layers. However, this is not the case for steel, whose corrosion product is non-continuous, soluble, permeable, and may grow indefinitely until the complete degradation of the metal. Therefore, corrosion protection is needed, which can be accomplished by the use of coatings (Gentil, 1996).

Coatings can be grouped into four categories, as organized by Pedeferri (2018): metallic coatings (for example, galvanized steels), inorganic coatings (e.g., glass lining or cementitious coatings), conversion coatings (e.g., chromating and phosphatizing), and paintings (or organic coatings), which will be further discussed in a dedicated Section.

2.3. REVIEW ON ORGANIC COATINGS

2.3.1. COMPONENTS

Anticorrosive paintings are mainly used as a corrosion control method because of how its cost-benefit relation and easiness of application (Gentil, 1996). Two main mechanisms are involved in the corrosion protection by paints: in addition to the physical barrier separating the metal substrate from aggressive environments, paints may also have specific elements in its composition, like corrosion inhibitors, that could prevent corrosion (McCafferty, 2010).

According to Pedeferri (2018), the components of a paint may be divided into two groups: the binder (or vehicle) and solvent (such as plasticizers) are in the liquid part; the pigments and addtives are in the solid group.

Binders are the most important constituent of the paints, and basically defines the coating type, according to its nature. It is the film-forming agent and transform itself into the continuous phase in which the remaining components of the paint are incorporated. Therefore, the film properties are very influential in the coating characteristics. Solvent evaporation, oxidation, crosslinking, and chemical reaction are some of the mechanisms by which the binders are converted from liquid to solid state on a substrate (McCafferty, 2010; Pedeferri, 2018).

Among the several types of paints, the ones from epoxy resins are among the most used coatings for industrial applications. They are obtained by the reaction of its reactive compounds – epoxy and hydroxyl groups – with a crosslinking agent (normally polyamide and polyamines, although many other can be used). One of the main factors supporting its widespread use is the wide variety of compositions and properties that can be achieved with this material, for many applications (Pedeferri, 2018).

Pigments and additives are solid particles added to the composition of paints to provide them specific properties that the binders do not possess. Among the

additives, some examples are: anti-foaming agents, anti-fungal agents, levelling agents, thixotropic agents, and many others (Gentil, 1996; Pedeferri, 2018).

The pigments can be classified by their main purpose in the coating, that can be, for example: to modify its performance properties, to alter the application properties, to provide colour, to hide the underlying material, or to reduce costs. According to Jones, Nichols and Pappas (2017), they can be grouped into four categories: inert, white, colour, and functional pigments.

White and colour pigments are related not only with the aspect finish of coatings, but also with provide them the characteristics of opacity and hiding power, which can be understood as the ability to obscure the underlying contrasting colours. On the other hand, inert pigments, also known as fillers or extenders, are mainly used to reduce costs, as they are generally not as expensive as other pigments. As some properties are a function of the volume of pigments in the film, inert pigments could increase this number and ultimately modify features in the paint such as mechanical and rheological properties.

Table 2.1 provides some examples of pigments from these categories (Gentil, 1996; Jones, Nichols and Pappas, 2017).

Functional pigments can alter the appearance, application characteristics and properties of the coatings, including its corrosion prevention performance. Several functions could be listed, although only a limited fraction of some relevant pigments is displayed in Table 2.2. Important types of functional pigments are used for purposes like anticorrosive, flatting (to reduce gloss), biocidal, antimicrobial, fire retarding, or infrared reflecting. Jones, Nichols and Pappas (2017) also report recent research achievements on nano-pigments, in application such as UV absorbing, for example,

Table 2.1 – Examples of inert, white and colour pigments (Jones, Nichols and Pappas, 2017).

Pigment	Use
Barium sulphate	Inert pigment with relative high density (4500 *kg/m³*)
Titanium dioxide	Principal white pigment used in coatings
Zinc oxide	Another white pigment
Calcium sulphates	Used in addition to other white pigments
Iron oxides (group)	Different oxides present in several colour pigments

Table 2.2 – Examples of functional pigments organized by their application (Jones, Nichols and Pappas, 2017).

Application	Pigments (examples)
Corrosion inhibitor	*Zinc phosphate*, zinc chromate, strontium chromate, barium phosphosilicates, barium borosilicates*
Cathodic action	*Zinc metal, in zinc-rich primers*
Antifouling	*Cuprous oxide*
Fungicide	*Zinc oxide*
Fire retardment	*Antimony oxide + chlorinated/ brominated polymers*
Gloss reduction	*Silicon dioxide*
Viscosity modifiers	*Quaternary ammonium salt-treated bentonite clay, fine particle size silica*

**Note: the corrosion prevention mechanism of zinc phosphate is not entirely understood. Some authors disagree on categorizing it as a corrosion inhibitor pigments because of its low solubility in water (Santos, 2018).*

The pigment volume concentration (PVC) – i.e., the volume percent of pigment in a dry coating layer, as defined in Equation (2.6) – is a parameter used to analyse the

effects of pigmentation in coatings, proposed by Asbeck and Loo (1949). They observed that at a certain value of PVC, an abrupt change in several properties takes place. This point is known as the critical pigment volume concentration (CPVC), as it is related to the pigment particle distribution in the paints. Depending on the paint application, a specific PVC-to-CPVC ratio is desired for the coating to achieve the required properties (Jones, Nichols and Pappas, 2017).

$$PVC = \left[\frac{(volume\ of\ hiding\ pigments + extenders)}{(volume\ of\ hiding\ pigments + extenders) + (volume\ of\ nonvolatile\ vehicle\ solids)}\right] \times 100 \qquad (2.6)$$

Anti-corrosion paints can be classified using the PVC-to-CPVC ratio, as shown in Figure 2.8. Depending on the ratio value, the coating protection mechanism changes from acting as a physical barrier to an active-type coating, as discussed further (Pedeferri, 2018).

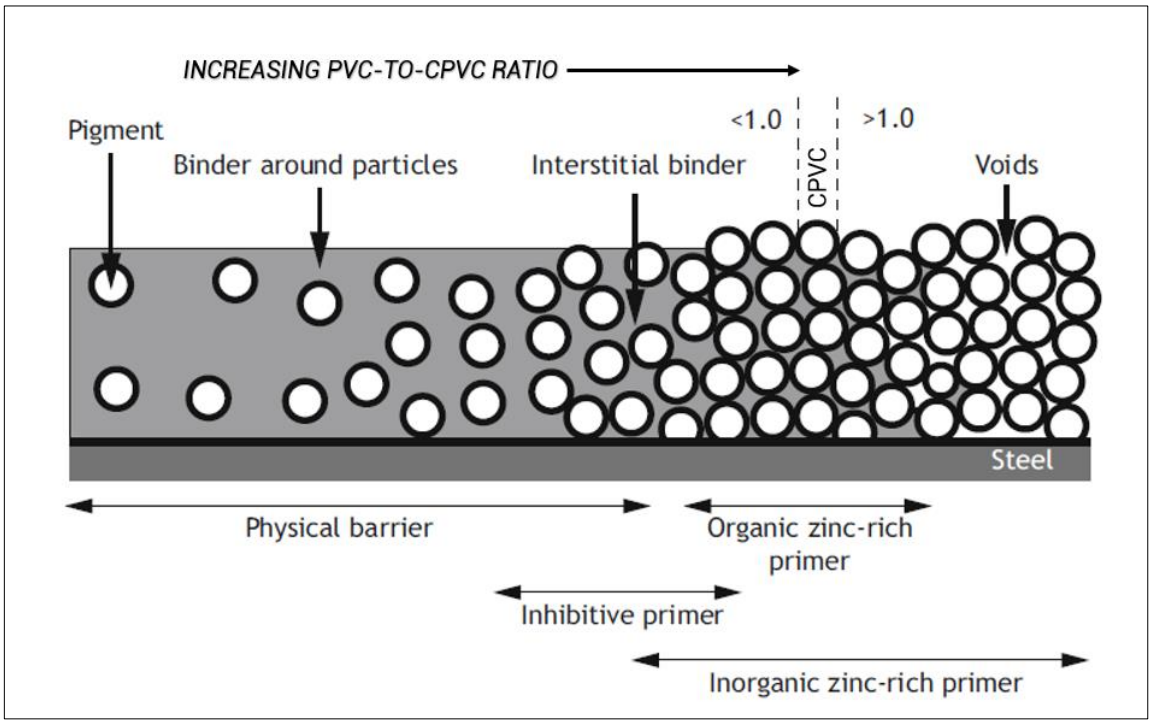

Figure 2.8 – Corrosion protection mechanisms as a function of the PVC-to-CPVC ratio – adapted from Pedeferri (2018).

Solvents, the volatile components, are another important constituent in paints, although it could be not present in some products. Their main contribution to the product is to facilitate its application and allow the formation of the film, after which they must evaporate thoroughly. A good solvent composition is critical to avoid the formation of film defects. Plasticizers are used to interact with the polymeric chains the binder and improve their properties of flexibility and plasticity (Pedeferri, 2018).

Finally, despite not being a component of the paint itself, the surface preparation prior to the application of coatings is vital for their performance against corrosion. As a matter of fact, in standardized coating systems for corrosion protection of components, where several layers of paints with different purposes are used, the surface preparation is one key component of these systems, as exemplified in standards such as ISO 12944-5 (ISO, 2018). For achieving a prepared substrate free of contaminants, and with an adequate surface profile for the application of paints, standards, such as ISO 12944-4 (ISO, 2017a), specify methods for water, solvent, acid, chemical and mechanical cleaning. For steels substrates, specific visual aspects after blast-cleaning procedures are normally required, which correspond to standardized grades covered in standards as ISO 8501-1 (ISO, 2007).

2.3.2. MARINE COATINGS

The materials used in ships, offshore structures and onshore facilities near seawater are subject to very aggressive environments. The use of coatings, together with cathodic protection systems, are the two major control methods against corrosion in these applications (Pedeferri, 2018).

Coatings applied on ship surfaces that are not underwater (above the waterline) are exposed to atmospheric corrosion, combined with high humidity and intense UV radiation conditions. Polyurethane and alkyd coatings are generally used, but the latter, although easiness of application, requires frequent maintenance. Another

interesting aspect about this area is found on military ships, where the colour grey is generally used for reduced their visibility. However, among the pigments used for this colour, carbon black, which is a great infrared absorber, was often present. This feature resulted in increased temperature inside the ships, motivating its substitution for other pigments (Jones, Nichols and Pappas, 2017).

Coatings used in interior spaces often require low levels of solvents for reducing fire hazards. For exterior deck surfaces, requirements on durability, abrasion resistance and often non-skid are stablish for coatings selection. Ballast tanks, mentioned in Section 1.3, also represent an important corrosion challenge, where epoxy formulations are applied. Fuel, oil, and septic tanks are often painted. According to Jones, Nichols and Pappas (2017), fuel tanks must be coated because seawater ballast is often transferred for these spaces after fuel is consumed.

Coatings subjected to seawater immersion conditions have to deal not only to the challenge of corrosion but also to the marine growth on their surfaces (*fouling*), which raise the ship drag, increase fuel consumption, and implies dry docking maintenance periods, resulting in high costs. That is the reason why coating systems for underwater areas are composed of anticorrosive and antifouling paints. Coatings in the splash zone (the structure areas close to the water surface) are particular challenging, since they are exposed to alternated cycles of salt water, dryness, and UV radiation. Additionally, glass reinforced fibre crafts are generally coated with polyester gel coats (Jones, Nichols and Pappas, 2017).

2.3.3. PROTECTION MECHANISMS

The prime consideration about the protection mechanism of coatings is the barrier effect, which aims to reduce the oxygen and water diffusion from the environment to the material to be protected. It is a function of the coating basic composition, its inner components and thickness. If a dense film is obtained after curing, the resistance to

water, oxygen and ions diffusion tends to be higher. Some pigments can enhance that resistance by acting as obstacles to the passage of ions or molecules through the coating, depending on their shape, content, and size. Solvents can also play a role in coatings permeability, as remaining volumes of solvent can favour water absorption (Gentil, 1996; Pedeferri, 2018).

Still, the corrosion protection of metals by organic coatings is not restricted only to their barrier properties. The first reason for this statement that, although the barrier effect does prevent water and oxygen from reaching the substrate, they do not prevent it eternally; therefore, these species permeate the coating eventually, creating and interface with the underlying metal. However, it was verified by authors that the rate of permeated species entering the films is substantially great than their consumption rate in corrosion processes in the metallic interface (Jones, Nichols and Pappas, 2017; Mayne and van Rooyen, 1954). Therefore, the barrier effect was not the only mechanism acting against corrosion.

Pedeferri (2018) refers to this other mechanism as an active effect. Actually, it relates to the specific pigments that, once adsorbed on the substrate, perform some type of “active protective action”, depending on the pigment. For example, zinc particles, in an adequate composition, promote a cathodic protection effect on the metal. This is the case of organic and inorganic zinc-rich primers. Other examples of active effect mechanisms are performed by corrosion inhibitors pigments, in which a passivating protective film is generated or strengthened on the metal surface, and self-healing coatings, which general mechanism relies on chemically reactive molecules that react with the matrix in the presence of a mechanical, thermal, or chemical stimulus, promoting sealing of inhibiting action. Figure 2.8 exhibits some of these mechanisms.

Additionally, a topic on the adhesion could also be discussed. Besides the paramount importance of surface preparation to the performance of a coating system, elements that could retain the adhesion the coating even in the occasion when water permeates through the film. Hence, pigments that act promoting wet adhesion

contribute to the corrosion prevention performance (Jones, Nichols and Pappas, 2017).

2.3.4. CORROSION

It is also important to discuss how corrosion could degrade an underlying coated substrate (underfilm corrosion). It will be a function of the permeation of water, oxygen and/or ions through the organic coating.

McCafferty (2010) describes the sequence of events that result in a coating failure due to corrosion. Water and oxygen molecules penetrate the organic coating, Water permeates into the paint by three mechanisms, which can be by diffusion, capillary action through pores and cracks, or by osmosis mechanisms (which could be enhanced by the presence of soluble salts or impurities on the substrate). Once reaching the substrate, the dissolution of metal starts at a local anodic site, which becomes acidic. If chloride ions are present in the environment, they also permeate through the paint, toward these sites. Supporting the anodic reaction, a local cathodic site is generated, which locally becomes alkaline. This promotes the disbanding of the coating from the metal substrate (a mechanism known as *cathodic delamination* – see Figure 2.9), degrading the coating and exposing the substrate. On the other hand, *anodic undermining* process can also occur, where the metal dissolution happens underneath the coating causes loss of adhesion, exposing the substrate. According to Schweitzer (1998), coated steel is more susceptible to cathodic delamination, while anodic undermining tends to be more common in coated aluminium.

The corrosion rate under coatings is also dependent on the electrical resistance of the paint. This will also be a function of the amount of water absorbed by the paint, which will depend on the properties of the coating. The salt content of the solution influences the coating conductivity (Pedeferri, 2018).

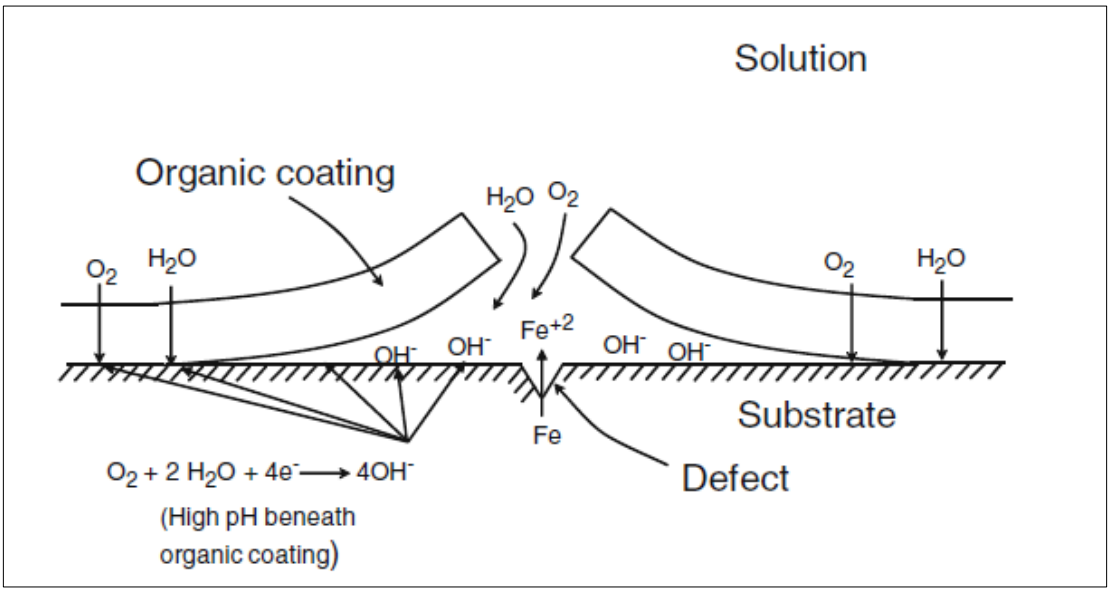

Figure 2.9 – Schematic representation of the cathodic delamination process.

2.4. COATING PERFORMANCE EVALUATION

The behaviour of organic coatings on preventing corrosion can be assessed by several methods such as accelerated tests, experimental electrochemical measurements, or field exposure tests (LeBozec et al., 2015; McCafferty, 2010). However, no test is capable to predict the performance of new coating systems (Jones, Nichols and Pappas, 2017).

The latter group (also referred as *use testing*) relates to data acquired on applying the coating systems and observing its conditions in actual use along the years. The information acquired can provide knowledge about the factors influencing the corrosion performance and support new formulations (Jones, Nichols and Pappas, 2017). Nevertheless, several years are necessary in order to acquire data. For example, in their article about the performance of marine and offshore coatings, LeBozec et al. (2015) collected data from coatings exposed to marine atmospheric corrosion for 3 years in dynamic conditions (where the paint was applied in a vessel) and 4 years in a static arrangement.

Simulated or accelerated tests are relatively reliable for analysing coating performance. They intent to simulate practical operating conditions, generally by using alternate cycles of different corrosion conditions to evaluate the coating behaviour. These cycles could be, for example: the continuous spray of salt water in an enclosed chamber, with high-humidity conditions; immersion cycles; exposure to several levels of relative humidity, temperature, and ultraviolet light. Several standards establish various accelerated corrosion tests, with different cycles, such as ISO 20340 and ISO 16701, resumed in Figure 2.10, in which the coating was subject to a 35°C/ 95% RH (relative humidity) condition, followed by a 45°C/ 50% RH cycle, alternated with a simulated salt rain (1 wt.% *NaCl*, *pH* 4) applied two times each week (LeBozec et al., 2015).

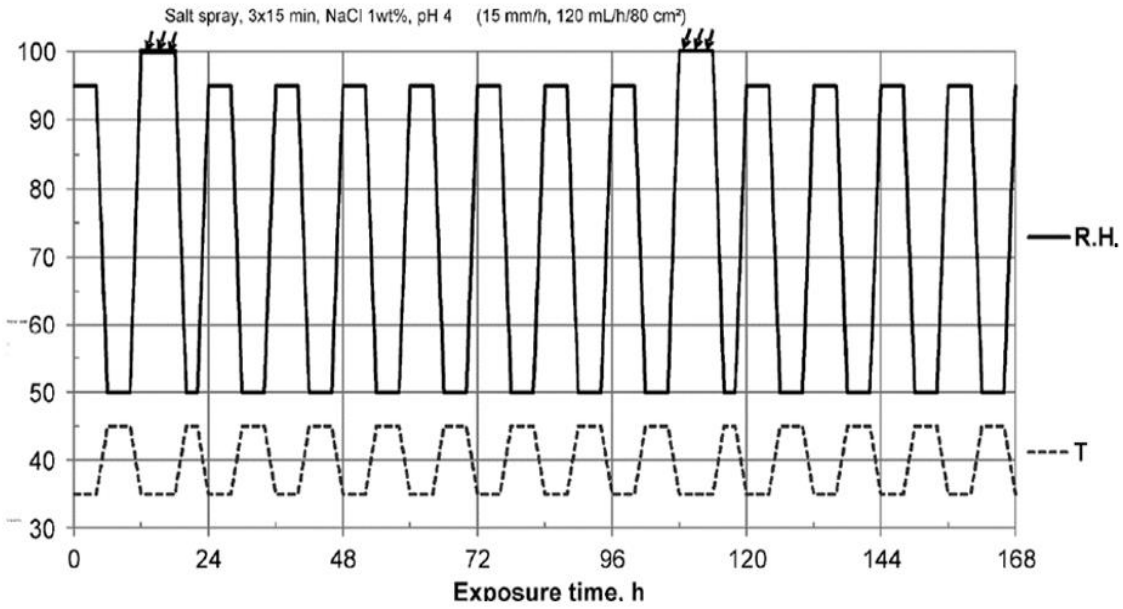

Figure 2.10 – Wet-and-dry cycles in ISO 16701 standardized accelerated test. "*R.H.*" stands for relative humidly and "*T*" for temperature (LeBozec et al., 2015)

Electrochemical methods, such as the electrochemical impedance spectroscopy (EIS), are used for studying coatings, which will be further studied in the following Sections. It is a non-destructive method based on the application of alternating

electrical signals at a range of frequencies, and the analysis of the apparent opposition to the current flow in the system (impedance). Based on the electrical circuit model shown in Figure 2.3, if EIS measurements were made in a coating sample exposed to an aggressive environment, it would be possible to acquire quantitative information on its behaviour like the rate of coating delamination, which is proportional to an increase in the capacitance signal. On the other hand, a coating with a good corrosion prevention performance would show a slow rate of increase in the capacitance response. Therefore, it is a powerful technique for comparing several coating formulations (Jones, Nichols and Pappas, 2017).

Several electrochemical techniques are used for evaluating the efficiency of corrosion prevention techniques and analyse the acting mechanisms on corrosion systems. The *linear polarisation resistance* (LPR) aims to measure the polarisation resistance of a corroding system by measuring the current response under a low applied potential. This technique is considered to be simple and non-destructive in nature. The *potentio/galvano dynamic* method is also used for evaluating the corrosion current density, the corrosion potential, and several parameters of corrosion systems. However, it is considered to be more expensive because of its required instruments. Another noteworthy method that can be used for on-line corrosion measurements is the *zero-resistance ammeter* (ZRA), where the corrosion rate is taken from measuring the galvanic current flowing between two dissimilar metals. These devices are used as part of *electrochemical noise* measurements which, unlike any other electrochemical method, allow the study of corrosion systems without introducing any electrical perturbation, providing the evaluation of free-corroding systems. Finally, an alternative electrochemical test was developed for evaluating the rates of cathodic delamination for different coating systems (Curioni, Monetta and Bellucci, 2015; Elayaperumal and Raja, 2015; Jones, Nichols and Pappas, 2017; McCafferty, 2010).

2.5. ELECTROCHEMICAL IMPEDANCE SPECTROSCOPY

Since electrochemical impedance spectroscopy (EIS) measurements were used in this project for studying coated samples, a dedicated section about this method is given in this Chapter. Nevertheless, this technique is not restricted to coating evaluation and corrosion assessment in metals, being instead related to a wider range of application such as characterization of batteries and fuel cells, quality inspection of foods, human body analysis, and bacterial concentration detection, for example (Grossi et al., 2019).

2.5.1. FUNDAMENTALS

The EIS technique is based on the development of the double-layer theory and derived equivalent circuit modelling on impedance data. Lvovich (2012) presents the sequence of authors and studies that have pavemented the progress on the electrochemical impedance theory.

Advances in equipment and computer technology had significantly impacted the area of electrochemistry, allowing the conception of techniques that could be applied to practical applications, such as the evaluation of coated metals during exposure to corrosive environments (Lvovich, 2012; Mansfeld, 1995).

The impedance can be defined as the resistance to current flow in a circuit and also its ability to store electrical energy. These two aspects are combined in a complex number and represent, respectively, its real and imaginary part. When evaluating the electrochemical behaviour of a coated sample, generally a sinusoidal AC voltage potential signal, with small amplitude, is applied in a range of frequencies. The current response (in a linear or pseudolinear system) in this case is also sinusoidal, but shifted in phase, and will depend on the characteristics of the electrochemical cell being studied (Lvovich, 2012).

The evolution of a coated sample exposed to an aqueous solution will depend on the evolution of the many interfaces in this system, which are not homogeneous. Each interface will be polarized in a particular manner when subjected to a potential difference and will change in a different way when this potential is reversed. For example, the double layers at a given metal/electrolyte interface will respond according to the distribution of their relaxation times, with a particular capacitive reactance (Macdonald and Johnson, 2005). Exploring the equivalent circuit previously mentioned in Figure 2.3, these and other responses of a coated sample under EIS measurement can be modelled by equivalent electric circuits (EEC), such as the one presented in Figure 2.11 where, in addition to the already mentioned polarisation resistance and double layer capacitance (respectively R_P and C_{dl}), other parameters are used to represent the characteristics of the system: R_Ω (also represented as R_s by some authors) represents the resistance between the reference electrode and the test electrode (also referred as “solution resistance”), C_C corresponds to the capacitance of the coating, and R_{po} is the resistance associated to the emergence of pores, which act as ionically conducting paths across the coating.

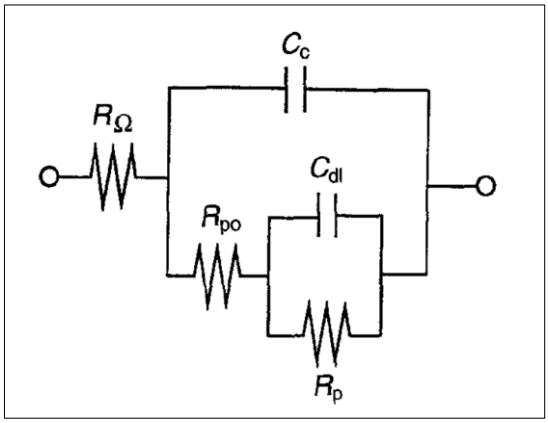

Figure 2.11 – Equivalent electrical circuit for a coated metal sample (Mansfeld, 1995).

The coating capacitance is defined by Equation (2.7), where A is the test electrode exposed area, d is the coating thickness, ε is the coating dielectric constant, and ε_0 is the dielectric constant of free space, equals to 8.85×10^{-14} F·cm^{-1}. It should be

highlighted that, as a coating degradation process happens, an increase in the capacitance would be measured by EIS, since the exposed area would increase (delaminated area) and, also, the thickness could be reduced (Mansfeld, 1995).

$$= \cdot {}_0 \cdot / \qquad (2.7)$$

The impedance output is generally expressed in terms of the impedance modulus | | and the phase angle shift, represented by Φ (phi). This data can be represented in two different plots, known as *Nyquist* and *Bode* plots. The first is composed of the real component of the impedance in the x-axis, and the negative value of the imaginary parts in the y-axis, creating the semicircle-shaped plot seen in Figure 2.12.

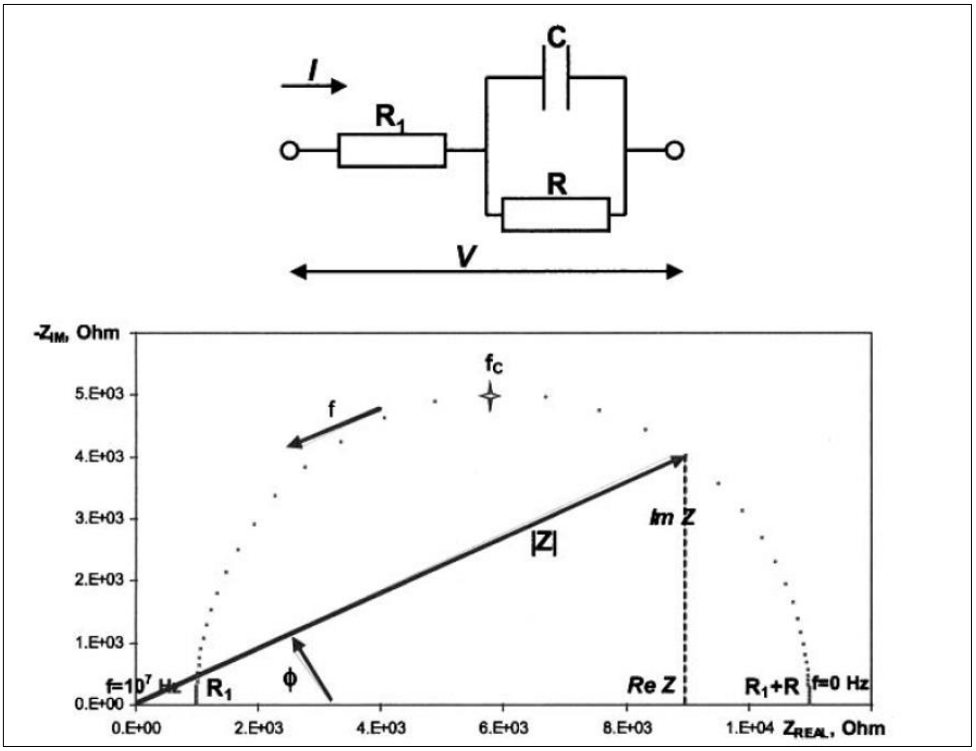

Figure 2.12 – Nyquist plot example for the corresponding EEC (Lvovich, 2012).

However, although this graph could provide useful insights on the conduction mechanisms of kinetic controlling the system, some authors are not keen on presenting EIS data using this kind of graph. The main critique relies on the fact that on detailed information about the frequency of each point is presented, which would require several labels in the plot indicating each frequency value. Additionally,

changes in the coating performance are not easily detect in this type of plot, as they are for the *Bode* plot. (Lvovich, 2012; Mansfeld, 1995).

The *Bode* plot is composed of two graphs: one showing the logarithm of the impedance modulus plotted against the logarithm of the applied frequency, and a similar one showing the phase angle versus the logarithm of frequency. Figure 2.13 shows the theoretical response of three coated samples with different degradation conditions. By using this representation, the effect of corrosion processes can be more clearly seen, as the impedance modulus in the low frequency range decreases in *(a)*. Less evidently, as the capacitance increases, the slopped segment line at medium frequencies shifts to the left. Also, as the coating degrades, an initial pure resistive behaviour evolves to a condition related to a two time constant equivalent circuit, represented as an intermediate plateau at curve *"3"*. It could also be commented that, at higher frequencies, the impedance reading is close to R_Ω, while for lower frequencies, the measurement is close to the sum of $R_\Omega + R_{po} + R_P$. Finally, each of these events is also reflect in changes in the phase shift graph. The parameters values used for these simulations can be found in the article by Mansfeld (1995).

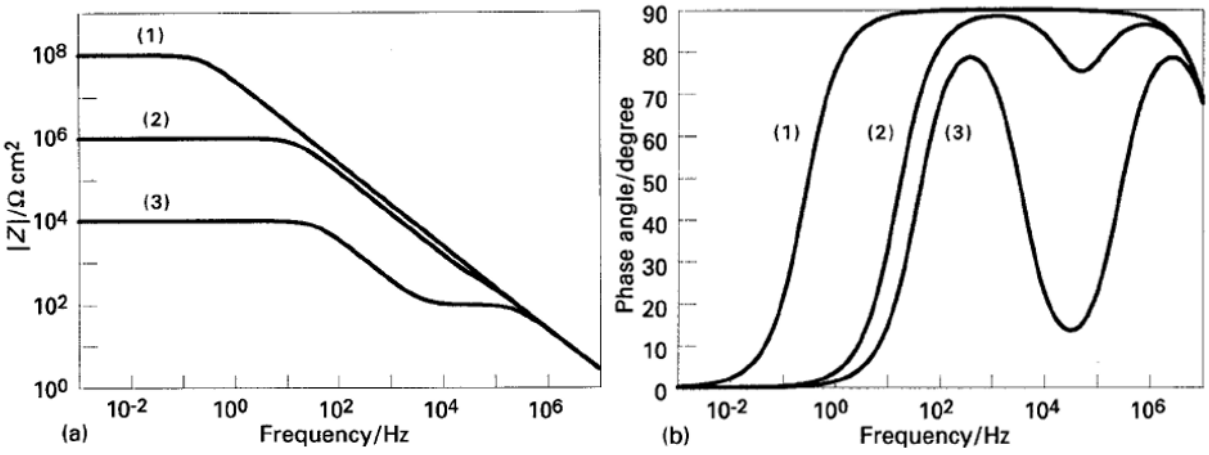

Figure 2.13 – Theoretical Bode Plots: *(a)* Impedance Modulus; *(b)* Phase angle shift. Curves "1", "2" and "3" represent different degradation stages of the coating. Adapted from Mansfeld (1995).

Additionally, if the sinusoidal values of voltage and current were used as axis in a x-y plot, the result would be an oval plot known as *Lissajous figure*. Figure 2.14 shows theoretical plots for this representation, depending on the phase shift angle.

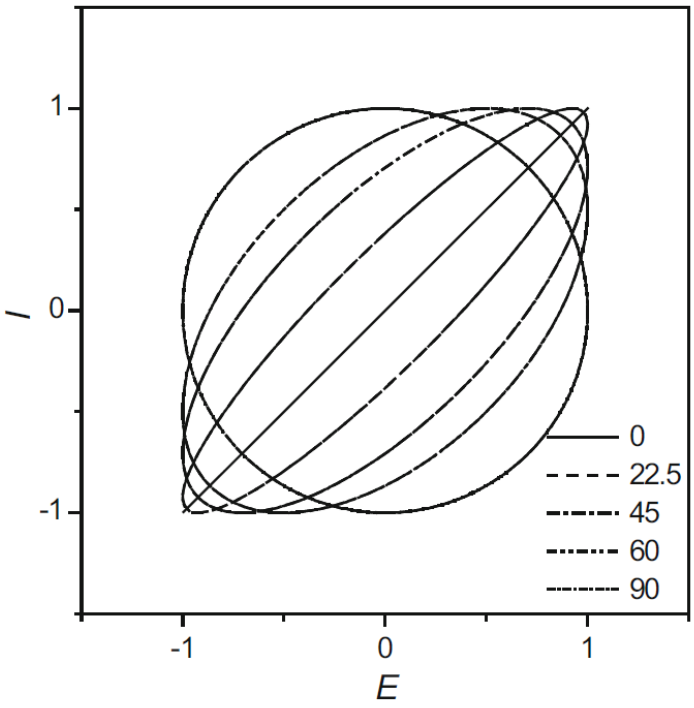

Figure 2.14 – Theoretical Lissajous figure (Potential *vs.* Current) for impedance data, for different phase shifts angles (in degrees) (Lasia, 2014).

For extracting quantitative information about EIS experiments, a suitable equivalent electrical circuit model must be selected for the fitting procedure, which basically means to correspond the impedance acquired data to the impedance response generated by the selected circuit. Generally, it is recommended to start this proceeding using one simple model and compare it with the measured data, which can be done graphically using adequate software. Adding new parameters may improve the fitting but should be use if they correspond to physical aspects of the corrosion system. Several parameters and circuits could be used for data fitting, depending on the characteristics of the sample being studied (Lasia, 2014).

Table 2.3 shows some ideal circuit elements used in EEC models. However, it is important to realize that, as stated by Lvovich (2012), to fit an equivalent circuit to a data acquired from a corrosion system is to resume a complex event that combine chemical, mechanical, electrical and mechanical aspect into purely electrical terms. Hence, there may be cases where the fitting could deviate from the acquired data.

Table 2.3 – Some circuit elements used in EEC models (Lvovich, 2012).

Components	Impedance
Resistor	
Capacitor	$1/j\omega$
Inductor	$j\omega$
Infinitive diffusion	$/\sqrt{j\omega}$
Constant phase element (CPE)	$1/[\ \ (j\omega)$

2.5.2. APPLICATIONS

Regarding corrosion studies, EIS has been broadly used for coatings evaluations. In the marine coatings sector, Kiosdou, Karantonis and Pantelis (2014) studied the barrier properties of two types of antifouling paints, an epoxy self-polishing and a silicone foul-release coatings, applied on steel substrates, by testing with electrochemical impedance spectroscopy, among other methods. EIS measurements were performed in laboratory conditions, using a three-electrode cell in a 3.5 wt.% *NaCl* solution with aerated deionized water, and also in specimens immersed in 2.5 *m* depth in field exposure conditions in the Gulf of Elefsina. The results shown that the silicone foul-release samples had better barrier properties compared to the self-polishing specimens, where a pore resistance value was detected after 4 months of tests in laboratory conditions.

Marine coating systems for underwater ship hull areas were evaluated by Stojanović et al. (2019). Steel plates previously shot-blasted to Sa 2½ condition according to ISO 8501-1. Each tested paint system had the same anticorrosive layers, totalling a 400 *μm*. For the antifouling component, two group of plates, with different types of products were tested – a group with self-polishing antifouling paints and another with biocide-free foul-release coatings. EIS measurements were used to evaluate the corrosion tendency for each plate in seawater, for 60 days, at room temperature. A sinusoidal 10 *mV* signal was used, in the frequency range of 100 *kHz* to 0.1 *Hz*. Three different equivalent circuit models, with 1-, 2- and 3-time constants, were used for fitting EIS data. At the beginning, the data was used using the EEC presented in Figure 2.3. With time, a non-porous coating behaviour and the presence of biofilm implied the used of more complex equivalent circuits. In opposition to the previous presented study, these authors have concluded that, after immersion, samples with the self-polishing products in their paint systems had better corrosion resistance, for the same thickness. An increase in corrosion with the development of biofilm on the plates was also verified, and the microbiological development was higher in plates where the solution was agitated. The variation between the results in the two studies about antifouling coatings could be due to environmental conditions or differences in the products used in each project.

For analysing the effects of microbiologically influenced corrosion (MIC) in submerged steel bridge piles, Permeh, Lau and Duncan (2019) have conducted EIS measurements in order to identify microbial activity and coating degradation related to the action of sulphate reducing bacteria (SRB). The levels of degradation were categorized using the measurements results. It was also noticed that SRB action have created layers with depleted biocide on the surface of antifouling paints. The frequency range used was from 1 *MHz* to 1 *Hz*. Four different equivalent circuits were used to fit EIS data. All of them had the constant-phase element (CPE), probably due

to the fact that the surfaces had not remained parallel during the test and deviated from an ideal capacitor.

An interesting project was conducted by Grossi et al. (2019), where a low-cost portable EIS measurement system was designed. The authors considered that the combination of scientific hardware and specific software normally required for impedance measurements virtually makes it unable for the method to be used in the field, that is, outside laboratory conditions. This has motivated the development of simpler and portable impedance analysers that attempt to fill that gap. For the teams' project, a 3D-printed structure, and an in-house electronic board for controlling the EIS measurements were designed. The conceived solution demonstrated good accuracy when tested with four distinct saline solutions.

The challenge of selecting equivalent electrical circuit to EIS data was explored by Van Haeverbeke, Stock and De Baets (2021). They purposed an identification algorithm, validated in impedance measurements from biological application. The algorithm was based on gene expression programming and was adjusted to search for the simplest circuit capable to fit a set of EIS data.

A method called localized electrochemical impedance spectroscopy (LEIS) was used in the studies by Dong et al. (2008) and Gong et al. (2019) for evaluating underfilm corrosion in steel samples. This technique utilises a scanning microprobe and is able to measure impedance in a microscopic scale. For example, the water diffusion in a localised coating defect, such as a blister. The results shown that LEIS depends on the defect size, and that the corrosion product creates a diffusion dominated process, which also in influenced by geometric factors.

A LEIS mapping procedure was conducted by the group of Mouanga, Puiggali and Devos (2013), around a defect area in a low carbon steel coated with a *Zn-Ni*-chromate conversion layer. Three-dimensional graphs, measuring the impedance modulus as a function of the x-and-y coordinates, were achieved. LEIS was also

used for the evaluation of pit growth controlling mechanisms, evaluated in iron-chromium alloys (Annergren, Zou and Thierry, 1999).

To evaluate the reproducibility of EIS method, a combined exercise was made between 19 laboratories, where the objective was the characterization, by impedance measurements, of three different systems, among which a dummy cell (an electrical circuit made of real electrical components) was used. The reproducibility results were better for the dummy cell, and relatively more scattered for the other two tested systems. The authors concluded that, despite being an excellent technique for evaluating electrochemical systems, requires careful planning and reproducibility verification. This exercise was referred as a *round-robin* and was published by Ritter et al. (2021).

Mansfeld (1995) explored other parameters obtained in EIS plots, namely the *breakaway frequency*, which is defined as the point in frequency where the phase angle equals 45°. His approach was to have a sensible evaluation criterion for coated samples that could be acquired outside the low frequency range, which requires time for acquiring data. Although useful, it was not precisely determined what quantity was actually related to the read parameter. Nevertheless, the proposed technique presented the benefit of acquire parameters about the coating in short time. Other "alternative" parameters were evaluated by Akbarinezhad et al. (2009) for ranking the performance of coatings, such as the *area under Bode plot*. However, the use of this parameter has yet not being found in many other academic resources.

2.5.3. DISADVANTAGES

Despite being a technique capable to provide a great amount of information about the coating corrosion prevention performance, impedance spectroscopy is a very challenging method. The main disadvantages can be summarized as: (i) its inherent

complexity; (ii) the specific requirements; and (iii) the difficulties in extracting quantitative data through fitting.

As EIS is based on impedance and complex numbers, which are intrinsically challenging, a solid background on mathematics, such as complex numbers, Laplace and Fourier transforms is necessary to understand the fundamentals behind the technique, so the interpretation of the results can be correctly assessed (Lasia, 2014; Macdonald and Johnson, 2005).

Electrochemical impedance measurements also demand special hardware equipment, specific procedures for acquiring data and the use of software that are often proprietary. A frequency response analyser (FRA) is necessary for translating the systems responses into sensible data, creating a build-up plot such as the Bode plot (Cogger, Webb and Wellstead, 1997). The software used for collecting data should have features such as the capability of reading at high and low-frequency regions and current auto-ranging on the measuring resistor, which should be adjusted in the course of the experiment since changes of several orders of magnitude are measured when testing coated samples. Also, a sufficient number of measurements at each frequency should be taken to reduce scattering. All these requisites, as mentioned by Mansfeld (1995), defines the material resource barrier that must be dealt in order to utilize EIS.

Finally, the challenge of circuit analysis and data fitting cannot be overlooked. A point could be made on the fact that circuit fitting present some limitations itself, as in situations where a theoretical system condition cannot be described as a complete equivalent circuit because some components may dominate the measurements, or when circuit elements can be rearranged in different ways, but the measured impedance is the same (Macdonald and Johnson, 2005). But, even a more important consideration resides on the fact that the interpretation of the EIS data additionally requires the presence of someone capable of dealing with all those challenges, in a near case-by-case rate. In summary, the individual would need, among other things,

to have the required knowledge about EIS, to be able to perform the experiments with the required equipment to acquire sensible data, to be able to interpret and select the appropriate equivalent circuit, and to perform a good data fitting. Overall, the resources in time, personnel, and equipment necessary to perform EIS measurements are quite overwhelming.

2.6. MACHINE LEARNING

The intrinsically complexity of electrochemical impedance spectroscopy and the hard obstacle of selecting and fitting equivalent electric circuit models into impedance data has apparently hindered EIS a more spread application of EIS outside academic researches (Bongiorno et al., 2022). However, approaches to increase the efficiency of time-consuming steps, like interpreting the data, and alternatives to the resource input requirements are being proposed. Among then, machine learning techniques present a possibility of efficiency improvement.

2.6.1. FUNDAMENTALS

Machine learning corresponds to a segment of computer science where attempts are made to identify patterns between input and output data, aiming to create a way to predict outputs from new data and make sense of previously unknown inputs. Identification part is refereed as “learning”, which gives name to this field of study. Machine learning (ML) algorithms can deal with a huge amount of data, transforming inputs into a great amount of output knowledge, and it is used for tasks such as image recognition, pattern identification, and strategy optimisation. In short, ML can be used whenever data needs to be interpreted, based on mathematical algorithms (Ghatak, 2017; Schuld, Sinayskiy and Petruccione, 2015).

The term “machine learning” has relations with *deep learning* and *artificial intelligence*. Ghatak (2017) separates their definitions as follows:

- *Artificial intelligence (AI):* a broad term used to encapsulate any method in which computers mimic human intelligence through logic methods;
- *Machine Learning (ML):* a subset of AI that uses statistical techniques to improve the accuracy of functions connecting inputs and outputs. Although it is impossible to find this exact function, the best approximate function is searched through the ML process. In another sense, the ML techniques try to better perform – according to a specific metric – the task of predicting outputs from inputs using the acquired experience in training; and
- *Deep learning*: it is defined as a scalable adaptation of machine learning, which expands the range of estimated functions, using multi-layered neural networks to large amounts of data.

To perform its task of learning, algorithms must be trained using a data set of inputs and outputs, where the relations between these instances are evaluated according to a model, which basically represents the path that is used from assessing the connection between the input and the output. The training results needs to be checked, which is done through cross-validation. The generated errors provide information on the algorithm performance.

Some common tasks that ML could execute are (Ghatak, 2017):

- Estimation of a probability function: for clustering tasks;
- Classification: i.e., to identify in which class a certain input belongs; and
- Regression: used for predicting numeric values.

Schuld, Sinayskiy and Petruccione (2015) divide the learning effort of ML algorithms in three categories. The *supervised* learning is where an inferred mapping is extracted from a dataset of correct input-output relations, in which patterns are recognized and classified. In the *unsupervised learning* type, patterns are scanned with the use of prior examples, creating subgroups (or clusters) that can summarize

an extensive volume of information. Finally, the *reinforcement learning* step is where feedbacks are applied to the predictions made by the algorithm, in order to optimize them.

Several models of machine learning algorithms can be used. A resume of some of these algorithms was presented in the works of Galvão et al. (2020):

- *k-Nearest neighbours*: measures the similarity between data instances to classify them into classes, to then predict if a new data point should be grouped as belonging to one class or another, depending on its features;
- *Decision trees*: data is divided into smaller subsets until patterns are recognized. These different groups are similar to tree branches, connected at nodes that represent decision alternatives. Several sets of branches and nodes can be created, in such a way that the final "leaf" consisted of data that could not be further divided;
- *Classification rules*: based on "if-else" analytical statements to logically evaluate the data. If a rule is suitable for a subset, this is separated from the rest of the data, until no more data remains unclassified. This method is better used for non-numerical data;
- *Artificial neural networks*: inspired by how a human brain works, this method uses nodes (artificial neurons) that can transmit information from one to the other (resembling brain synapses). These neurons are organized as input, output, and intermediary (hidden) layers. In these latter layers, neurons are arranged in a model using activation functions, which basically command the way information is pass from one neuron to the next and which criteria must be used;
- *Support vector machine method*: combines features of the linear regression modelling and the k-nearest neighbour algorithm to generate a surface (hyperplane), separating data according to different characteristics; and

- *Ensemble methods*: allow the combination of different models by varying the data artificially.

2.6.2. APPLICATIONS IN CORROSION STUDIES

Organic corrosion inhibitors performances were studied by various ML techniques, aiming to verify which of these inhibitors are most efficient for aluminium alloys used in aeronautical applications. An extensive range of results from the different ML algorithms was acquired and evaluated. For the created datasets, the random forest algorithm has provided the best accuracy and precision (Galvão et al., 2020).

Parameters obtained by a *Fe*/*Cu* galvanic corrosion sensor for the atmospheric corrosion of steel were used in machine learning algorithms by Pei et al. (2020). Support vector regression, artificial neural network and random forest models were used, but the latter has shown the higher accuracy. Among the tested parameters, relative humidity, temperature, and rainfall were verified as having more impact than the effect of carbon monoxide, nitrogen dioxide, ozone, sulphur dioxide and airborne particles.

The evaluation of an image corrosion classification method was the aim of Sanchez, Aperador and Cerón (2019). The ML method used was support vector machine, and visual features from microscopic surface images were used as input. The results were later compared to electrochemical techniques.

Machine learning techniques were used on electrochemical noise measurements data of localised corrosion processes on steel samples passivated in Na_3PO_4 by Alves et al. (2018) in order to identify corrosive substance and classify different types of localised corrosion mechanisms.

Diao, Yan and Gao (2021) studied the corrosion resistance of low-alloy steel used in marine environment to develop corrosion rate prediction models using ML algorithms. The input parameters were the steel composition and environmental factors, and the

random forest ML model was selected. Other methods were later used to identify the dominating factors on the corrosion rate. The analysis of the predictions shown a good level of accuracy of the corrosion rate, stating the usefulness of machine learning for corrosion evaluation studies.

An artificial neural network algorithm was used for developing a corrosion prediction model for carbon steel in mixtures based on methyl-diethanolamine (MDEA), an aqueous amine solution used for absorbing gases such as CO_2 and H_2S out of natural gas production lines, also contributing for reducing greenhouse gas emissions. Data on multiple parameter conditions and corrosion rates were used to train and test the machine learning model, which architecture is shown in Figure 2.15. The input layer had five input variables – MDEA concentration, total amine concentration, pH, conductivity, and solution type; the hidden layer had eight neurons; and the output layer had one variable, the corrosion rate. The prediction results were evaluated using plots where the experimental values were on the x-axis while the ML predicted values were at the y-axis (Li et al., 2021).

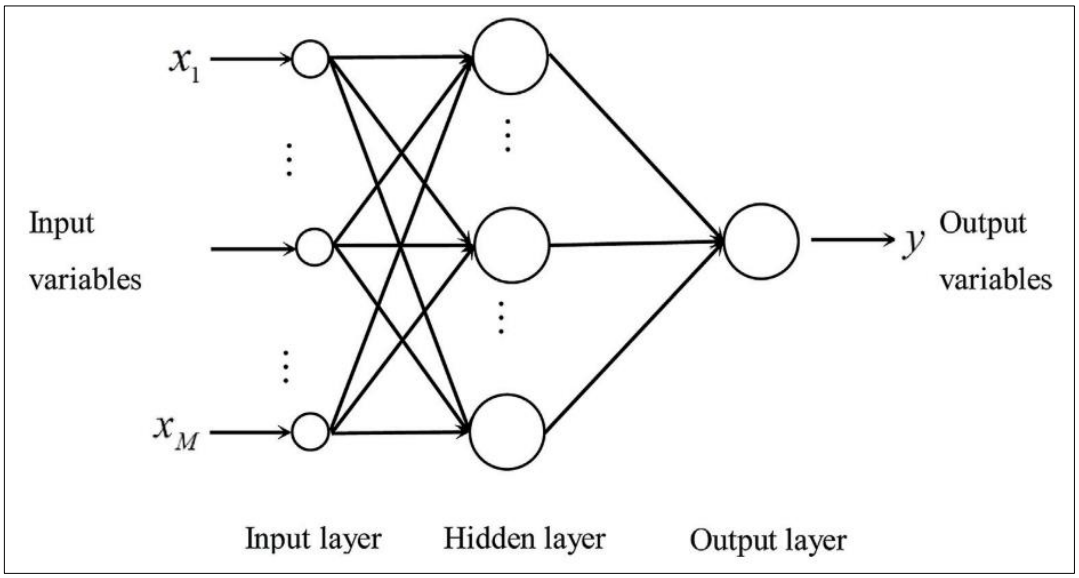

Figure 2.15 – Artificial neural network model used by Li et al. (2021).

Machine learning methods have been also applied in combination with electrochemical impedance spectroscopy. Wang et al. (2020) used EIS and an artificial neural network ML algorithm to study the corrosion on steel buried pipelines under stray current excitation. The machine learning approach was used to measure the effect of the parameters on the impedance data, which were the stray current density, corrosion time and chloride ion concentration. Equivalent circuit modelling fitting showed a dual-capacity reactance characteristic arc. The authors also considered that the selected ML algorithm could be used to evaluate the acquired EIS data, providing a monitoring solution for the problem of stray current corrosion.

Bongiorno et al. (2022) investigated the application of artificial neural network algorithm to the task of EIS data interpretation, which represents a time and resource-consuming task. Two different types of algorithms were developed: one for identifying the suitable equivalent circuit (classification-type) and other to calculate the values of the EEC parameters (regression or fitting-type). Computer generated simulated EIS data was used in order to evaluate the influence of the dataset size on the ML algorithms performance. It was discovered that a dataset with a number of about 200 examples are approximately sufficient for the training of both types of algorithms, stimulating the use of ML approaches for interpretating data from actual EIS experiments.

The goal in the project of Gong et al. (2019) was to generate polarisation curves and electrochemical impedance spectra for pure copper in different chloride ion concentration, using experimental data. The justification for this objective was the consideration that electrochemical measurements are time-consuming, expensive, and generate a relative high amount of waste since several experiments are needed to characterize different environment conditions. A number of machine learning algorithms were tested for this objective, where the random forest algorithm shown the best results.

2.7. IDENTIFIED KNOWLEDGE GAPS

As it was presented in the previous Sections, the use of machine learning for corrosion systems evaluations has been recently acquiring more space on academic production. Several models have been development for different areas of studying, including for electrochemical impedance spectroscopy.

EIS has been broadly used for the evaluation of coating performance, as was presented in Section 2.5.2. Marine coatings are among one of subject of these studies. However, this technique presents some challenges, especially for its complexity, resource-consuming and equipment requirements.

In this sense, research has been developed in order to overcome these disadvantages. One of the approaches is the use of trained machine learning algorithms that could interpret EIS data, whether for classification of fitting purposes.

Therefore, in this project, EIS experiments were performed in order to generate real impedance data to be used for the training and testing of a ML fitting-type algorithm. Also, data from electrochemical impedance measurements from marine coatings tested in accelerated corrosion conditions were used for the testing and training of a ML classification-type algorithm. These two approaches were used to explore the use of machine learning for improving the efficiency of coating performance evaluation.

Finally, an alternative for EIS measurements was tested, in an attempt to create a similar kind of coating performance evaluation solution, based on machine learning, using electrochemical signals that could be acquire from less expensive equipment.

3. MATERIALS AND METHODS

3.1. PROJECT PLAN

3.1.1. INVESTIGATION PATHS: PROOF OF CONCEPTS

The project will investigate the use of machine learning approaches on analysing data from electrochemical impedance spectroscopy experiments through three distinctives paths, as introduced below:

1. By using EIS raw data taken from samples coated with different formulations of anticorrosive epoxy paints (“marine coatings”), subjected to accelerated cyclic corrosion tests over approximately 2.5 years, together with images from visual inspections of the samples in various moments in time. The visualized objective in this case is to verify if a trained machine learning algorithm could perform a classification evaluation of the coatings, based on their impedance spectra and their visual aspect;

2. By performing electrochemical impedance spectroscopy on six samples coated with paints containing different sets of pigments in their composition, and which corrosion prevention performance is consciously distinct among then (“model coatings”). After performing several EIS experiments, the coating parameters were extracted by fitting equivalent electrical circuit on the obtained spectra, in order to create datasets for a machine learning algorithm that would be able to analyse new EIS data and evaluate their performance quantitatively, without the need for a new equivalent electrical circuit fitting step. The parameters calculated by after testing the algorithm were compared with the visual aspect of the samples after the experiments; and

3. By applying methods using different electrochemical signals to the same above-mentioned samples to create new datasets, combining the system responses to these experiments and the parameters obtained from the previous item. The new

trained machine learning algorithm would then, in theory, be able to evaluate the coatings performances without the necessity of the specific hardware and software required for EIS.

3.1.2. PROJECT INPUTS

3.1.2.1. MARINE COATINGS

The electrochemical impedance spectroscopy data from marine coatings was provided by *AkzoNobel*. The coatings were applied on mild steel panels, previously blasted cleaned to the *Sa 2.5* (or Sa *2 ½*) condition according to ISO 8501-2 (2007) to create the adequate surface profile. The method of application of the paints was airless spray. Two coating layers with dry film thickness of 160 *µm* were applied, totalling 320 *µm*.

Four different anticorrosive marine coatings were evaluated in the accelerated cyclic corrosion test, identified below as Coatings *A* to *D*. They vary on the level of solids and the quantity of aluminium flakes in their composition. A brief description of the products is shown in

Table 3.1. A total of twelve coated samples were tested, since three panels were prepared for each coating.

Table 3.1 – Coatings used in the accelerated cyclic corrosion tests (information provided by *AkzoNobel*)

Coating	Type of coating	Level of solids	Al flake content
A	Anticorrosive epoxy-amine primer	Moderate	9 wt.%
B	Anticorrosive epoxy-amine primer	High	9 wt.%
C	Anticorrosive epoxy-amine primer	Moderate	0 wt.%.

D	Anticorrosive epoxy-amine primer	High	3 wt.%

Each panel received a different code, with the last number ranging from 71 to 82, according to the Table 3.2. Figure 3.1 (coating *A*), Figure 3.2 (coating *B*), Figure 3.3 (coating *C*) and Figure 3.4 (coating *D*) show the condition of the panels before the beginning of the accelerated test. In the images, the marked rectangles indicate the areas that were periodically tested by EIS, as further described in the following paragraphs.

Table 3.2 – Coated panels and their respective coatings.

Panel Codes			Coating
TC3778 / 71	*TC3778 / 72*	*TC3778 / 73*	*A*
TC3778 / 74	*TC3778 / 75*	*TC3778 / 76*	*B*
TC3778 / 77	*TC3778 / 78*	*TC3778 / 79*	*C*
TC3778 / 80	*TC3778 / 81*	*TC3778 / 82*	*D*

After the total cure of the paints, the samples were subjected to an experimental accelerated cyclic corrosion test, developed by *AkzoNobel*, simulating the in-service conditions present in ships water ballast tanks. The cycles included cyclic thermal and immersion stress, in such a way that the coating degradation mechanisms were stimulated. Periodically throughout the test the samples were removed and visually assessed for defects. In the occasion of detecting a corrosion induced defect on the surface of the panels, the week number was marked beside it. Also, EIS tests were performed on the panels surface when they were removed for inspection, to evaluate the coatings conditions as the cycles went by.

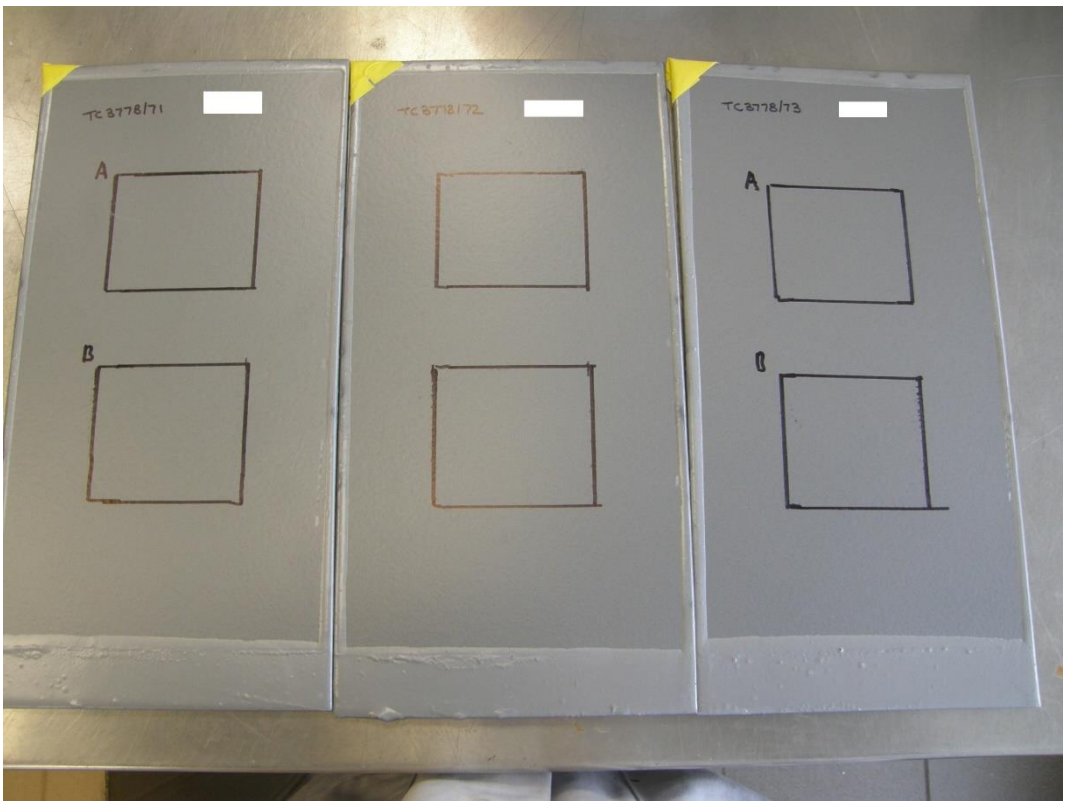

Figure 3.1 – Coated panels for Coating A (credits do *AkzoNobel*).

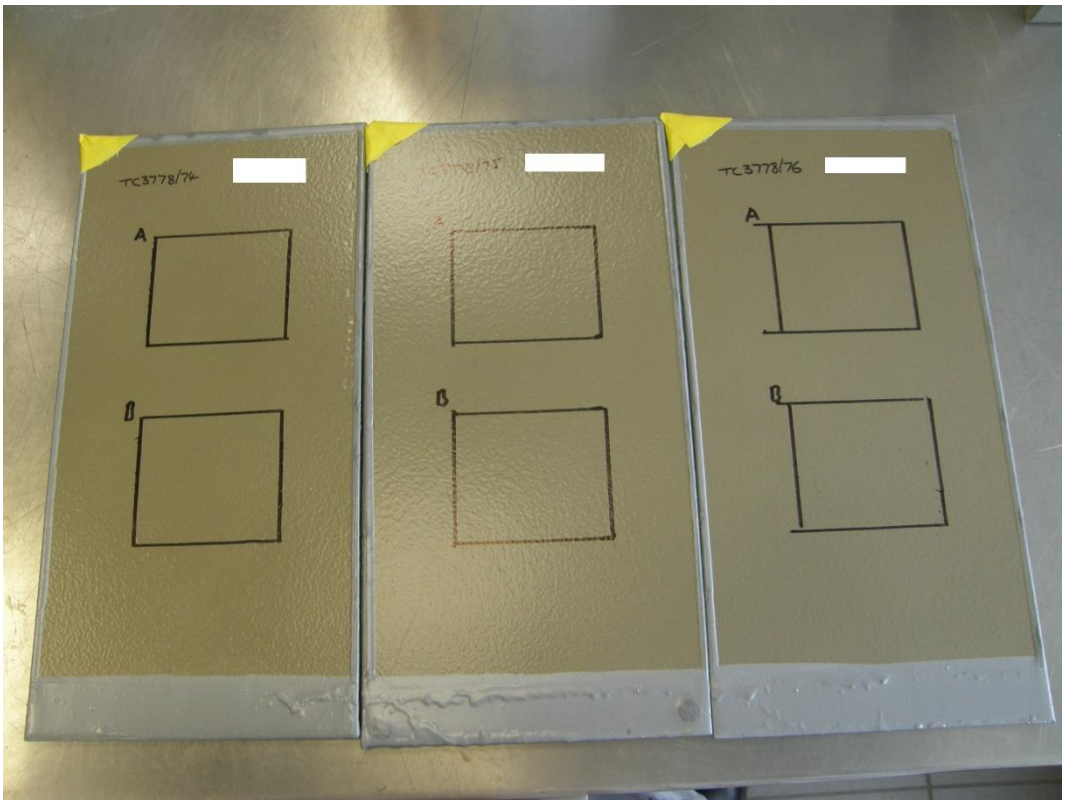

Figure 3.2 – Coated panels for Coating B (credits do *AkzoNobel*).

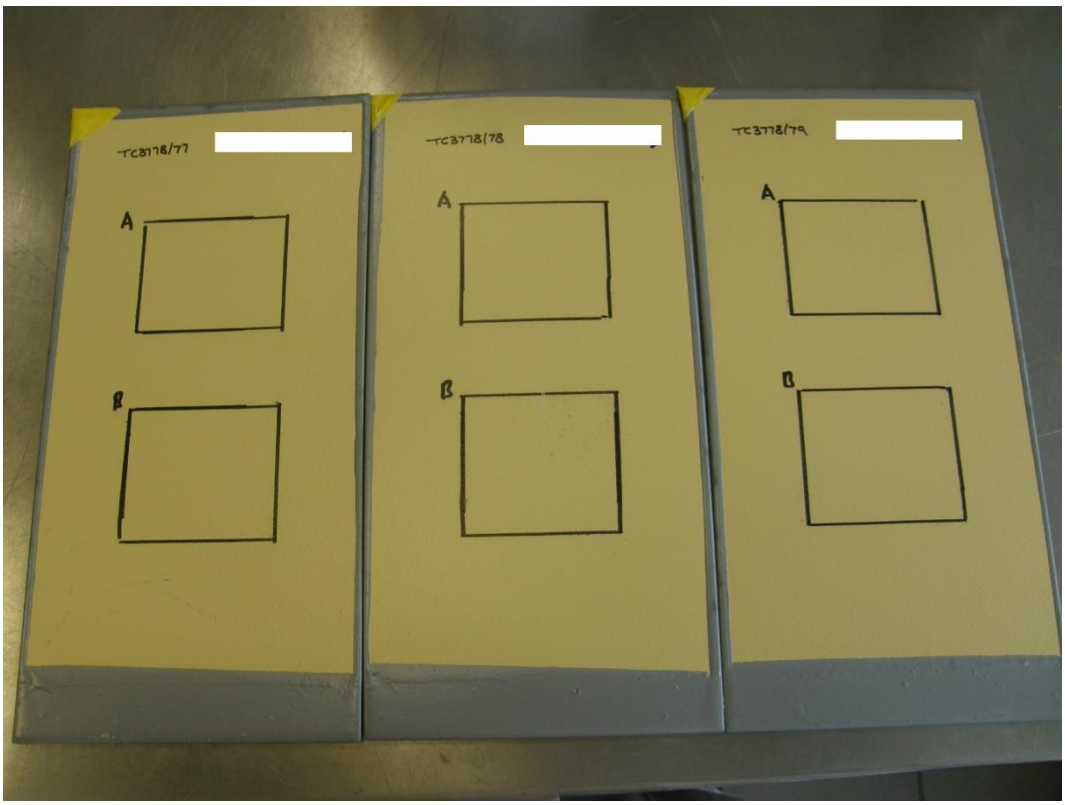

Figure 3.3 – Coated panels for Coating C (credits do *AkzoNobel*).

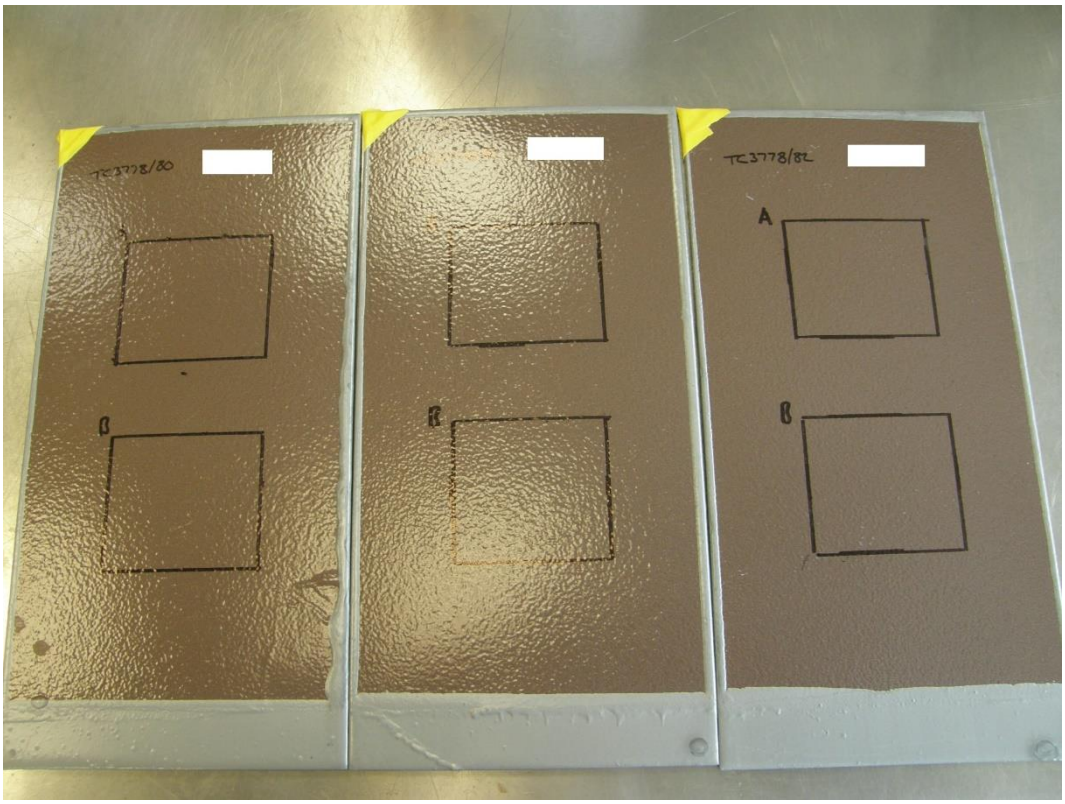

Figure 3.4 – Coated panels for Coating D (credits do *AkzoNobel*).

The electrochemical impedance measurements were performed in two distinct areas of the panel surface, on an area of 8cm×7cm (42cm²). In a few cases, and extra area was tested in the opposite side of the panel, also coated. A two-electrode system was used. A small uncoated area of steel served as the working electrode (WE), located under the small yellow triangular band in the top left corner of the panels, as shown in Figure 3.1 to Figure 3.4. The counter electrode (CE) was a small piece of stainless steel placed inside a sponge probe soaked with an electrolyte of 3.5 wt.% *NaCl* solution. A sinusoidal potential signal with an amplitude of 200 *mV* at the open circuit potential was applied to the system, in the frequency range from 10^4 *Hz* to 1 *Hz*. The tests were made utilizing an *Ivium® Compactstat™* potentiostat.Figure 3.5 shows the schematic arrangement of EIS measurement on the marine coating samples.

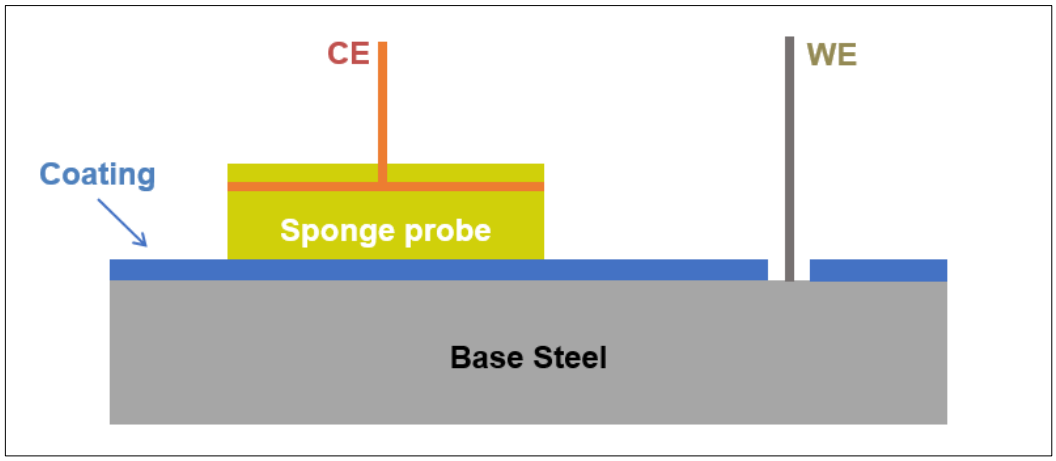

Figure 3.5 – Schematic arrangement of the two-electrode system used for electrochemical impedance measurements on the marine coating samples

The total duration of the accelerated cyclic corrosion test was 145 weeks. However, for four samples, one of each coating, the test was stopped after cycle week 101 (panels 73, 74, 78 and 82). Later, for four other panels, the test was interrupted after week 127 (panels 71 and 72, from coating *A*, and panels 77 and 79, from coating *C*). The remaining panels, from coatings *B* (75 and 76) and *D* (80 and 81) were tested until week 145.

The complete mass of obtained data consisted of nearly 480 log files with the EIS spectra and about 240 photographs showing the conditions of the panels at different moments throughout the test. A spreadsheet containing the values of the impedance modulus for the EIS analysed areas on the samples, per cycle week, was also provided. Credits to *AkzoNobel*.

3.1.2.2. MODEL COATINGS

For the project studies described in items 3.1.1.2 and 3.1.1.3, six coatings with dissimilar sets of pigments were used. In spite of having the same pigment volume concentration (PVC), which was about 30%, the types of pigments in their composition were different, in such a way that their expected corrosion prevention performance could vary. These coatings are henceforth referred as “model coatings”.

Table 3.3 show the sets of pigments that distinguish each of the six model coatings. For facilitate their identification, they shall be referred by as the combination of the main element of their pigments, as seen in the Table. The remaining composition of these paints are similar.

The model coatings were applied on panels of two different types of substrates: cold rolled mild steel and AA2024-T3, an aluminium alloy with copper as the principal alloying element. Before the application of the coatings, the steel panels were degreased with solvents, air dried, and sanded using a P180 grit with a lubricant composed of water and 10 wt.% of alabastine. After, the steel was rinsed with distilled water and dried with a paper towel. On the other hand, the aluminium alloy panels were prepared by wet abrasion, followed by a solvent cleaning step. The model coatings were provided by *AkzoNobel*.

Table 3.3 – Distinctive sets of pigments in each model coating.

Coatings	Characteristic pigments
TiCa	Titanium dioxide; calcium sulphate
TiBaCa	Titanium dioxide; barium sulphate; calcium sulphate
TiBaCaZn	Titanium dioxide; barium sulphate; calcium sulphate; zinc phosphate
TiBa	Titanium dioxide; barium sulphate
TiBaZn	Titanium dioxide; barium sulphate; zinc phosphate
TiZn	Titanium dioxide; zinc phosphate

Smaller samples were prepared from the received panels, so they could be used in the electrochemical cells, which will be described in Section 3.3.1. The steel coated samples had dimensions of approximately 100 × 45 × 0.5 *mm*, while the aluminium alloy coated samples were about 70 × 50 × 0.8 *mm*. Every panel had the information about the thickness of the applied coating. Figure 3.6 shows the general aspect of the model coatings on aluminium alloy and steel before the beginning of the experiments.

Prior to the actual project tests, the experimental design prepared for this part of the study was tested using two model coatings (*TiCa* and *TiZn*) applied on steel. After, the experiment was made using all the samples. Table 3.4 displays the coatings applied on steel, identified by their pigments and thickness. Simarly, Table 3.5 presents the information about the coated aluminium samples.

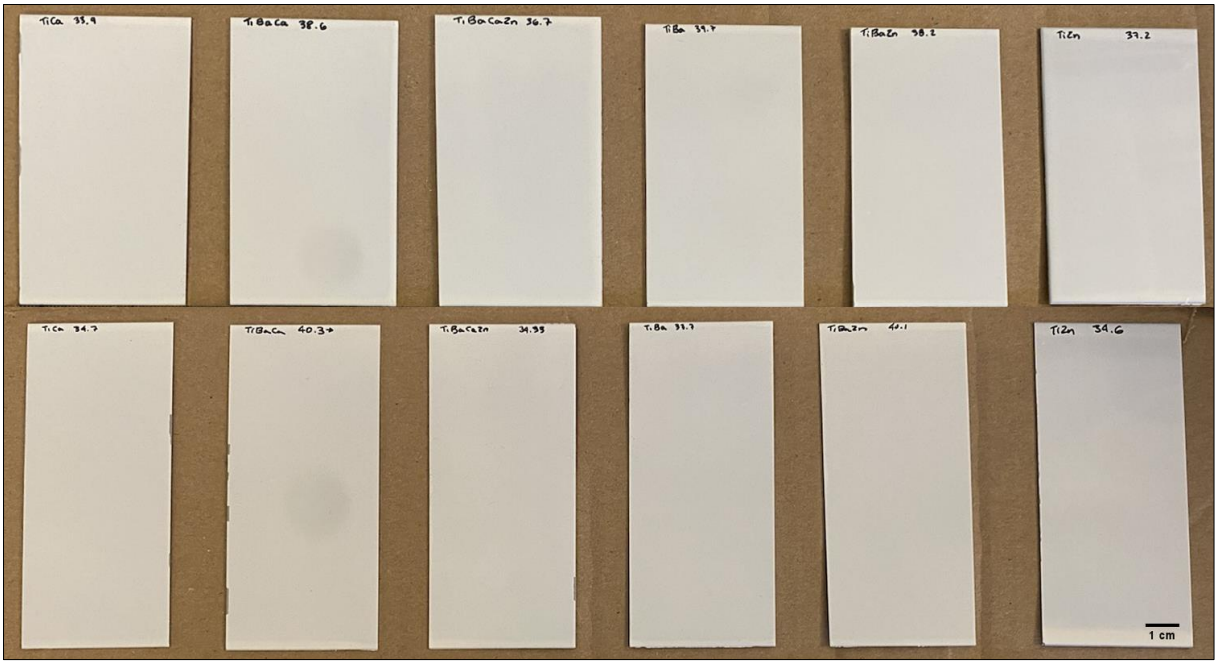

Figure 3.6 – Model coatings on aluminium alloy (on top) and mild steel (below) substrates.

Table 3.4 – Information about model coatings on steel substrate

Coatings	Coating thickness [*μm*]	
	Preparation tests	Experiment
TiCa	34.7	34.7
TiBaCa	–	40.3
TiBaCaZn	–	34.3
TiBa	–	37.7
TiBaZn	–	40.1
TiZn	33.4	33.4

Table 3.5 – Information about model coatings on aluminium alloy substrate

Coatings	Coating thickness [*μm*]
TiCa	38.9
TiBaCa	38.6
TiBaCaZn	36.7
TiBa	39.7
TiBaZn	38.6
TiZn	37.2

3.2. MACHINE LEARNING FOR EIS SPECTRA CLASSIFICATION

3.2.1. DATA CURATION

In order to prepare the data for exploring the possibilities of machine learning approaches, the EIS raw data and image files of the visual aspects of the coated panels were labelled according to the coating, samples, and cycle week. This data curation made it possible to investigate possible correlations between the EIS signals and the physical aspect of the measured areas in specific moments of the accelerated cyclic corrosion test. In this context, some examples of the data provided by the industrial manufacturer (*AkzoNobel*) will be presented in this Section to make the correlation analysis clearer.

From Figure 3.7 to Figure 3.10, the evolution of the maximum values of the impedance modulus are presented. The values were acquired at the lower frequency range of the EIS measurements, throughout the cycle weeks. It is possible to see that the samples from coating *C* have suffered the greater reduction in the impedance modulus values during the test. The plots were made using the software *OriginPro 2020b 9.7.5.184*.

Figure 3.11 to Figure 3.14 show the visual aspect of the marine coated samples after week 101. This particular moment in time was selected since none of the samples were yet removed from the accelerated cyclic corrosion test run. The images show the several marked defects that were developed in different moments, until that stage of the test. The numbers beside the defects indicate in which week they were noticed. As it can be seen, in the cases where defects happened, many of them were outside the EIS testing area (which were the rectangles marked with the letters “A” and “B” on the coatings surface). However, some of them did happen inside the EIS measurement areas, especially in coating *C*. Hence, the EIS spectra related to the presence of defects where analysed and compared to other spectra measured when defects were not present. The condition on the back of the panels is also presented in Figure 3.15 to Figure 3.18. The cases where an extra area was measured by EIS (area “C”) can also be seen.

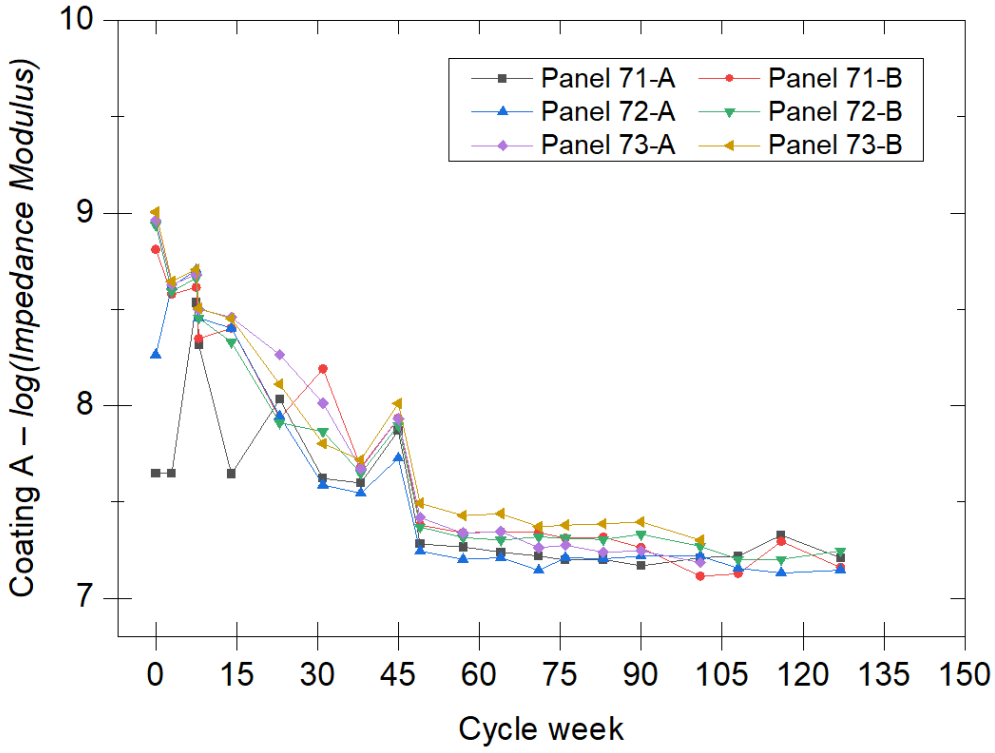

Figure 3.7 – Maximum impedance modulus evolution (coating A).

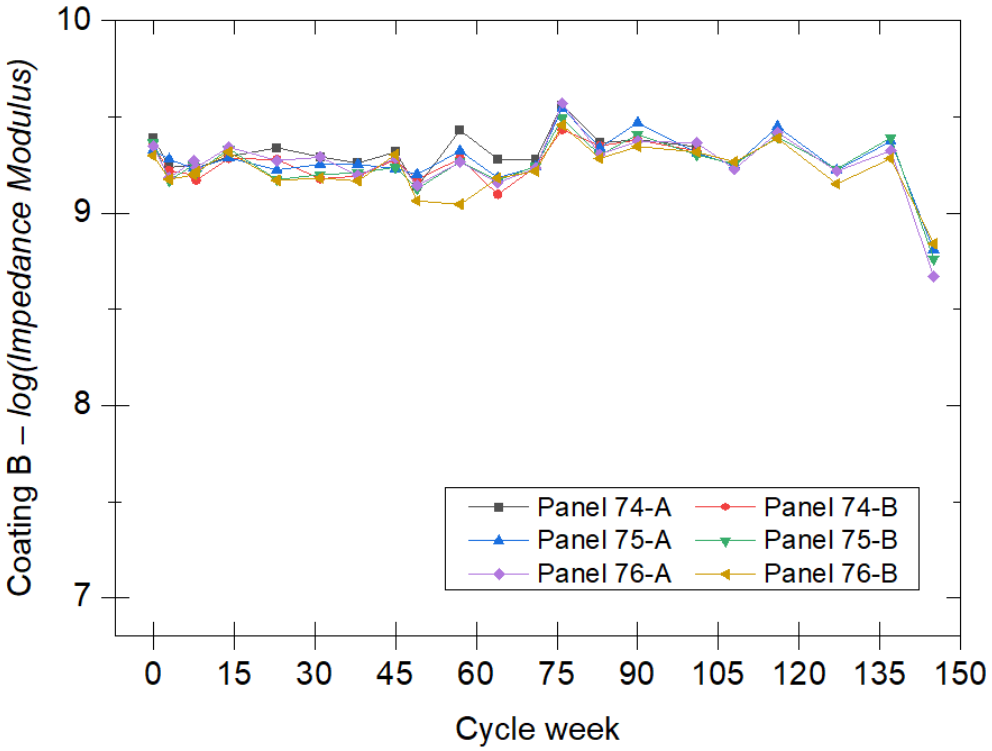

Figure 3.8 – Maximum impedance modulus evolution (coating B).

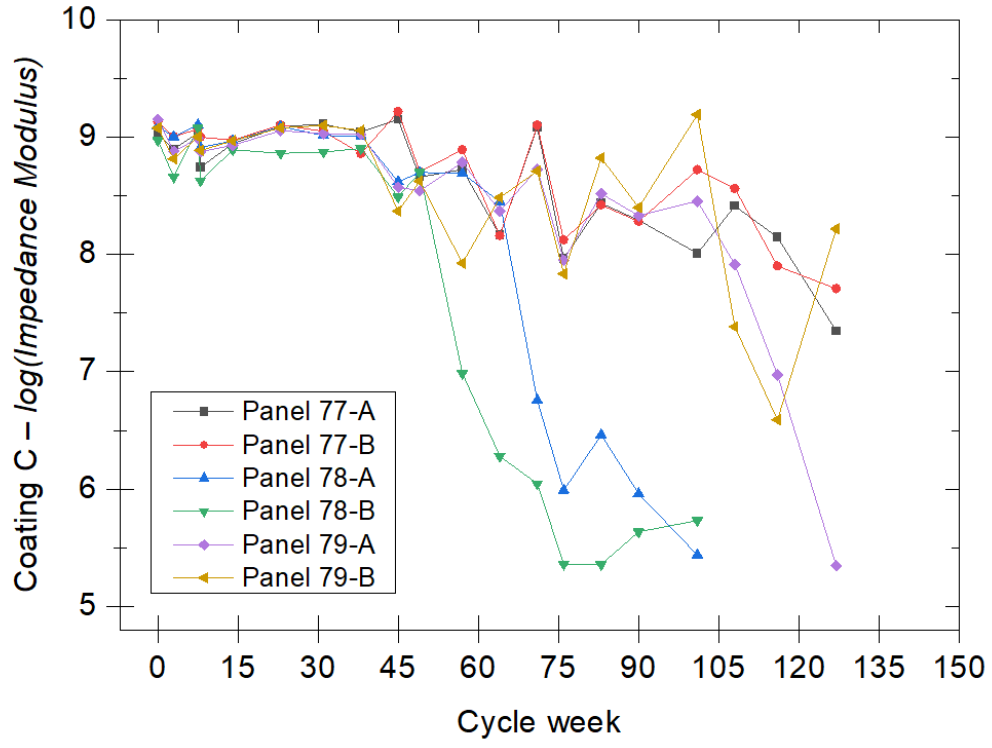

Figure 3.9 – Maximum impedance modulus evolution (coating *C*).

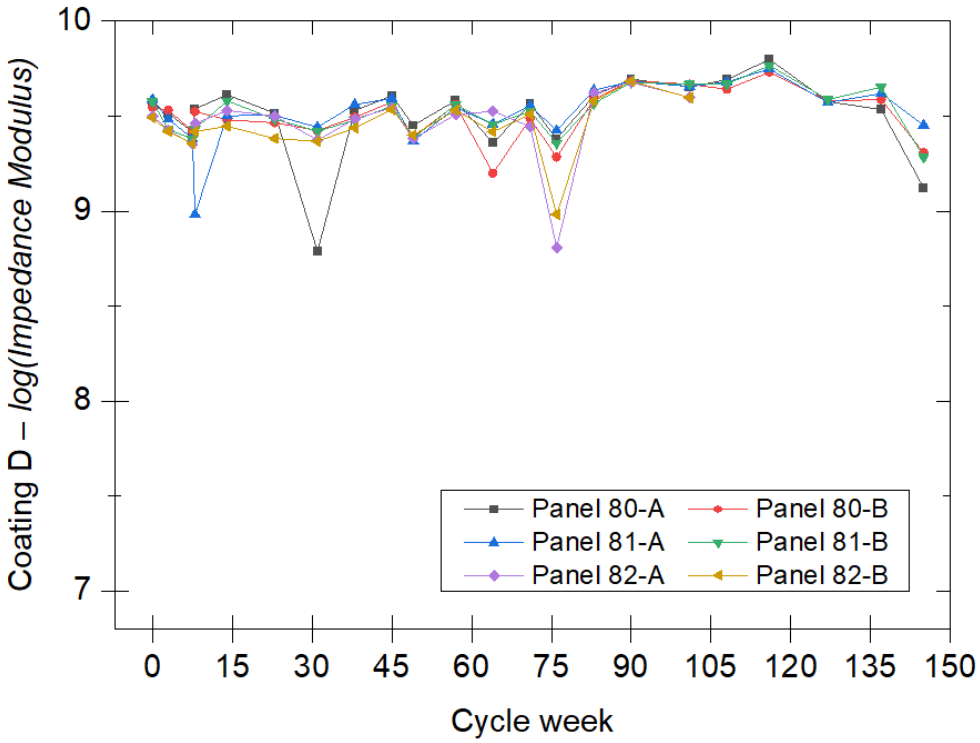

Figure 3.10 – Maximum impedance modulus evolution (coating *D*).

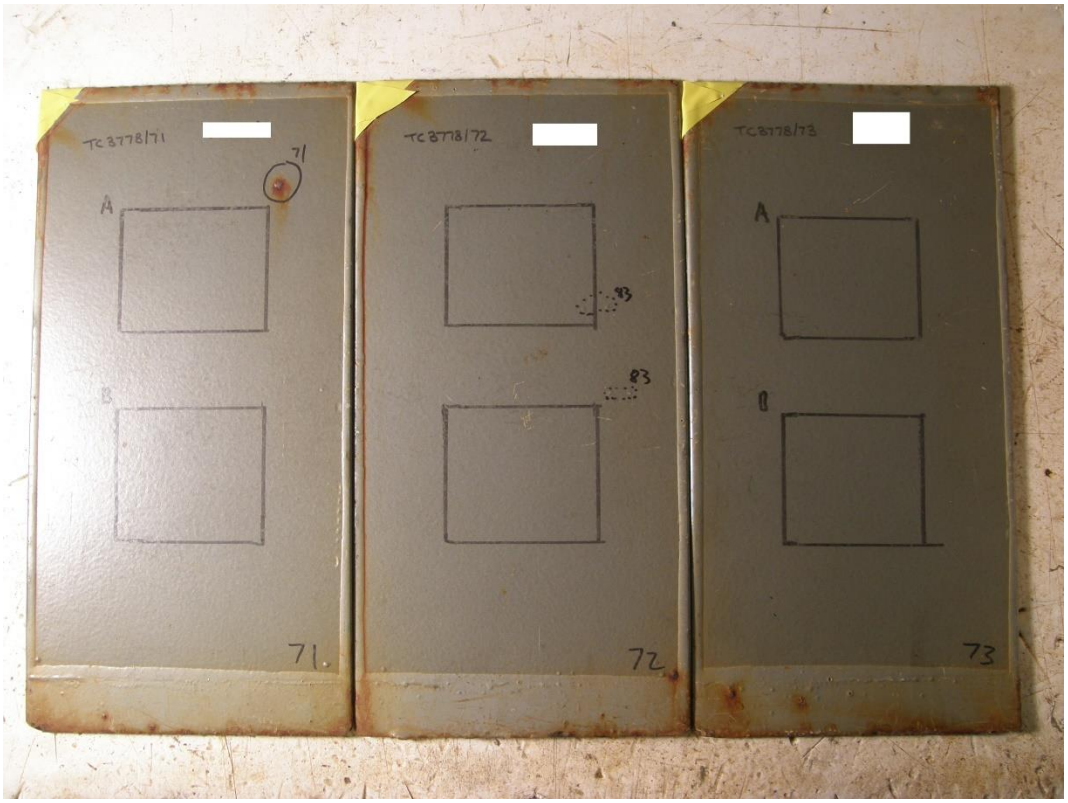

Figure 3.11 – Coating *A* panels at week 101.

Figure 3.12 – Coating *B* panels at week 101.

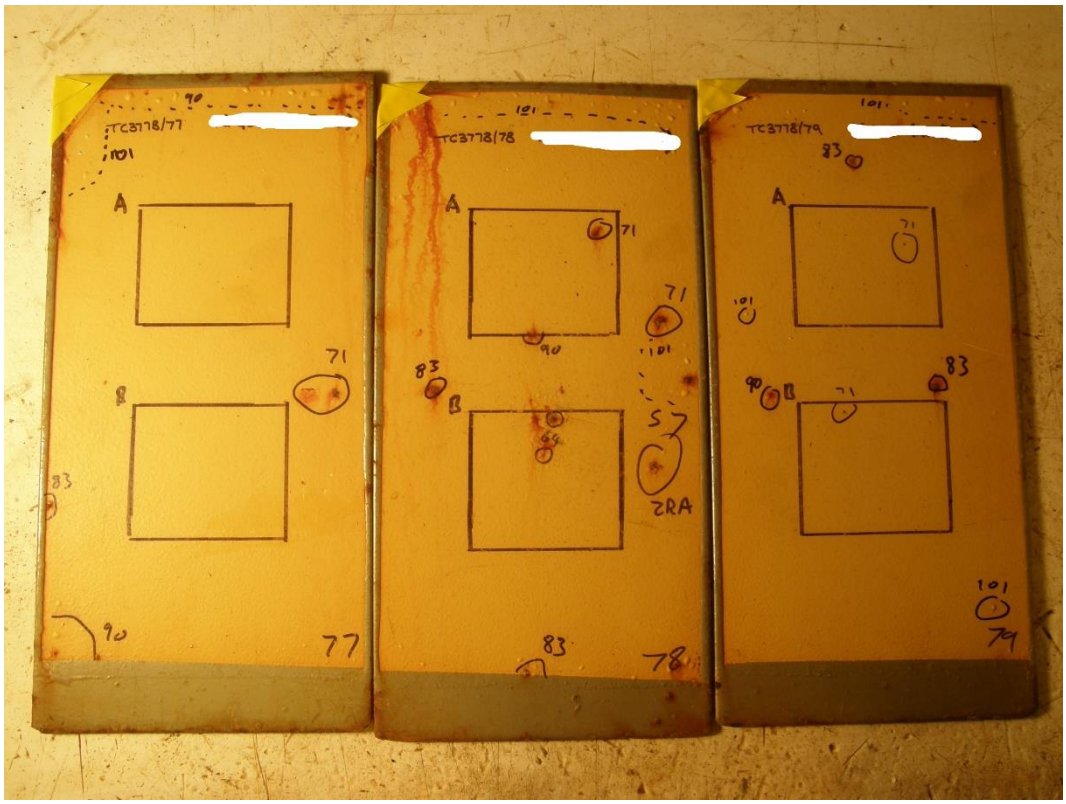

Figure 3.13 – Coating *C* panels at week 101.

Figure 3.14 – Coating *D* panels at week 101.

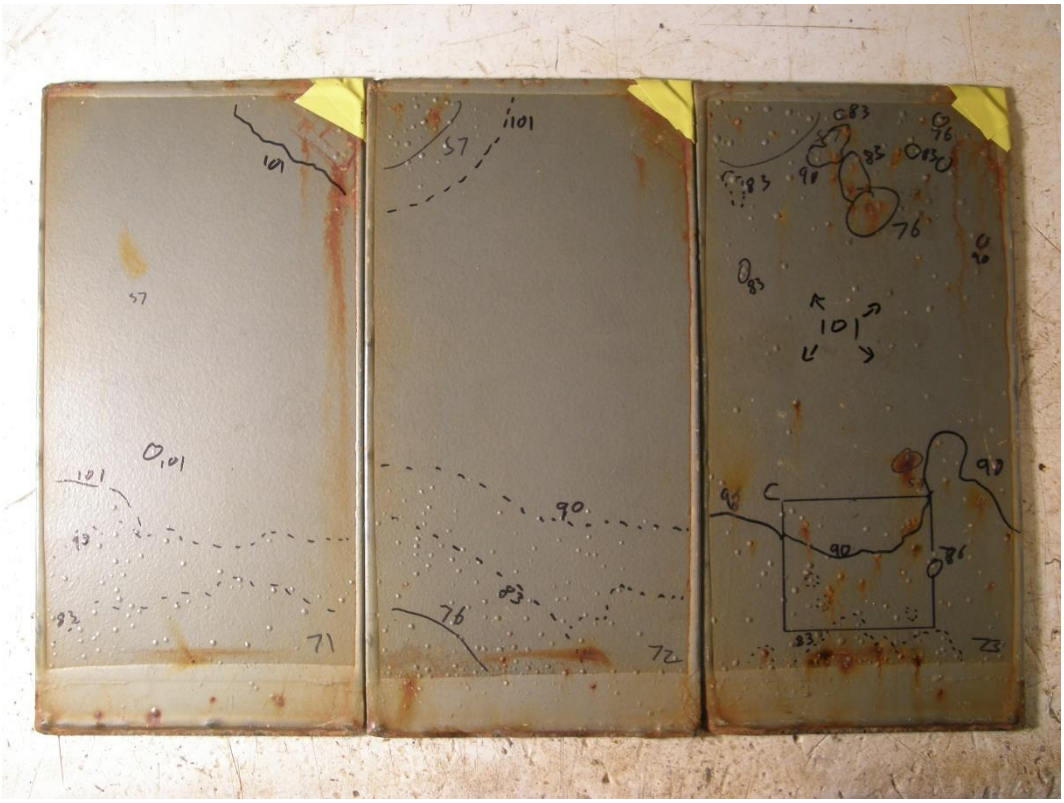

Figure 3.15 – Coating *A* panels at week 101 (opposite side).

Figure 3.16 – Coating *B* panels at week 101 (opposite side).

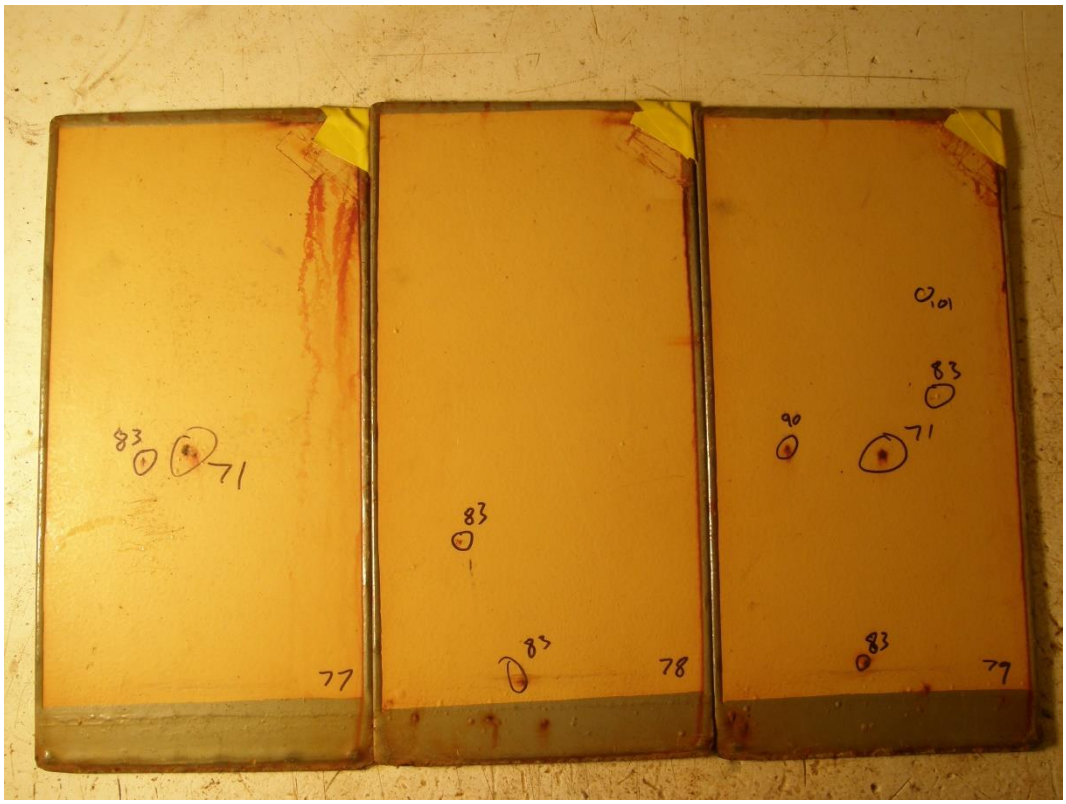

Figure 3.17 – Coating *C* panels at week 101 (opposite side).

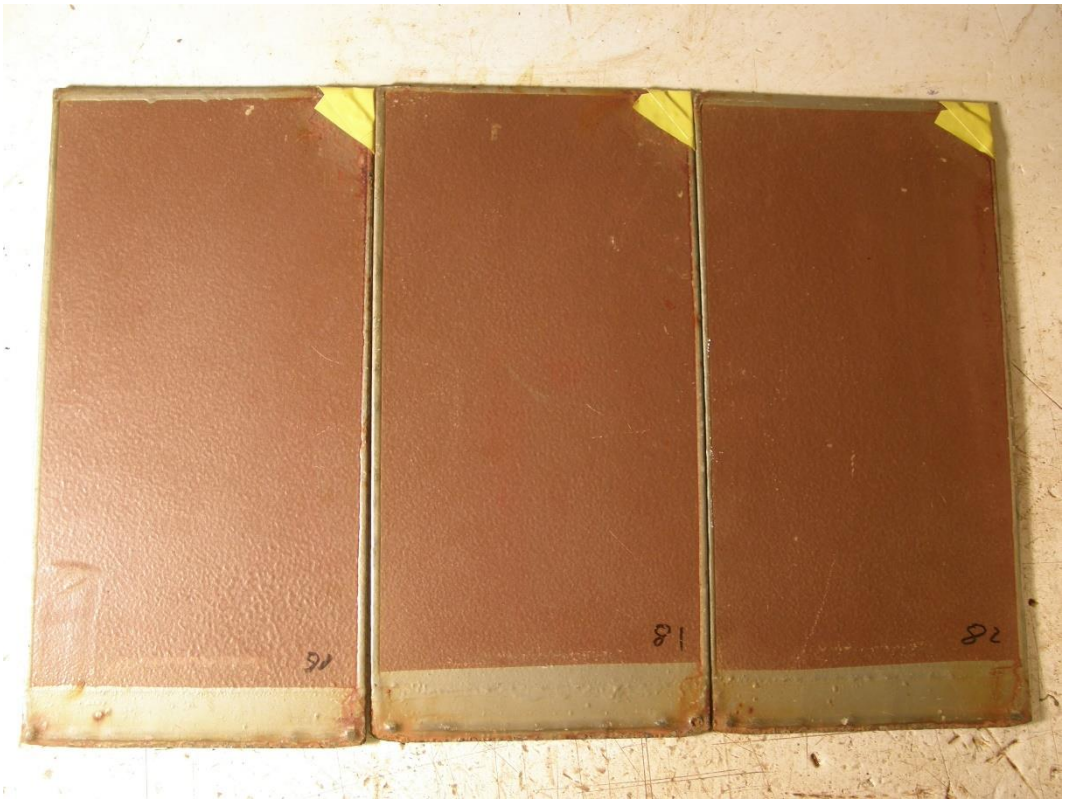

Figure 3.18 – Coating *D* panels at week 101 (opposite side).

After analysing the data provided on the visual aspect of the panels, each marked defect was mapped according to its area and cycle week, which was registered in a spreadsheet that could correlate the week in which a defect was noticed and the respective value of the impedance modulus. By comparing the impedance modulus evolution before and after the emerging of a defect, and also by studying the corresponding EIS spectra, it was possible to detect correlations between the presence of defects on the EIS tested areas and changes in the electrochemical measurements. Figure 3.19 illustrates one example of this correlation, where a drop in the impedance modulus was detected, what could be due to the presence of a defect on the tested area.

This has motivated an approach for pre-processing the data for a machine learning algorithm that could receive values from the EIS measurements made on areas with or without defects. The objective here was to check if this algorithm would be capable

of performing a classification evaluation of the EIS data generated in the accelerated cyclic corrosion tests.

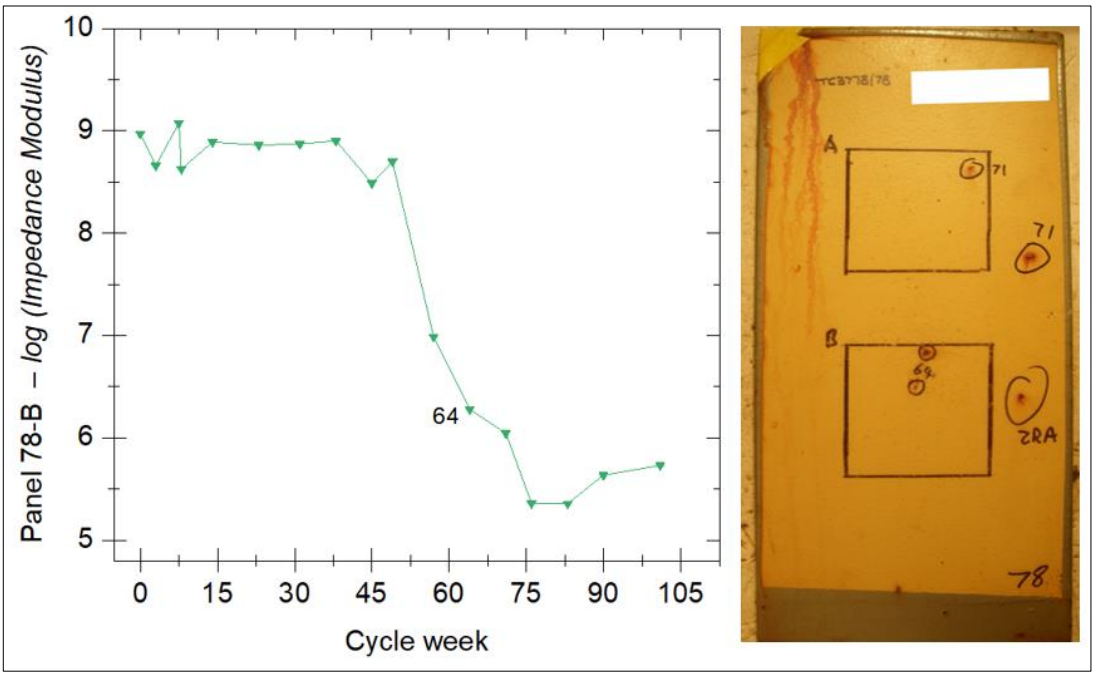

Figure 3.19 – Correlation example between the impedance modulus evolution and the detection of a defect at Panel 78 (Coating C), area “B” (lower rectangle).

3.2.2. PRE-PROCESSING DATA

EIS raw data contained the values for the impedance modulus and for the phase angle shifts obtained at each frequency point during the electrochemical measurement. As indicated in Section 3.1.2.1, EIS was performed in a frequency range from 10^4 *Hz* to 1 *Hz*. There was a total of 81 frequency points for every EIS measurement, each having a corresponding value for impedance modulus and phase angle shift. These values would be later used as input for the machine learning algorithm.

Subsets of electrochemical impedance spectra were divided into two groups: “without defects” (*subset A*) and “with defects” (*subset B*). A screening step had to be made, in order to select representative spectra. As the total number of electrochemical impedance measurements on areas with defects was not high, the total number of

spectra in the subsets was relatively low. For each group, the spectra with the higher and the lower impedance modulus in the low frequency range were selected for equivalent electrical circuit (EEC) fitting. The spectra selection and EEC fitting were made using the *ZView™ 3.5i* software from *Scribner Associates, Inc*.®. Figure 3.20 illustrates the ranges of each subset. Figure 3.21 presents the equivalent electrical circuits that were used for fitting and obtained parameters values for solution resistance, charge transfer resistance and for the constant-phase element instances related to the double layer capacitance.

For the training dataset, the obtained parameters values were used to create simulated EIS spectra for each subset. By using the maximum and minimum values of the parameters, the created simulated spectra remained in the ranges shown in Figure 3.20. The reason for using this approach was to have a larger amount of data for the training phase of the machine learning. The training dataset had 1000 spectra data. Subsequently, the frequencies, the impedance modulus, and the phase shift angles of the simulated spectra for each subset were combined with their corresponding subset identification letter (“A” or “B”) in a comma-separated values file (*csv*).

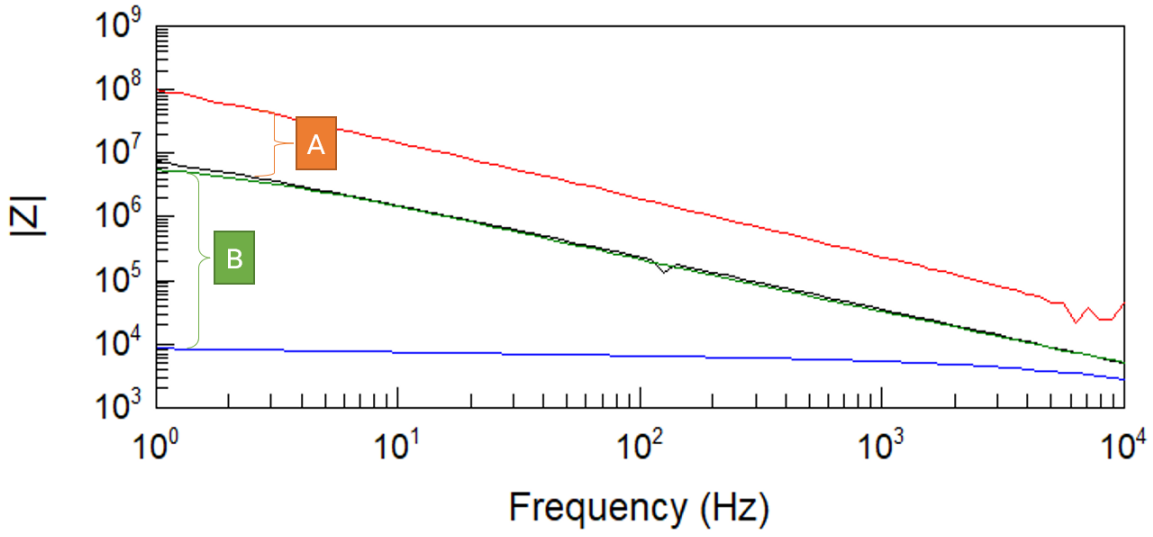

Figure 3.20 – EIS Bode plot for the impedance modulus showing the spectra ranges of the two subsets used for classification: “without defect” (subset *A*) and “with defect” (subset *B*).

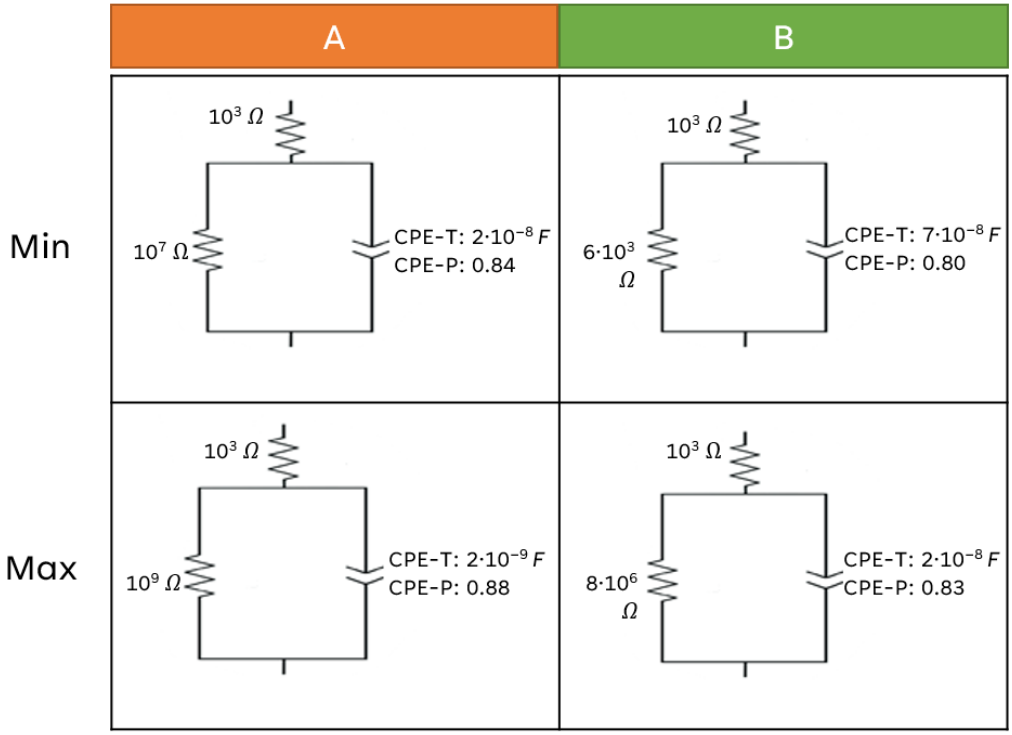

Figure 3.21 – Equivalent electric circuits for fitting and obtained parameter values for the upper and lower spectrum of each subset.

The testing dataset was pre-prepared by using the data of every original spectrum in the subsets, combined with their group identification letter. The total number of instances in the testing dataset were 31.

A final preparation step before uploading the datasets to the machine learning software was made, which consisted of arranging the data of each input instance as arrays, in which all the values of a specific entity (e.g., the frequency) were separated by semicolons (“;”), while the different inputs were separated by commas (“,”), as indicated in Figure 3.22, where the example shown had an output of three dimensions (in order words, three values of “results”). With the software *LabView*™ from *National Instruments*®, an in-house application was developed to prepare the data to the correct format – credits to Bongiorno et al. (2022). After that, the *csv* files were saved in compressed folders, as required by the ML software that was used.

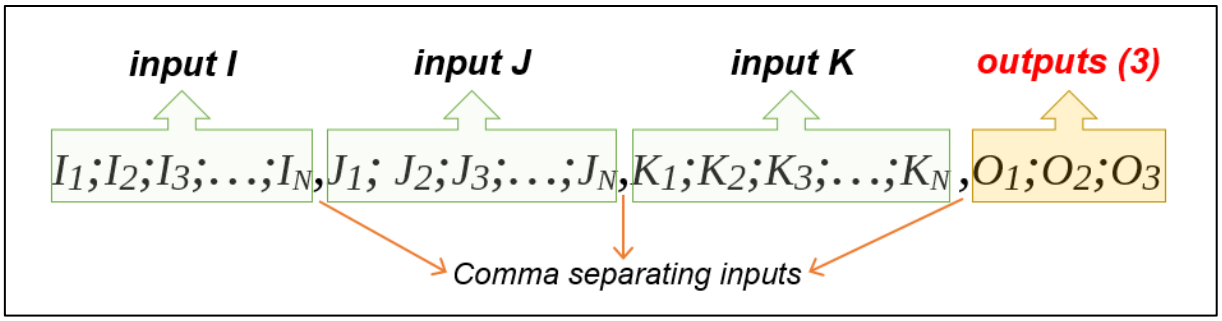

Figure 3.22 – Example of dataset format preparation before uploading to the machine learning software.

3.2.3. MACHINE LEARNING

The software used in the project was the *Deep Learning Studio 1.1.0*, from *DeepCognition*. In this case, the software was running in a *Lenovo Thinkpad X240* (*Intel® Core™ i5,* 8 *GB RAM*).

An artificial neural network (ANN) machine learning model was used, consisting of three sets of alternated dense and dropout layers (Figure 3.23), closed by a final dense layer. The model architecture is credited to Bongiorno et al. (2022). In these sets, the dense layers had different numbers of neurons at each step. The last dense layer had the same dimension of the output array element (in this case, only one).

For training a classification-type ML algorithm, the activation function used in the first three dense layers was the rectified linear unit (*ReLU*), while for the last one, the *Softmax* activation function was applied. For the dropout layers, the dropout fraction used was 0.1. The loss function used binary crossentropy. Additional information about the parameters used in the ML model architecture can be seen in Table 3.6.

The data in the training dataset was divided, so there 80% of the input-output sets where used for actually training the algorithm, and 20% used for the validation step. After the machine learning training and testing, the results were evaluated according to its accuracy, its precision and its classification's recall.

Table 3.7 summarizes the equations used for the evaluation of the ML classification-type algorithm performance.

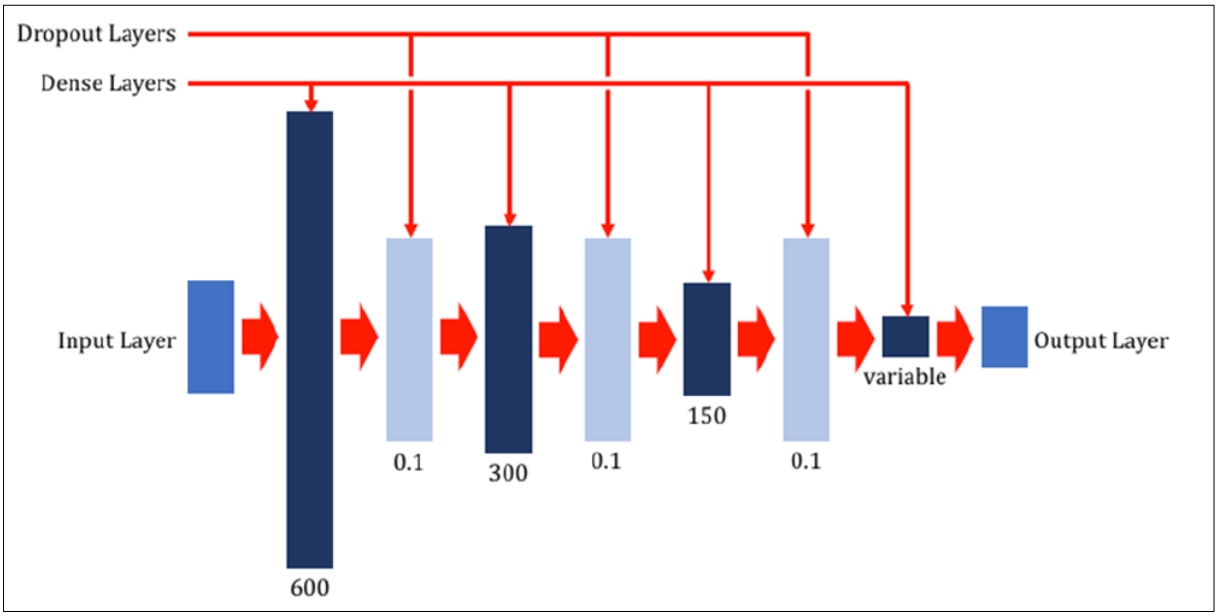

Figure 3.23 – Basic scheme of the machine learning model used for machine learning training. Credits to (Bongiorno et al., 2022).

Table 3.6 – Additional parameters for used for training the classification-type ML algorithm. Credits to Bongiorno et al. (2022).

Epoch number: 1000	*Optimizer:* Adam	*Decay*: 0	β_1: 0.9
Learning rate: 0.001	*Batch size:* 32	ε: 10^{-8}	β_2: 0.999

Table 3.7 – ML classification-type algorithm performance calculations

Accuracy	$= \frac{Numb\ \ of\ \ h\ \ pr\ \ dict}{mb\ \ of\ pr\ \ dict}$	(3.1)
Recall – for class "x"	$= \frac{Numb\ \ of\ co\ \ ct\ pr\ \ dict\ \ fo\ \ "cl\ \ ss\ \ "}{Numb\ \ of\ "cl\ \ ss\ \ "\ \ xamp\ \ in\ \ h\ \ da\ \ set}$	(3.2)
Precision – for class "x"	$= \frac{Numb\ \ co\ \ ct\ pr\ \ dict\ \ fo\ \ "cl\ \ ss\ \ "}{Numb\ \ of\ \ me\ \ "cl\ \ ss\ \ "wa\ \ pr\ \ dict}$	(3.3)

3.3. MACHINE LEARNING FOR EIS QUANTITATIVE ANALYSIS

3.3.1. SAMPLES PREPARATION

Before starting the electrochemical experiments on the model coatings, the samples went through a preparation step. Firstly, the samples edges and their opposite sides were painted with a two-components high-solids epoxy coating (*Interzone 954*™). Then, a mixture of beeswax (CAS registry number 8012-89-3) and Gum rosin (or natural resin; CAS registry number 8050-09-7), in a 3:1 ratio, was prepared, heated, and applied over the edges and faces of the samples, leaving only a squared exposed area of the coating of 3 × 3 *cm* (9 cm^2). This masking procedure on the samples was made so their interaction with the electrolyte remained concentrated on the squared exposed area. Figure 3.24 and Figure 3.25 illustrate the aspect of the samples after this step.

3.3.2. EXPERIMENTAL SETUP

The model coatings samples were tested by electrochemical impedance spectroscopy using a three-electrode cell, as described in Figure 3.26. The electrolyte used was a solution of 5 wt.% *NaCl* solution. The counter-electrodes were small titanium strips, of approximately 1 cm width. The reference electrodes were prepared using the procedure described in the following paragraphs.

Silver wires were immersed in 0.1*M HCl* solution and superficially treated by a galvanostatic method applying a 10 mA/cm^2 fixed current for 4 minutes, resulting in a superficial thin layer of *AgCl*. This treatment was carried with using a *Solatron Analytical® ModuLabXM*™ potentiostat. Afterwards, the treated wires were placed in small plastic tubes (made from new plastic pipettes with their upper extremity removed) filled with 5 wt.% *NaCl* solution, where they remained in equilibrium with the surrounding solution.

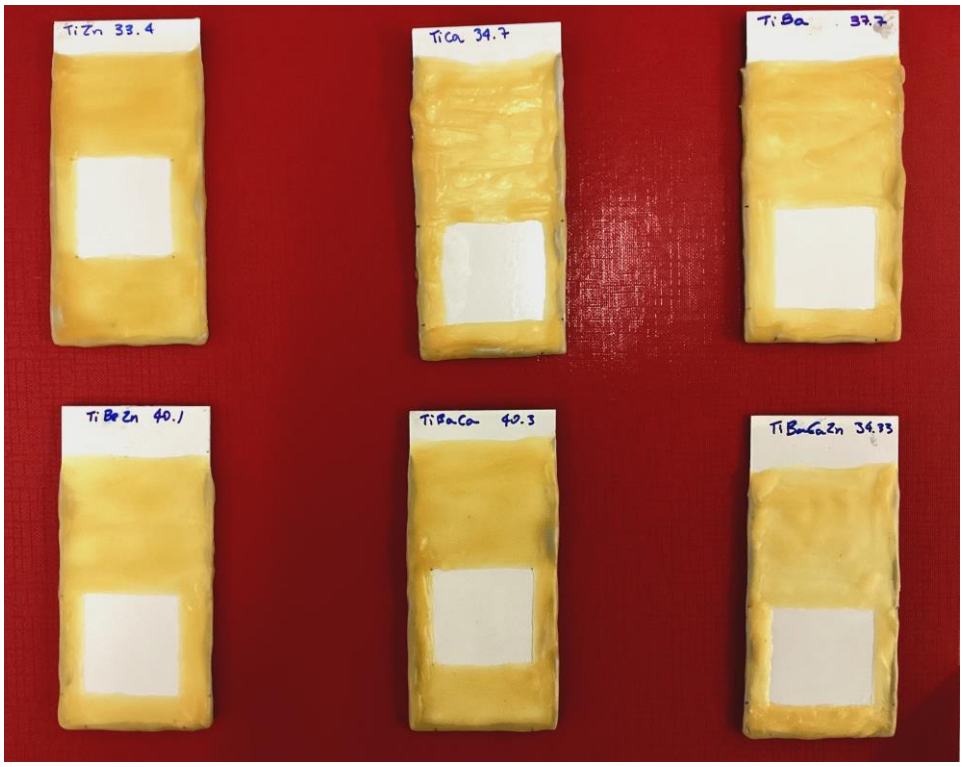

Figure 3.24 – Steel model coating panels after sample preparation.

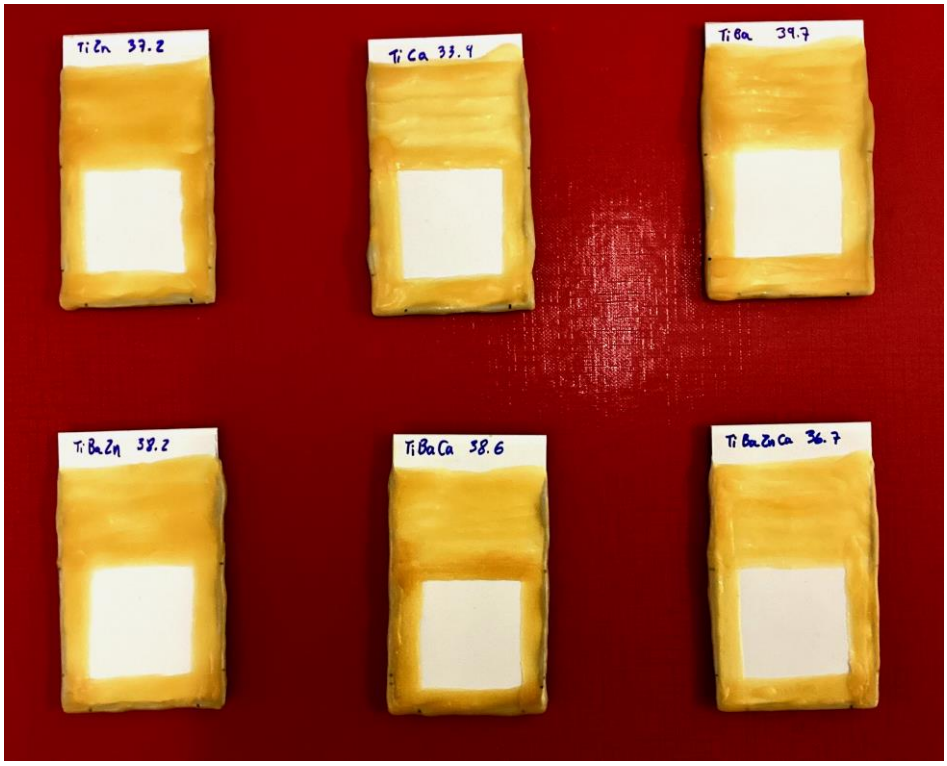

Figure 3.25 – Aluminium alloy model coating panels after sample preparation.

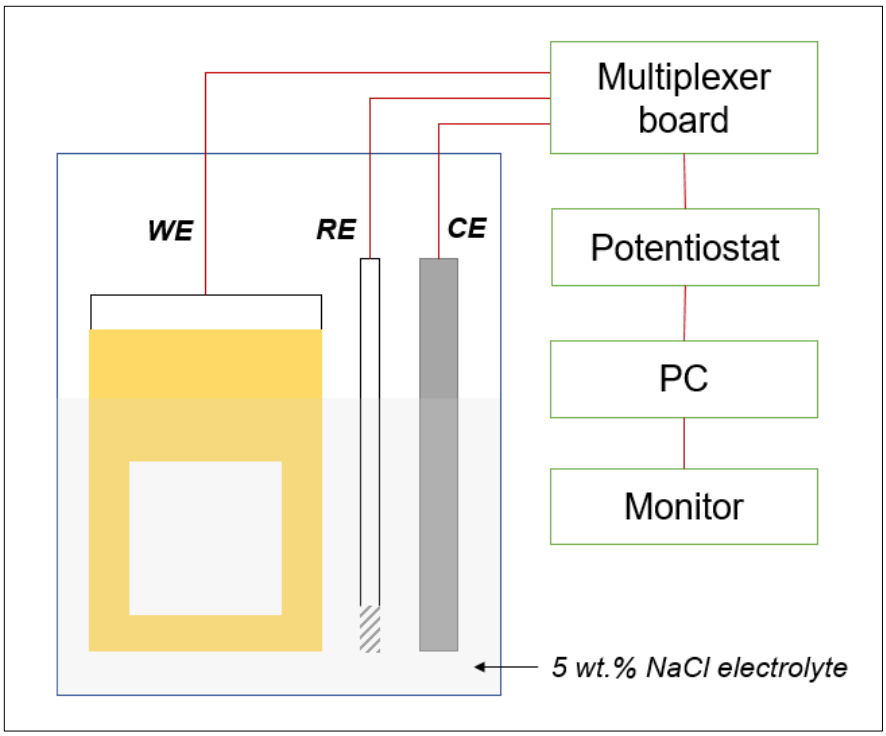

Figure 3.26 – Schematic representation of the three-electrode cell used in the electrochemical experiments showing the working electrode (WE), reference electrode (RE), and counter electrode (CE).

For the salt bridge of the reference electrodes, a solution containing 5 wt.% *NaCl* and 4 wt.% of *Agar* (CAS registry number 9002-18-0) was prepared, with the aid of a heater and stirrer. Once the mixture was ready, the lower extremity of the pipette was immersed in it, in such a way that the solution went inside. After cooling, the Agar solidified inside the tube, creating the salt bridge. At the upper part of each reference electrode, the silver wire was connected to an electric cable, and the tube was sealed using beeswax, as shown in Figure 3.27.

Figure 3.28 shows one of the actual three-electrode electrochemical cell, where the sample (working electrode), the counter electrode and the reference electrode are placed in a plastic bag and supported with a sample holder. Rubber bands were also used to secure the plastic bag on the holder. The electrolyte was later inserted in the cell with the aid of a syringe.

Two *LattePanda* computers (*4G RAM, 64G eMMC* specifications) were used for the experiments. A *Ivium*® *Compactstat*™ and a *Ivium*® *Vertex*™ potentiostats were used for the aluminium alloys and steel samples, respectively. The electrochemical experiments were controlled using the *IviumSoft*™ by *Ivium Technologies*®. Also, the EIS methods were prepared using this software.

The EIS test varied from 10^5 *Hz* to 10^{-2} *Hz*, with a sinusoidal input of 100 *mV versus* the open circuit potential, which was monitored for 30 seconds, with an interval of 1 second. Ten points were acquired per each decade, and the total number of frequency points in each measurement was 71. The acquisition period was 1.5 second.

Figure 3.27 – Reference electrode prepared for the electrochemical experiments.

For the purpose of acquiring enough data for a satisfactory machine learning algorithm training, the experimental setup used two 10-channels multiplexer electronic board (Figure 3.29), connected between the electrochemical cells and the potentiostat, to control the sequence of experiments. The benefits of its use were many – for example, it was not necessary to manually load each electrochemical

method for every cell and start each experiment one by one. On the contrary, once the cells were correctly connected to the board channels, and the test methods were properly loaded into the potentiostat software, the experiments were performed on the samples one after the other. For controlling the sequence in which the board channels were activated, and the electrochemical measurement methods that were performed, another in-house application, elaborated on *LabView*™, was created. The credits for the board's design and for the *LabView*™ programme are from Bongiorno et al. (2022).

The channels of the multiplexer boards were previously tested by using a "*dummy" cell* in which electrical components were arranged as two different circuits similar to the expected conditions of the EIS experiments on the coatings. By analysing the acquired data, it was possible to verify which channels were not working properly. Figure 3.30 shows the electrical circuits used with the "dummy" cells for testing the channels on the multiplexer board.

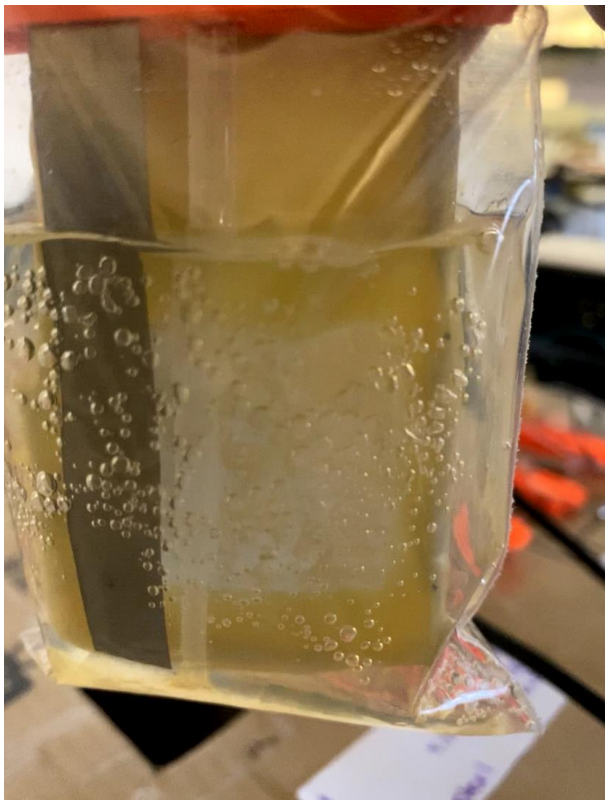

Figure 3.28 – Detail of one electrode cell (*TiCa* model coating on steel).

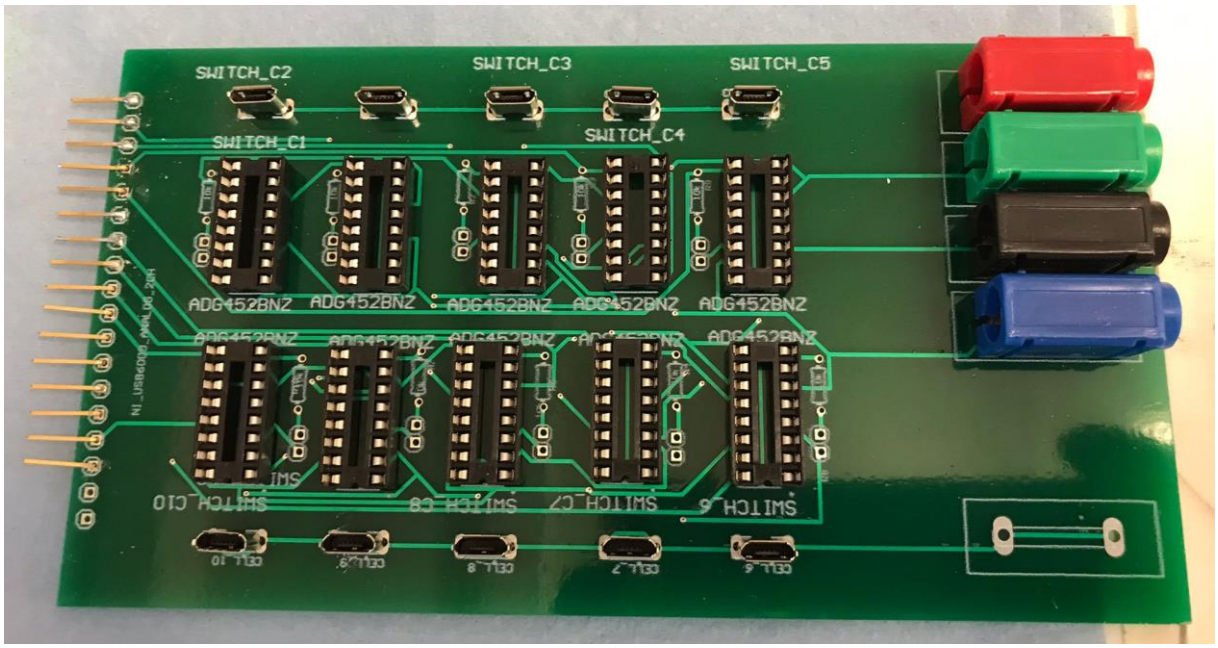

Figure 3.29 – Multiplexer board

The electrochemical impedance spectroscopy experiments were performed in two different runs for approximately two weeks each, in the days when the laboratory was accessible. In each day of measurement, two EIS tests were executed, one before and one after the electrochemical methods presented in Section 3.4. Previously, the methods were tested in a shorter run, with only two steel coated samples.

Electrochemical experiments, with all methods, were performed in the model coatings. The time points (i.e., the number of hours between the experiment and the initial immersion of the model coating samples in the electrolyte) are indicated in . Table 3.8.

After the conclusion of the experiments, the samples were removed from the electrochemical cells, slightly cleaned with deionized water for removing any excess of electrolyte, and then photographed. Subsequently, a non-caustic dichloromethane-free gel paint stripper (*Rustings® Strypit™*) was used to remove the model coating and expose the condition of the underlying substrate, which were also photographed.

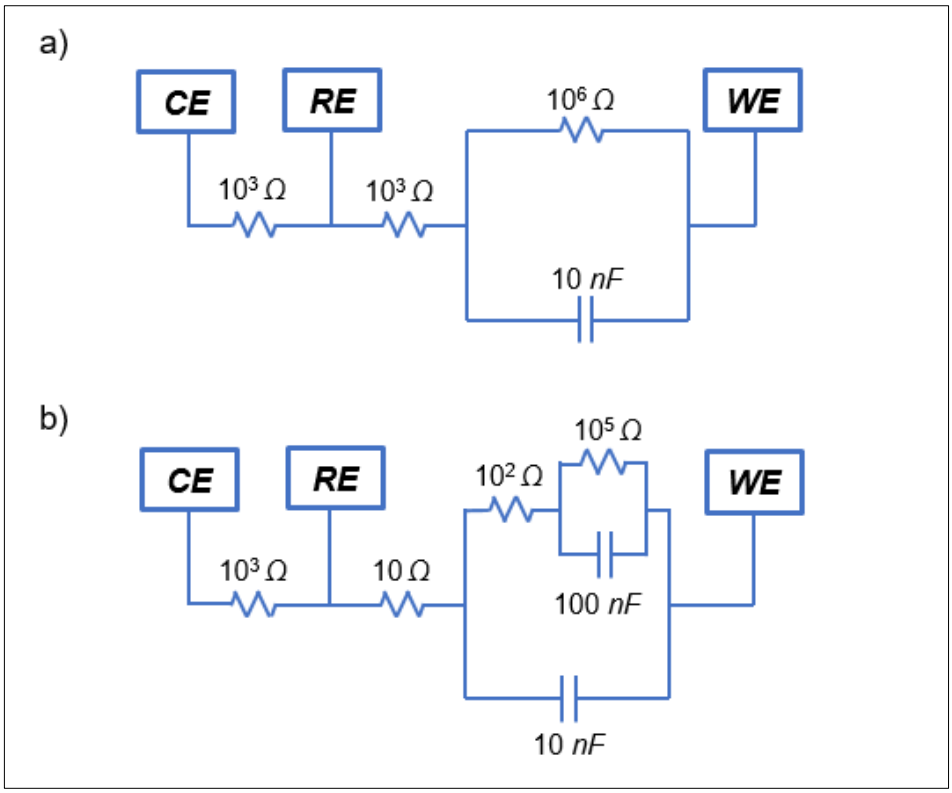

Figure 3.30 – Circuits used in the dummy cells for testing the multiplexer board: (a) circuit with one time constant, and (b) circuit with two time constants.

Table 3.8 – Time points for the electrochemical tests.

0h	120h
2h	144h
24h	168h
48h	192h
72h	312h
96h	336h

3.3.3. DATA TREATMENT

The obtained electrochemical impedance spectra were analysed and selected for the equivalent electrical circuit fitting step. Measurements that were unusable due to some disarrangement during the test were not used for the datasets. The equivalent

circuits were fitted to the remaining EIS data, using the software *ZView™ 3.5i* software from *Scribner Associates, Inc*.®. It was possible to see that some spectra shown the aspect of an equivalent electric circuit with two time constants, while the rest had the one time constant characteristic aspect. Therefore, two EEC models (Figure 3.31) were used for fitting the EIS spectra. In the image, *Rs, R1, R2* are the resistive parameters, while *CPE1* and *CPE2* constant phase elements represent the capacitive parameters.

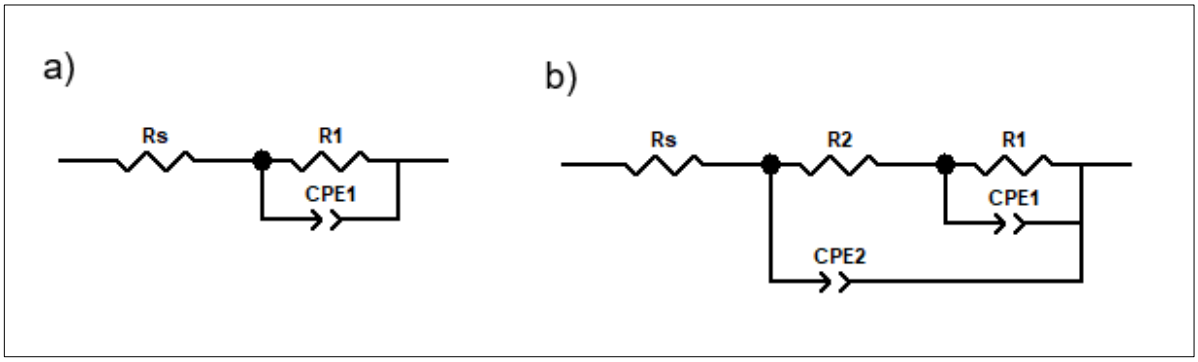

Figure 3.31 – Two equivalent electric circuits used for fitting the EIS spectra: (a) EEC with one time constant, and (b) EEC with two time constants.

Once the parameters for each spectrum were obtained, they were ready to be combined to the data from the electrochemical measurements to prepare the datasets for machine learning. However, as some EIS spectra had a total of three fitted parameters, while the others had five (as it can be seen in Figure 3.31), two separated datasets would then have to be made, since their output array dimensions would be different, preventing the use of the whole data for the same model (considering the software being used for this project). In order to avoid this, the values from the resistive and capacitive elements were combined into two parameters – total resistance and total capacitance. In this way, the whole amount of data could be used, once the output array dimension was now equal to 2.

Initially, two distinctive datasets were created, one for each substrate, using the data acquired in the tests with the model coatings.

The *LabView™* in-house programme cited in Section 3.2.2 was used to prepare the data to the correct format – credited to Bongiorno et al. (2022). After that, the *csv* files were saved in compressed folders.

3.3.4. MACHINE LEARNING

The software used in the project was also the *Deep Learning Studio™ 1.1.0*, from *DeepCognition®*, in this case installed on a *Lenovo ideapad 320-15IKB* (*Intel® Core™ i7-7500U CPU,* 2.70 *GHz,* 8 *GB RAM*).

An artificial neural network (ANN) machine learning model was also used, consisting of three sets of alternated dense and dropout layers, closed by a final dense layer, as proposed by Bongiorno et al. (2022). However, the purpose in this case was to train a ML fitting algorithm. Therefore, its model is slightly different from the one prepared for the ML classification-type algorithm. The linear activation functions were applied for all the dense layers for this model, while the loss function chose was the mean squared error. The other model parameters are similar from Section 3.2.3. The machine learning model separated the amount of data for training, validation and testing as 60%, 20% and 20%, respectively.

After the ML training, the predicted values were compared to the original values obtained via fitting. Also, the performance of the fitting-type algorithm was assessed by calculating the mean squared error and the average percent error for each parameter, as described in Table 3.9.

3.4. MACHINE LEARNING USING DATA FROM OTHER METHODS

3.4.1. EXPERIMENTAL SETUP

The same three-electrode electrochemical cells that were used for the EIS measurements were also tested using different electrochemical signals, as introduced in item 3 from Section 3.1.1. In summary, they consisted of one of the six

model coatings as the working electrode, the titanium strip as the counter electrode, the manufactured *Ag/AgCl* reference electrode (described in the Section 3.3.2), immersed in the 5 wt.% *NaCl* solution. As there were six coated samples for each of the two substrates, a total of 12 electrochemical cells were tested.

Table 3.9 – ML fitting-type algorithm performance evaluation measurements

Mean squared error, for "*x*"	$MSE = \frac{\sum_{=1}(\quad - \quad)^2}{}$	(3.4)
Average percent error, for *"x"*	$AE = \frac{\sqrt{MSE}}{AV}$	(3.5)

Note: AV corresponds to the average value (for "x")

The methods for the different electrochemical signals were prepared using the software *IviumSoft*™ by *Ivium Technologies*®. For the purpose of facilitating their identification, these signals will henceforward be denominated as "sweeps" and "pulse" signals.

The "sweep" electrochemical methods were based on the standard cyclic voltammetry measurement option, available in *IviumSoft*™ software. They basically consisted of a cyclic linear fluctuation of the potential, above and below OCP. Three amplitude ranges were tested, in separated methods: a higher range, from –1.00 *V* to +1.00 *V*; a medium one, from –0.20 *V* to +0.20 *V*; and, lastly a lower sweep, from –0.05 *V* to +0.05 *V*. The use of different scan rates was also investigated — thus, for each amplitude range, two methods were prepared, one with a higher scan rate and another one with a lower one. In total, six "sweep" methods were used, as described in Table 3.10. Each "sweep" method had three cycles of potential variation. In those methods, the open circuit potential was monitored for 10 seconds, with a 1 second interval. The equilibration time used was 15 seconds, with an interval time of half a

second. A schematic representation of the different “sweeps” is presented in Figure 3.32, where the potential increment (*ΔE*) range of each method can be perceived.

Table 3.10 – Sweep electrochemical methods

Sweep method	Potential amplitude	Scan rate
“High-Fast”	± 1.00 *V*	100 *mV/s*
“High-Slow”	± 1.00 *V*	10 *mV/s*
“Medium-Fast”	± 0.20 *V*	50 *mV/s*
“Medium-Slow”	± 0.20 *V*	5 *mV/s*
“Small-Fast”	± 0.05 *V*	5 *mV/s*
“Small-Slow”	± 0.05 *V*	0.5 *mV/s*

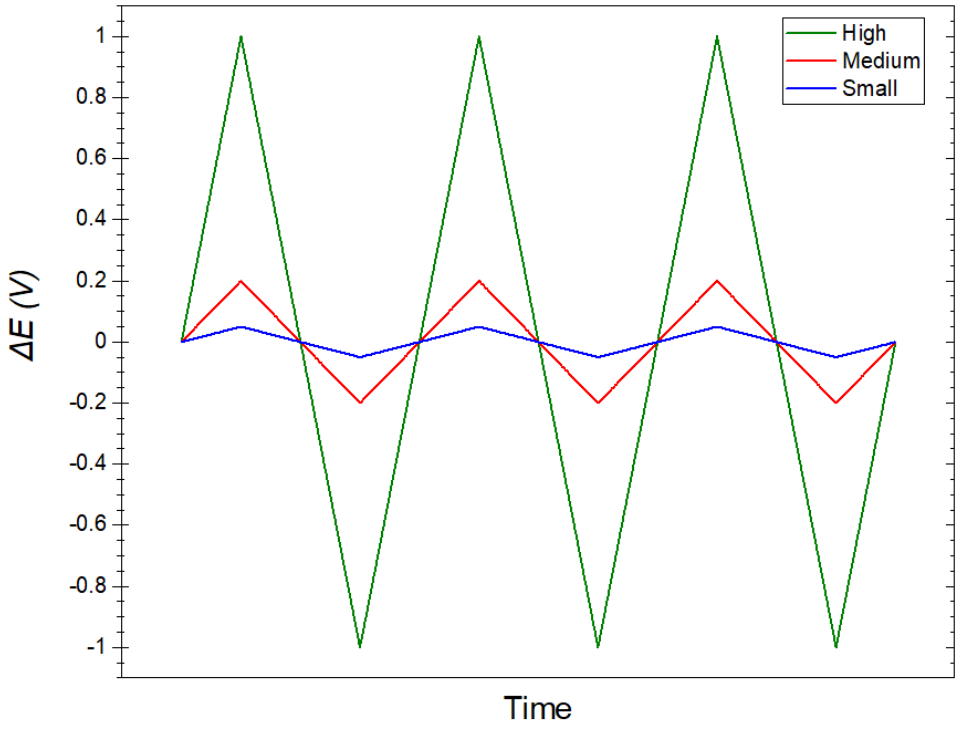

Figure 3.32 – Schematic representation of the potential “sweep” methods.

The “pulse” electrochemical method was created using the ChronoAmperometry measurement type, available on the Transients menu of methods in *IviumSoft*™. It consisted of alternated potentiostatic-like cycles, where the potential was held at specific values for the duration of the cycle. Figure 3.33 represents the general aspect of the method, showing the potential increment *ΔE* over time. In summary, after an initial period of 3 seconds at open circuit potential, each following cycle had 10 seconds, in which the potential was raised and decreased to the plateaux of ±0.10 *V*, ±0.15 *V*, and ±0.20 *V*, in different cycles. Between the positive and negative input signal, the potential was kept at OCP for one cycle. With a last cycle of 3 seconds, where the potential was also held at OCP, the total number of cycles in the method were 13. Additionally, the following parameters were used: the OCP was monitored for 3 seconds, with an interval time of 1 second. The equilibration time was 2 seconds, with an interval time of half a second.

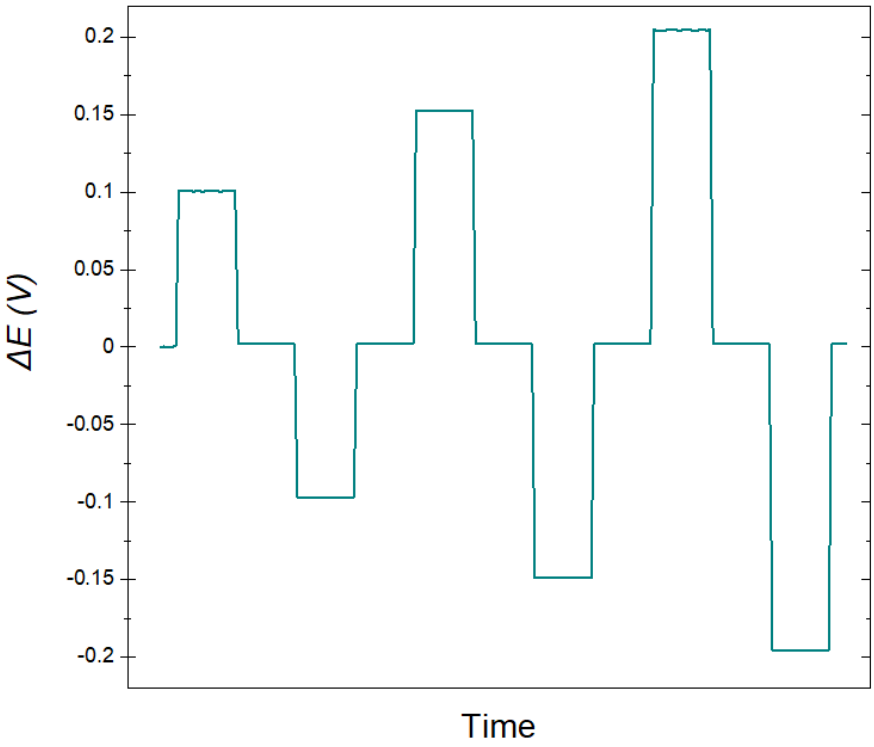

Figure 3.33 – Schematic representing the “pulse” electrochemical method.

The “sweep” and “pulse” methods were loaded in the *LabView*™ application that controlled the electrochemical measurements. An initial “void” method, with no electrochemical input, had to be created for enabling the application to run properly.

A total of ten electrochemical methods were performed on the coated samples at each time Table 3.11 show the methods used in the test. For the “sweeps” and “pulses” methods, data was collected for each of the time points indicated in Table 3.8, except for the first, at *0h*. For the EIS experiments, the *0h* data was collected.

As stated in Section 3.3.2, after the conclusion of each run, the samples were removed from the electrolyte, cleaned, and photographed before and after the stripping of their respective coating.

Table 3.11 – Electrochemical methods used in the test.

1	“Void”	6	Sweep Medium-Slow
2	EIS	7*	Sweep Small-Fast
3*	Sweep High-Fast	8*	Sweep Small-Slow
4*	Sweep High-Slow	9	Pulses
5	Sweep Medium-Fast	10	EIS (last)

3.4.2. DATA TREATMENT

Data from the “sweep” and “pulse” electrochemical experiments were used to created new datasets. For each specific sample and time point, the acquired values from the different methods were used as inputs, and the outputs were the respective values of the fitted parameters (see Section 3.3.3). For the dataset created from the “sweep” data, the inputs were the values of potential, the variation in potential (delta-potential), and the current. Each generated “sweep” log file had 160 data points. For the “pulse” dataset, the inputs were the registered values of the potential, time, and current. In this case, every “pulse” log file had 232 data points.

For each method, three comma-separated dataset files were created, using the *LabView*™ application: one using only data from the steel coated samples, one using only data from the aluminium alloy coated samples, and one using both data. The files were later saved in compressed folders, as mentioned in previous sections.

3.4.3. MACHINE LEARNING

The same artificial neural network model, described in Section 3.3.4, was used for the training a fitting-type machine learning algorithm, which aim was to predict the PARAMETER values related to the coating conditions, but based on the acquired data from different electrochemical measurements, from the “sweeps” and “pulse” methods. The algorithm was later evaluated by comparing the original used values with the ML predictions.

3.5. FLOW CHARTS

The figures below illustrate the resumed project paths as basic flow charts. Figure 3.34 presents the steps in exploring the EIS data from the marine coatings (item 3.1.1.1). Figure 3.35 shows the route from electrochemical impedance spectroscopy experiments to a trained machine learning algorithm (item 3.1.1.2). Finally, Figure 3.36 displays the use of different electrochemical measurements, aiming for the development of an algorithm that could provide coating evaluation with different techniques then EIS (item 3.1.1.3).

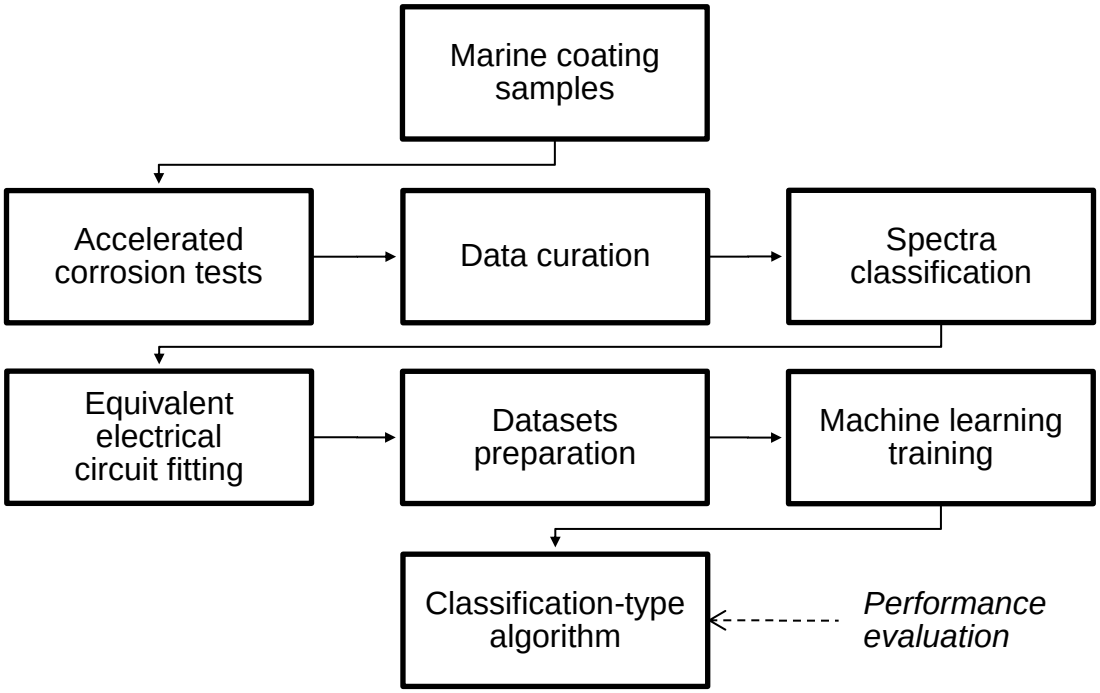

Figure 3.34 – Flow chart for item 3.1.1.1.

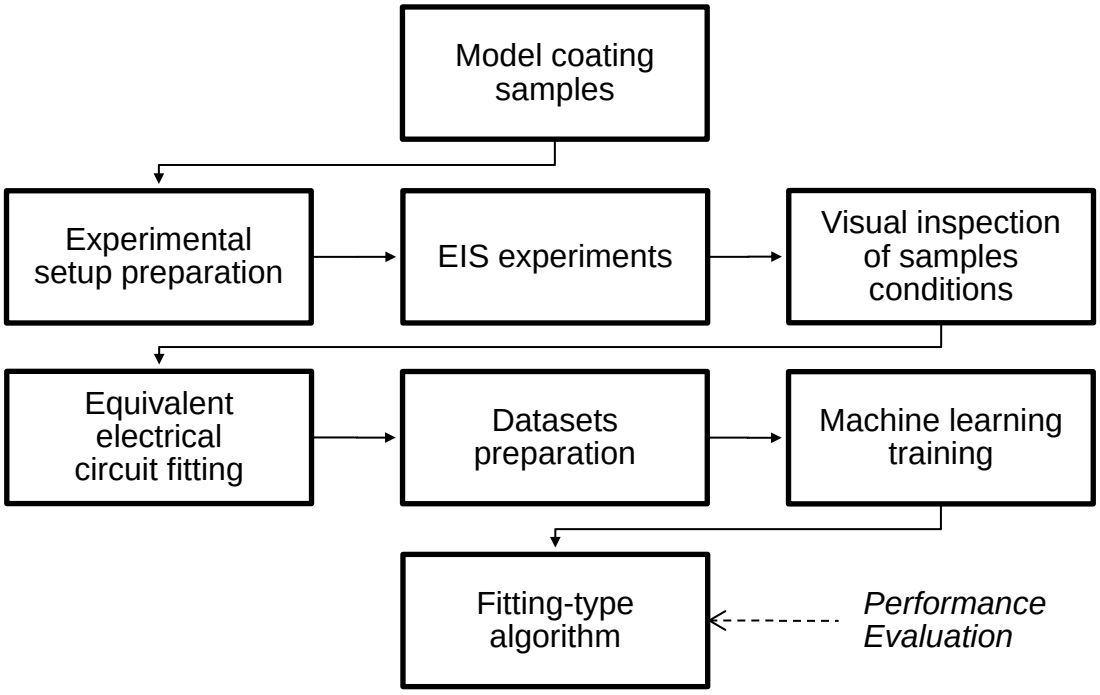

Figure 3.35 – Flow chart for item 3.1.1.2.

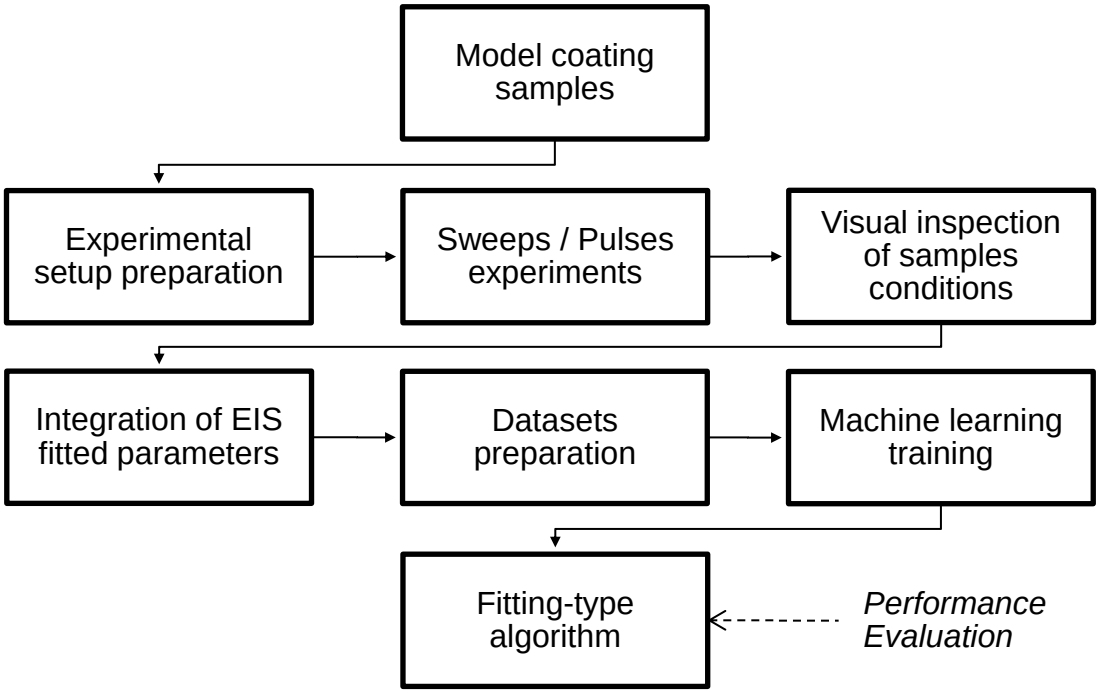

Figure 3.36 – Flow chart for item 3.1.1.3.

4. RESULTS AND DISCUSSION

4.1. RESULTS FOR MARINE COATINGS

4.1.1. EIS FROM ACCELERATED CORROSION TEST

Figure 4.1 show representative impedance spectra evolution of selected samples from coatings *A* to *D*, throughout the accelerated cyclic corrosion test, as Bode plots. The intention at this point is to show the general aspect of this evolution. Therefore, the data from some cycle weeks were omitted in order to make this representation clearer. Also, spectra data with noise had to be removed.

As previous mentioned in Section 3.2.1, coating *C* demonstrated a higher decrease in the value of the maximum impedance modulus. As a result, their spectra evolution has shown some of the characteristic changes related to coating degradation, as studied in Section 2.

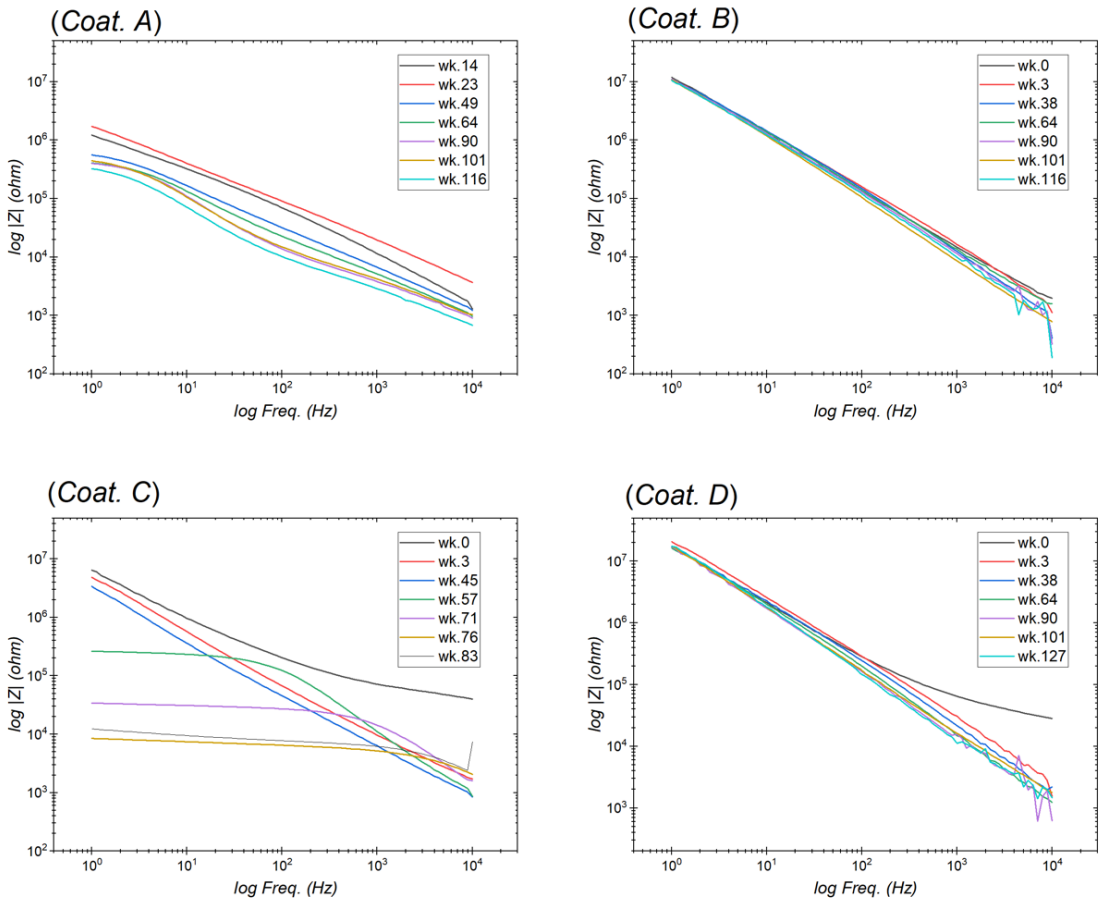

Figure 4.1 – EIS from accelerated cyclic corrosion tests.

By comparing the EIS spectra from Figure 4.1 with the characteristics of the marine coatings used in the accelerated cyclic corrosion tests, presented in Table 3.1, it is possible to understand why coating *C* had an inferior result compared to others, since it has no addition of aluminium flakes pigments and a moderate level of solids. The other three coatings, that had from 3 wt.% to 9 wt.% of the aluminium pigments, were more resistant to the test conditions, which is in part due to their composition. However, the amount of taluminium flakes in the composition has shown a smaller effect when compared to the level of solids. That can be understand by comparing the composition of coatings *B* and *D* with their impedance spectra measurements, which are very similar, even though the amount of *Al* is different. Actually, it seems that the level of solids had a bigger effect on the coating corrosion resistance, since these coatings, both high-solids, had a better performance than coating *A,* which had a moderate level of solids, albeit having 9 wt.% of aluminium pigments.

4.1.2. VISUAL ASPECT

The visual aspect of each panel, at each last registered condition, is shown in *APPENDIX A* – MARINE COATINGS ASPECT AFTER ACCELERATED TEST. At the front side, although the general aspect of the coatings does not show a generalized degradation, defects have emerged in coatings *A* and *C*, starting from week 57 (according to the provided data). At the back side, the degradation was more accentuated in some panels.

4.1.3. MACHINE LEARNING

After the training of the machine learning classification-type algorithm, the testing dataset was used to predict the designed classes, i.e., "*without defect*" (A) and "*with defect*" (B). This dataset used real values of impedance modulus (in *log*), phase shift

angles, and frequency (in *log*), acquired from the EIS measurements on the marine coating samples.

For this *proof of concept*, the 31 predicted classes have shown an accuracy of 100%, in relation to the actual classification. Table 4.1 shows the evaluation details. The obtained results are probably a consequence of the small size of the testing dataset, and also due to the facts that: *(i)* only one of the four coatings evaluated has shown a significant reduce in measured values; and *(ii)* the emergence of the defects was not concentrated on the areas tested by EIS. Therefore, only a fraction of the whole generated spectra was effectively related to a defect, reducing the availability for creating a greater testing dataset.

Nevertheless, the performance of the application of this ML approach in extracting sensible evaluations about the performance of coatings was considered to be gainful, since the trained solution has the potential to perform several spectra evolution at a much lesser time then it would be required in a case-by-case analysis.

Table 4.1 – ML classification-type algorithm testing results

N° of predictions (total)	31	N° right predictions – class *A*	18
N° of total right predictions	31	N° right predictions – class *B*	13
N° of examples – class *A*	18	Recall – class *A*	100%
N° of examples – class *B*	13	Recall – class *B*	100%
N° of predictions – class *A*	18	Precision – class *A*	100%
N° of predictions – class *B*	13	Precision – class *B*	100%

4.2. RESULTS FOR MODEL COATINGS

4.2.1. VISUAL ASPECT

The visual aspect of the modal coatings after the electrochemical tests, before and after the stripping of the paint, is presented in *APPENDIX B* – MODEL COATINGS AFTER ELECTROCHEMICAL TESTS.

It is worth to mention that some of the coatings remained very adhered to their substrate. Therefore, scratches and residual paint can unfortunately be seen in some images, especially in the group of the aluminium alloy panels.

By the visual aspect, it was possible to verify the effect of the different pigmentation (see Table 3.3) on the corrosion performance of the model coatings, as it supposed to be. Coatings with the anticorrosive pigment (zinc phosphate) had better performances. The samples with higher amount of calcium sulphate have suffered more degradation in the experiment conditions, which made their removal from each substrate very easy, as the coated seemed disbonded. This could be the result of an underfilm corrosion process, such as cathodic delamination, discussed in Section 2.

4.2.1. EXPERIMENTAL DATA RESULTS

At this point, a disclaimer needs to be made: the basic objectives in performing electrochemical impedance spectroscopy measurements on the coated samples in the project were to acquire a significant number of EIS spectra, fit equivalent electric circuits into the data, and acquire the parameters, so that information could be built in datasets for training, validating, and testing machine learning algorithms. Therefore, albeit the experiments were made at different time points, the main goal was not to study the time evaluation of the coatings. Nevertheless, this information would be interesting to report in the dissertation, since it could provide insights about the entire context being studied.

However, despite allowing the acquisition of enough useful data for the fitting step, a considerable part of the spectra data presented too much noise. Up to a point, this was an understandable issue that happened when the measured signal was too small for a proper reading by the potentiostats employed in the tests. Worse, some other measurements data were lost due to connection problems in the multiplexer board, when unsensible spectra was acquired.

The reason why this have not affected the fitting step in a critical way is due to the fact that, in this stage, all the acquired spectra was fed as one for the datasets. In the case of presenting the time evolution of each coating, however, the spectra would be separated into smaller groups, and the effect of having unusable data caused some of these studies to be, in resume, incomplete – i.e., there was not useful data covering the whole timespan of the experiment.

Another critical issue happened with the electrochemical “sweep” methods, in the “high” and “low” designs. The data obtained with these methods was not conclusive. Therefore, only data from the “medium-fast” and “medium-slow” sweep methods, together with the “pulse” method, was used for feeding the datasets for the ML fitting-type algorithm.

4.2.2. MACHINE LEARNING

4.2.2.1. USING EIS DATA

The results after the training, validation and testing of the machine learning model for the fitting-type algorithm are presented in the form of a graph, where the x-axis represents the experimental values, and the y-axis represents the values predicted by the machine learning after being trained.

A sloped line with a function $f(x) = x$ was introduced to facilitate the understanding of the results, in the following way: if the points in the graph are close to the line, that

means that the prediction values are close to the experimental value and, so, the and the prediction is relatively satisfactory. Conversely, if the data points are scattered away from the slopped line, the prediction was not precise.

Figure 4.2 shows the results for the predictions of the total resistance and total capacitance using data from the steel coated samples. On the other hand, Figure 4.3 shows the results for the same parameters for the aluminium alloy coated samples. The results have shown a satisfactory prediction capability for both substrates. The better results were achieved in the algorithm prepared with the aluminium alloy coated samples.

Additionally, Table 4.2 show the mean squared error (MSE) and average percent error (AE) for each case.

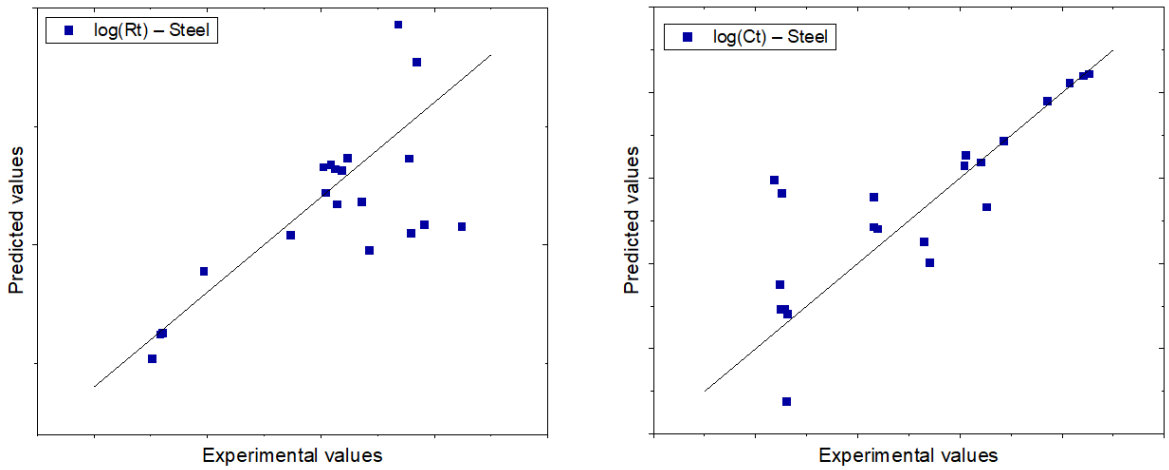

Figure 4.2 – Algorithm cross-plot – EIS – data from steel coated samples

4.2.2.2. USING OTHER ELECTROCHEMICAL METHODS DATA

The same presented approach was used for evaluating the results obtained by the ML algorithm fed with data from the other electrochemical methods. However, in this case, the dataset was prepared using data from both substrates. The results are

presented in Figure 4.4 and Table 4.3 for the “Pulse” method. In the cross-plot of total resistance, it appears that some kind of shift in the values had occurred, since them seem to be aligned below the $f(x) = x$ line. However, no apparent reason was found.

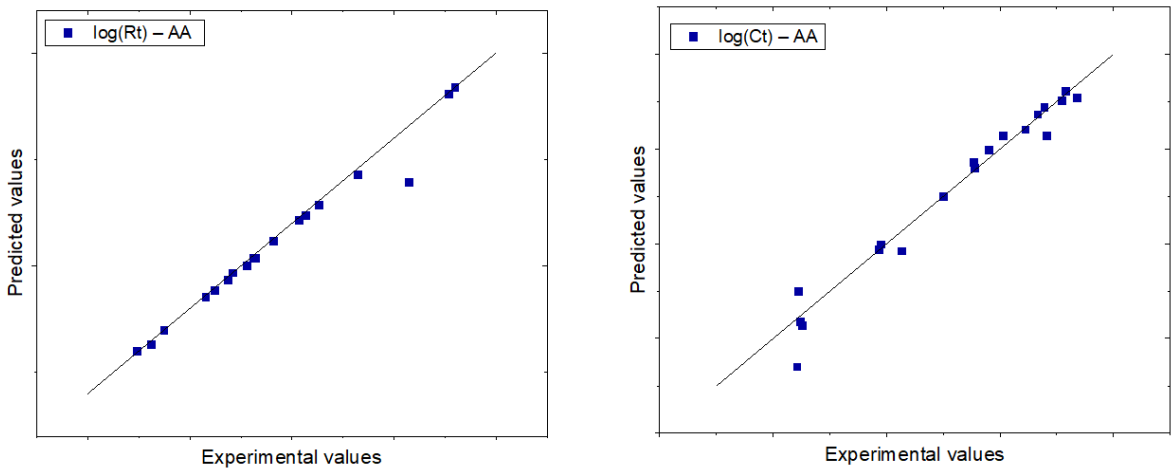

Figure 4.3 – Algorithm cross-plot – EIS – data from AA coated samples

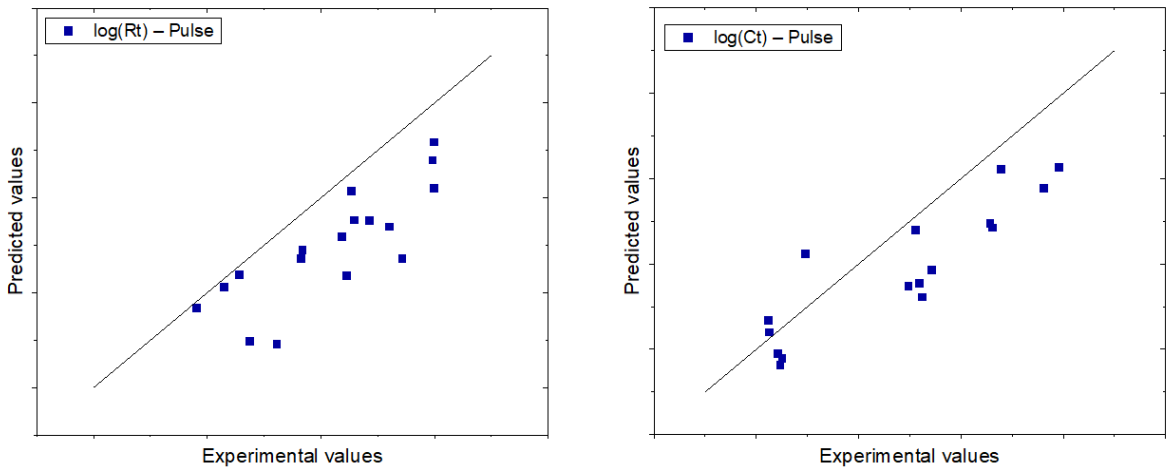

Figure 4.4 – Algorithm cross-plot – pulse method

Table 4.2 – EIS based algorithm classification

Steel	Total resistance		Total capacitance	
	MSE= 5.29	AE= 37%	MSE= 1.60	AE= 41%
AA	Total resistance		Total capacitance	
	MSE= 0.10	AE= 6%	MSE= 0.11	AE= 11%

Table 4.3 – Pulse based algorithm evaluation

Pulse	Total resistance		Total capacitance	
	MSE= 2.07	AE= 23%	MSE= 1.78	AE= 48%

For the “sweeps”, the data was acquired from the medium amplitude swaps. Therefore, Figure 4.5 and Table 4.4 shows the results for the “medium-fast” and “medium-slow” sweep method.

Table 4.4 - Sweep based algorithm evaluation

Medium-Fast	Total resistance		Total capacitance	
	MSE= 0.37	AE= 10%	MSE= 0.68	AE= 30%
Medium-Slow	Total resistance		Total capacitance	
	MSE= 0.07	AE= 5%	MSE= 0.39	AE= 17%

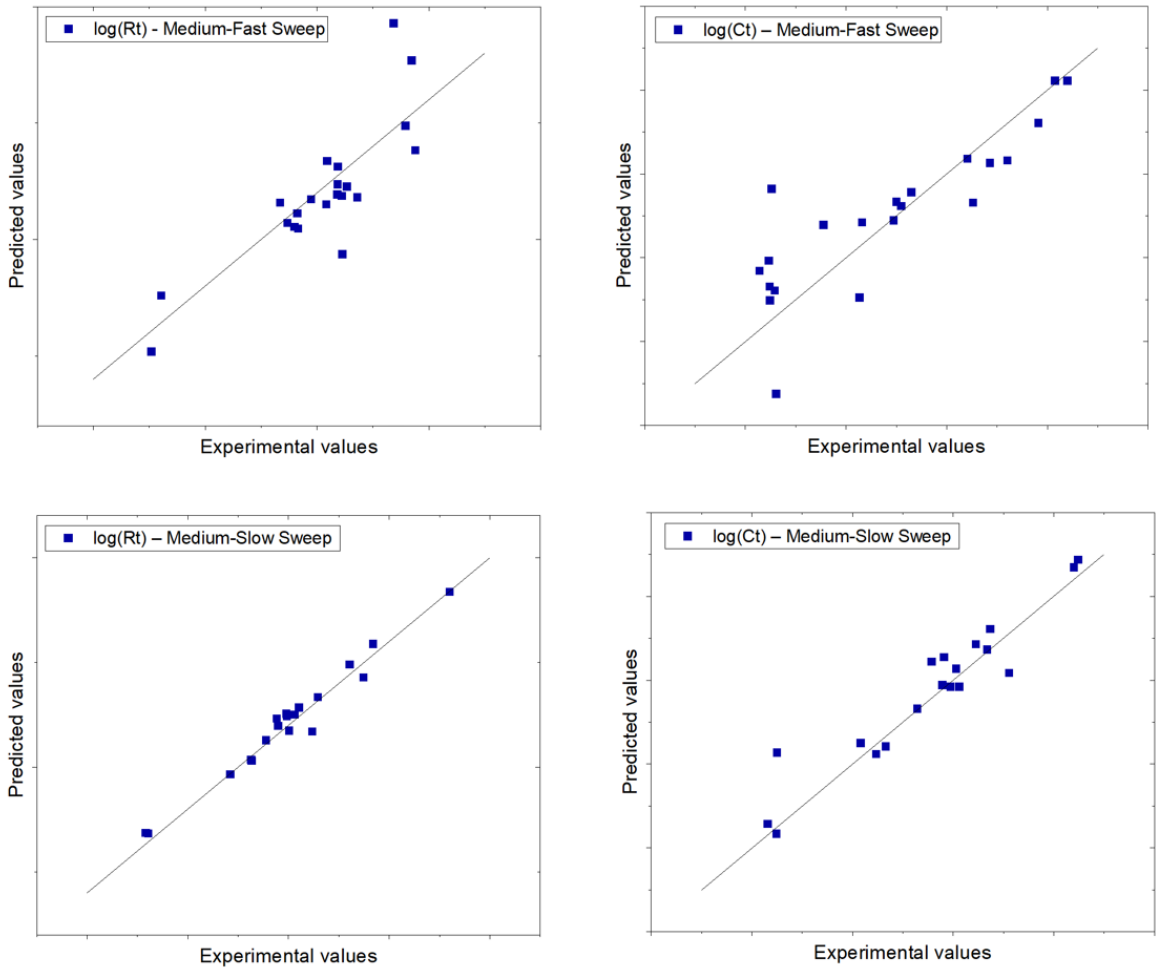

Figure 4.5 – Algorithm cross-plot – sweep methods

Despite being more scattered than the results from the ML using data sourced from EIS, these results represent a very satisfactory achievement since they were acquired from alternative methods. The achieved performance motivates further investigation and development of the technique.

However, a valid critique could be made on the fact that the output values used for the training and predicted by the algorithms do not correspond precisely to the parameters of a given corrosion system. Since, for this project, a strategy for overcoming the necessity of preparing different algorithms due to different number of fitted equivalent circuit elements that could emerge from an evolving corrosion system, at the end the achieved values are not capable of discern the type of

equivalent circuit and, ultimately, the corrosion conditions at the coated metal. Nevertheless, this approach has been used to evaluate the capability of the machine learning algorithm to identity the relations between electrochemical data inputs and outputs, which has been achieved.

5. CONCLUSIONS AND FUTURE WORK

This project has sought to implement machine learning approaches to the context of electrochemical impedance spectroscopy. The objective was to explore if the inherent complexities of this method could be better processed by machine learning, in order to achieve an improvement in efficiency.

EIS and visual inspection data from marine coatings, exposed to accelerated corrosion tests, were curated, and allowed the preparation of a classification-type algorithm. Impedance measurements, together with alternative proposed methods, were applied to model coatings, with different pigmentation sets, in order to generate datasets for the training, validation and testing of a different fitting-type algorithm. Both of these developments were proposed as “proof of concepts”.

By using an artificial neural network model and real data from coated samples, the machine learning algorithms have performed satisfactorily. The results motivate further investigation of the experimental methods. The simplifications used in this project, especially in the issue of selecting the suitable equivalent electric circuit for the fitting step, should be further investigated. Also, experimental tests that could provide more useful data would allow more points in the datasets to be fed into the machine learning algorithms. However, an efficient trade-off should be found, since the increase in the dataset size would require more time spent in the fitting step, which is still a task that has to be performed in a case-by-case scenario. Despite the fact that, using the machine learning approach, this would only had to be done a few times, for preparing the datasets, this challenge still represent a matter that could be targeted by future researches.

6. REFERENCES

Akbarinezhad, E., Bahremandi, M., Faridi, H. R. & Rezaei, F. (2009). 'Another approach for ranking and evaluating organic paint coatings via electrochemical impedance spectroscopy' *Corrosion Science*, 51 (2), pp. 356-363. DOI: 10.1016/j.corsci.2008.10.029.

Alves, L. M., et al. (2018). 'Identification of corrosive substances and types of corrosion through electrochemical noise using signal processing and machine learning' *Journal of Control, Automation and Electrical Systems*, 30 (1), pp. 16-26. DOI: 10.1007/s40313-018-00423-0.

Annergren, I., Zou, F. & Thierry, D. (1999). 'Application of localised electrochemical techniques to study kinetics of initiation and propagation during pit growth' *Electrochimica acta*, 44 (24), pp. 4383-4393. DOI: 10.1016/S0013-4686(99)00154-1.

Asbeck, W. K. & Loo, M. V. (1949). 'Critical pigment volume relationships' *Industrial and engineering chemistry*, 41 (7), pp. 1470-1475. DOI: 10.1021/ie50475a042.

Bongiorno, V., Gibbon, S., Michailidou, E. & Curioni, M. (2022). 'Exploring the use of machine learning for interpreting electrochemical impedance spectroscopy data: Evaluation of the training dataset size' *Corrosion Science*, 198. DOI: 10.1016/j.corsci.2022.110119.

Brunel, I. (2011). 'Steam navigation. The 'great western' steam-ship', *The life of isambard kingdom brunel, civil engineer*, pp. 231-245.

Cogger, N. D., Webb, R. V. & Wellstead, P. E. (1997). *Frequency response analysis - technical report 10*: Solartron Instruments.

Curioni, M., Monetta, T. & Bellucci, F. (2015). ‘Modeling data acquisition during electrochemical noise measurements for corrosion studies’ *Corrosion Reviews*, 33 (3-4), pp. 187-194. DOI: 10.1515/corrrev-2014-0047.

Danfoss (2018). *How to comply with new ballast water regulation*: Danfoss A/S. Available at: https://www.danfoss.com/en/about-danfoss/articles/dcs/how-to-comply-with-new-ballast-water-regulation/ (Accessed: 03 September 2022).

De Baere, K., et al. (2013). ‘Reducing the cost of ballast tank corrosion: An economic modeling approach’ *Marine Structures*, 32 pp. 136-152. DOI: 10.1016/j.marstruc.2012.10.009.

Diao, Y., Yan, L. & Gao, K. (2021). ‘Improvement of the machine learning-based corrosion rate prediction model through the optimization of input features’ *Materials & Design*, 198. DOI: 10.1016/j.matdes.2020.109326.

Dong, C. F., Fu, A. Q., Li, X. G. & Cheng, Y. F. (2008). ‘Localized eis characterization of corrosion of steel at coating defect under cathodic protection’ *Electrochimica Acta*, 54 (2), pp. 628-633. DOI: 10.1016/j.electacta.2008.07.016.

Doshvarpassand, S., Wu, C. & Wang, X. (2019). ‘An overview of corrosion defect characterization using active infrared thermography’ *Infrared Physics & Technology*, 96 pp. 366-389. DOI: 10.1016/j.infrared.2018.12.006.

Elayaperumal, K. & Raja, V. S. (2015). *Corrosion failures : Theory, case studies, and solutions*. Hoboken, New Jersey John Wiley & Sons, Inc.

Eyres, D. J. (2006). 'Materials and strength of ships', *Ship construction*: Jordan Hill: Elsevier Science & Technology.

Ferreiro, L. D. (2020). *Bridging the seas : The rise of naval architecture in the industrial age, 1800-2000*. Cambridge : The MIT Press.

Galvão, T. L. P., et al. (2020). ‘Elucidating structure–property relationships in aluminum alloy corrosion inhibitors by machine learning’ *The Journal of Physical Chemistry C*, 124 (10), pp. 5624-5635. DOI: 10.1021/acs.jpcc.9b09538.

Gentil, V. (1996). *Corrosão*. 3a edn. Rio de Janeiro, RJ – Brazil: LTC — Livros Técnicos e Científicos Editora S.A.

Ghatak, A. (2017). *Machine learning with r*.

Gibbs, J. W. (1878). *On the equilibrium of heterogeneous substances*. New Haven, Connecticut: Transactions of the Connecticut Academy of Arts and Sciences.

Gong, X., et al. (2019). ‘Machine learning assistance for electrochemical curve simulation of corrosion and its application’ *Materials and Corrosion*, 71 (3), pp. 474-484. DOI: 10.1002/maco.201911224.

Grossi, M., Parolin, C., Vitali, B. & Riccò, B. (2019). ‘Electrical impedance spectroscopy (eis) characterization of saline solutions with a low-cost portable measurement system’ *Engineering Science and Technology, an International Journal*, 22 (1), pp. 102-108. DOI: 10.1016/j.jestch.2018.08.012.

Gudze, M. T. & Melchers, R. E. (2008). ‘Operational based corrosion analysis in naval ships’ *Corrosion Science*, 50 (12), pp. 3296-3307. DOI: 10.1016/j.corsci.2008.08.048.

Hope, J. (2022). *Life on the high seas: Ss great britain history*. The Bristol Magazine: MC Publishing Limited. Available at: https://thebristolmag.co.uk/ss-great-britain-history/ (Accessed: 27 August 2022).

ISO (2007). *8501-1: Preparation of steel substrates before application of paints and related products — visual assessments of surface cleanliness — part 1: Rust grades and preparation grades of uncoated steel substrates and of steel substrates after overall removal of previous coatings*. Switzerland. ISO Copyright Office.

ISO (2017a). *4: Paints and varnishes — corrosion protection of steel structures by protective paint systems — part 4: Types of surface and surface preparation*. Switzerland. ISO copyright office.

ISO (2017b). *12944-2: Paints and varnishes — corrosion protection of steel structures by protective paints systems — part 2: Classification of environments*. Switzerland. ISO Copyright Office.

ISO (2018). *12944-5: Paints and varnishes — corrosion protection of steel structures by protective paint systems — part 5: Protective paint systems*. Switzerland. ISO Copyright Office.

Jones, F. N., Nichols, M. E. & Pappas, S. P. (2017). *Organic coatings : Science and technology*. 4th edition edn. Hoboken, NJ, USA: John Wiley & Sons, Inc.

Kiosdou, E. D., Karantonis, A. & Pantelis, D. I. (2014). 'Evaluation of barrier properties of antifouling coatings on naval steel' *Chemical Engineering Transactions*, 41. DOI: 10.3303/CET1441051.

Koch, G. H., et al. (2005). 'Cost of corrosion in the united states', in Myer Kutz Associates, I. D., New York (ed.) *Handbook of environmental degradation of materials*: William Andrew Publishing, pp. 3–24.

Lasia, A. (2014). *Electrochemical impedance spectroscopy and its applications*. New York, NY: Springer.

LeBozec, N., et al. (2015). 'Performance of marine and offshore paint systems: Correlation of accelerated corrosion tests and field exposure on operating ships' *Materials and Corrosion*, 66 (3), pp. 215-225. DOI: 10.1002/maco.201307340.

Li, Q., et al. (2021). 'Modeling the corrosion rate of carbon steel in carbonated mixtures of mdea-based solutions using artificial neural network' *Process Safety and Environmental Protection*, 147 pp. 300-310. DOI: 10.1016/j.psep.2020.08.035.

Ljungström, H. (2018). *Great western*. Available at: http://thegreatoceanliners.com/articles/greatwestern/ (Accessed: 26 August 2022).

Lvovich, V. F. (2012). *Impedance spectroscopy: Applications to electrochemical and dielectric phenomena*. John Wiley & Sons.

Macdonald, J. R. & Johnson, W. B. (2005). 'Fundamentals of impedance spectroscopy', in Barsoukov, E. & Macdonald, J. R. (eds.) *Impedance spectroscopy.* 2nd edn: John Wiley & Sons, Inc.

Mansfeld, F. (1995). 'Use of electrochemical impedance spectroscopy for the study of corrosion protection by polymer coatings' *Journal of Applied Electrochemistry*, 25 (3), pp. 187-202. DOI: 10.1007/BF00262955.

Mansfeld, F. & Kendig, M. W. (1985). 'Electrochemical impedance spectroscopy of protective coatings' *Materials and Corrosion*, 36 (11), pp. 473-483. DOI: 10.1002/maco.19850361102.

Masunaga, S. (2020). 'That rust on your shower head? It's a $6-billion problem for the navy, cruise ships and more', *Los Angeles Times*. [Online]. Available at: https://www.latimes.com/business/story/2020-01-13/navy-ship-rust (Accessed: 03 September 2022).

Mayne, J. E. O. & van Rooyen, D. (1954). 'The mechanism of the corrosion-inhibitive action of paints, with special reference to basic pigments' *Journal of applied chemistry (London)*, 4 (7), pp. 384-394. DOI: 10.1002/jctb.5010040708.

McCafferty, E. (2010). *Introduction to corrosion science*. New York, NY : Springer New York.

Mouanga, M., Puiggali, M. & Devos, O. (2013). 'Eis and leis investigation of aging low carbon steel with zn–ni coating' *Electrochimica Acta*, 106 pp. 82-90. DOI: 10.1016/j.electacta.2013.05.021.

Orazem, M. E. & Tribollet, B. (2017). *Electrochemical impedance*

spectroscopy. 2nd edn. Hoboken, New Jersey.: John Wiley & Sons, Inc.,.

Pedeferri, P. (2018). *Corrosion science and engineering*. Milan, Italy: Springer Nature Switzerland AG.

Pei, Z., et al. (2020). 'Towards understanding and prediction of atmospheric corrosion of an fe/cu corrosion sensor via machine learning' *Corrosion Science*, 170. DOI: 10.1016/j.corsci.2020.108697.

Permeh, S., Lau, K. & Duncan, M. (2019). 'Characterization of biofilm formation and coating degradation by electrochemical impedance spectroscopy' *Coatings*, 9 (8). DOI: 10.3390/coatings9080518.

Pourbaix, M. (1974). *Atlas of electrochemical equilibria in aqueous solutions*. 2nd English edn. Houston, Texas: National Association of Corrosion Engineers.

Ritter, S., et al. (2021). 'Results of an international round-robin exercise on electrochemical impedance spectroscopy' *Corrosion Engineering, Science and Technology*, 56 (3), pp. 254-268. DOI: 10.1080/1478422X.2020.1850070.

Sanchez, G., Aperador, W. & Cerón, A. (2019). 'Corrosion grade classification: A machine learning approach' *Indian Chemical Engineer*, 62 (3), pp. 277-286. DOI: 10.1080/00194506.2019.1675539.

Santos, I. S. d. (2018). *Influência da preparação de superfície no desempenho de tintas de fundo aplicadas a estruturas marítimas sob proteção catódica*. MSc, Federal University of Rio de Janeiro, Rio de Janeiro.

Scaliger, C. (2014). 'The start of something: Though most americans have likely not heard of josiah willard gibbs, he was an american physicist upon whose works much of science and math revolve' *The New American*, 30 (22), p. 33+. https://link.gale.com/apps/doc/A391719070/AONE?u=jrycal5&sid=bookmark-AONE&xid=e65cf11f Available at:

https://link.gale.com/apps/doc/A391719070/AONE?u=jrycal5&sid=bookmark-AONE&xid=e65cf11f.

Schuld, M., Sinayskiy, I. & Petruccione, F. (2015). 'An introduction to quantum machine learning' *Contemporary Physics*, 56 (2), pp. 172-185. DOI: 10.1080/00107514.2014.964942.

Schweitzer, P. A. (1998). *Encyclopedia of corrosion technology*. New York: Marcel Dekker.

Stojanović, I., Farkas, A., Alar, V. & Degiuli, N. (2019). 'Evaluation of the corrosion protection of two underwater coating systems in a simulated marine environment' *Jom*, 71 (12), pp. 4330-4338. DOI: 10.1007/s11837-019-03669-4.

Van Haeverbeke, M., Stock, M. & De Baets, B. (2021). 'Practical equivalent electrical circuit identification for electrochemical impedance spectroscopy analysis with gene expression programming' *IEEE Transactions on Instrumentation and Measurement*, 70 pp. 1-12. DOI: 10.1109/tim.2021.3113116.

Wang, Z., et al. (2020). 'Cutting performance and wear mechanism of spark plasma–sintered silicon nitride ceramics tool in dry turning of 41cr4 hardened steel' *The International Journal of Advanced Manufacturing Technology*, 107 (7-8), pp. 3415-3424. DOI: 10.1007/s00170-020-05277-y.

APPENDIX A – MARINE COATINGS ASPECT AFTER ACCELERATED TEST

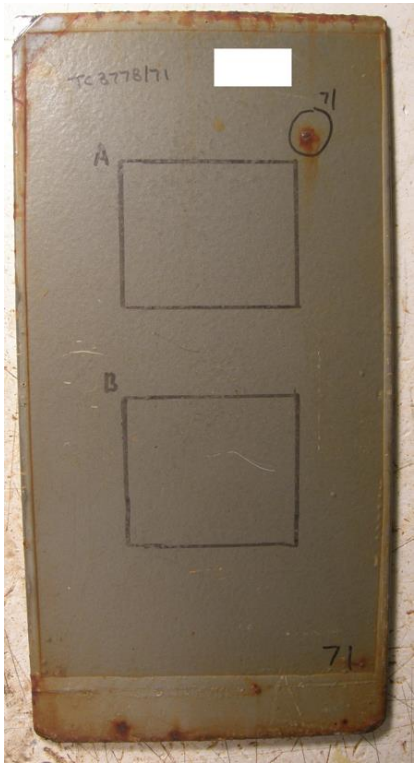

Coating *A* - Panel 71 - Front - Wk.127

Coating *A* - Panel 71 - Back - Wk.127

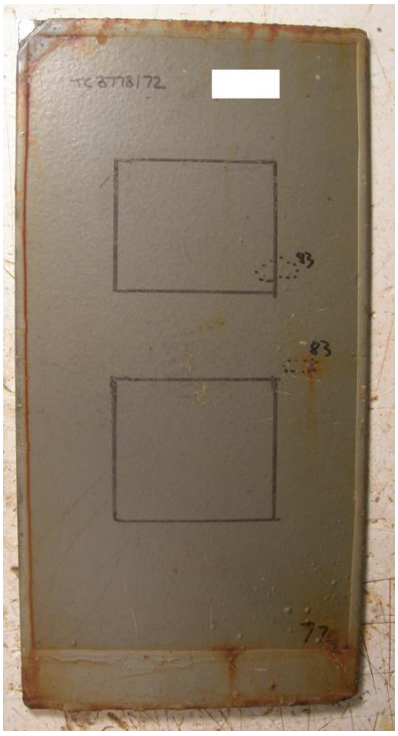

Coating *A* - Panel 72 - Front - Wk.127

Coating *A* - Panel 72 - Back - Wk.127

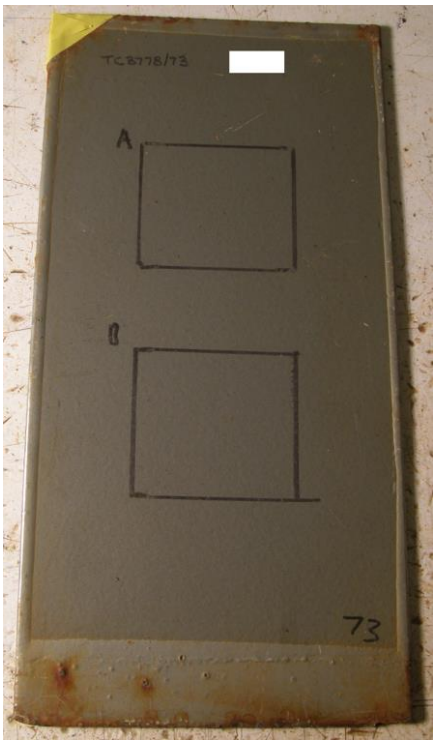

Coating *A* - Panel 73 – Front - Wk. 101

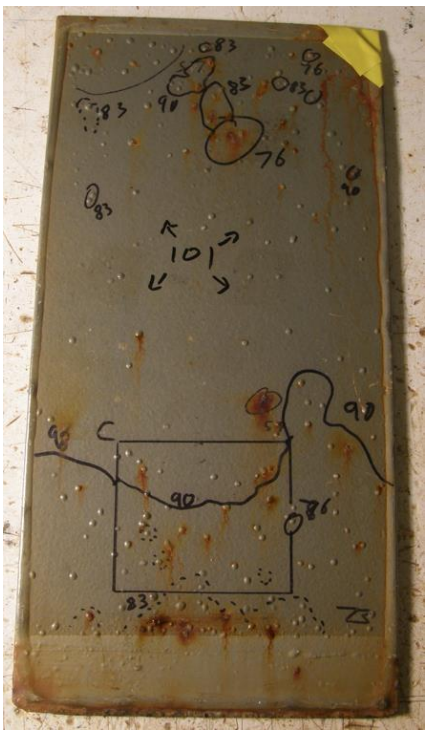

Coating *A* - Panel 73 – Back - Wk. 101

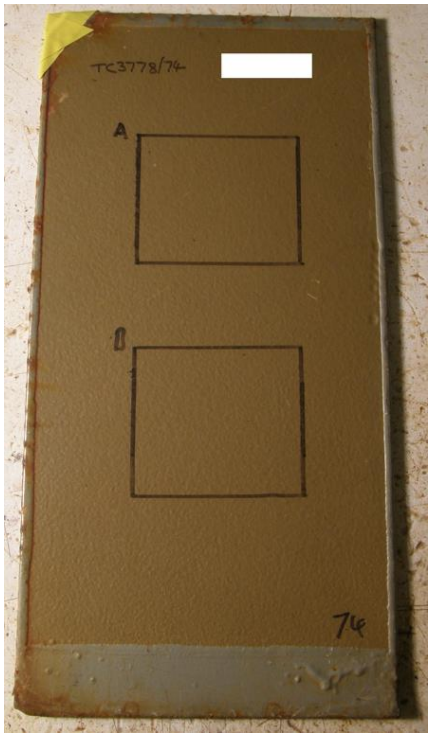

Coating *B* - Panel 74 - Front - Wk. 101

Coating *B* - Panel 74 – Back - Wk. 101

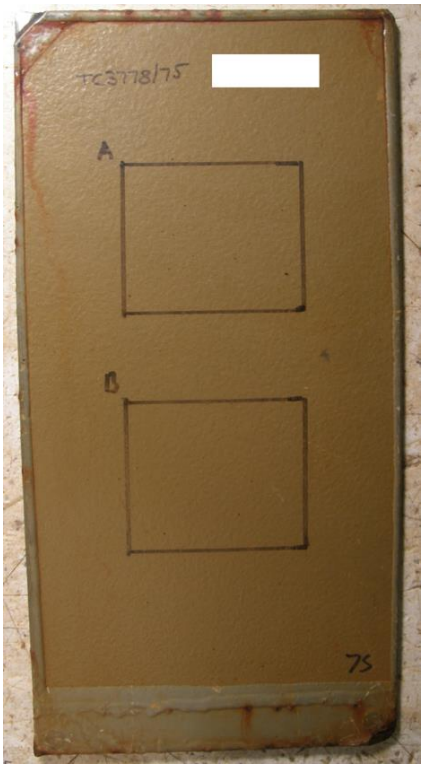

Coating *B* - Panel 75 - Front - Wk.145

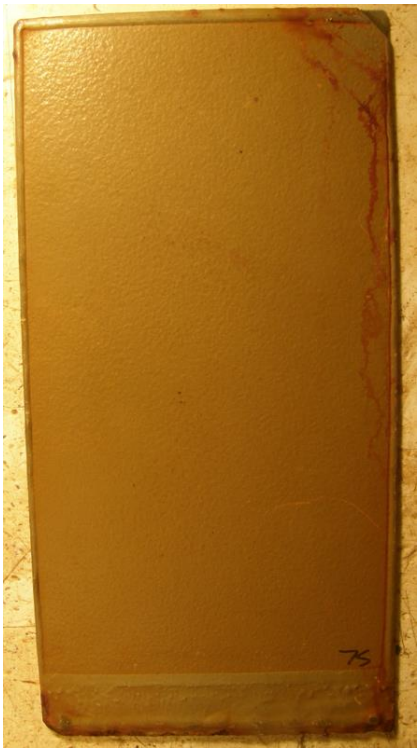

Coating *B* - Panel 75 - Back - Wk.145

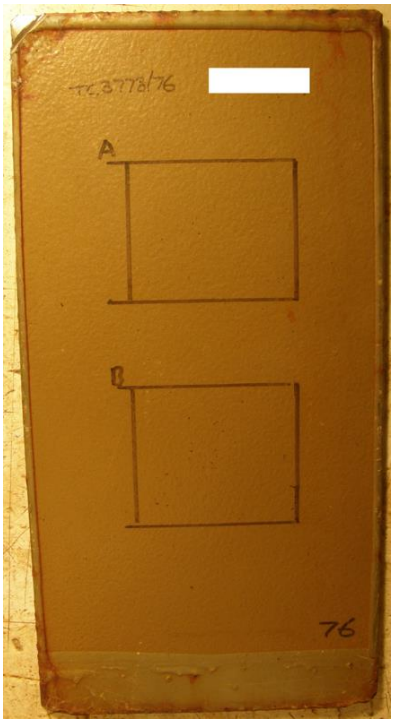

Coating *B* - Panel 76 - Front - Wk.145

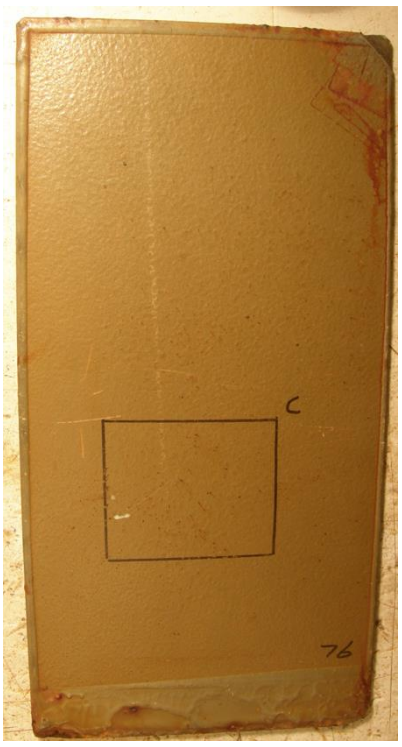

Coating *B* - Panel 76 - Back – Wk.145

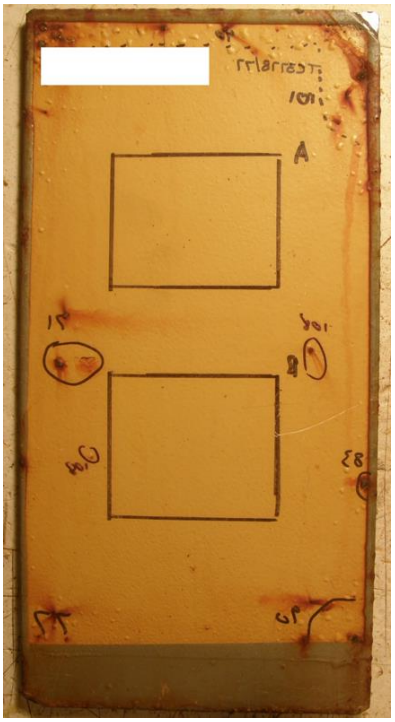

Coating *C* - Panel 77 - Front - Wk.127

Coating *C* - Panel 77 - Back - Wk.127

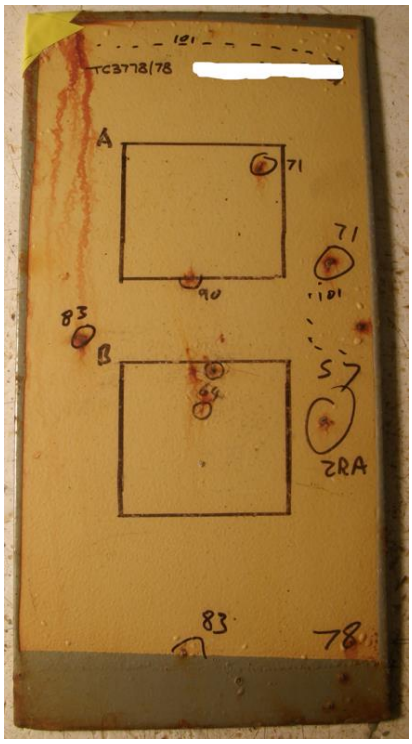

Coating *C* - Panel 78 - Front - Wk.101

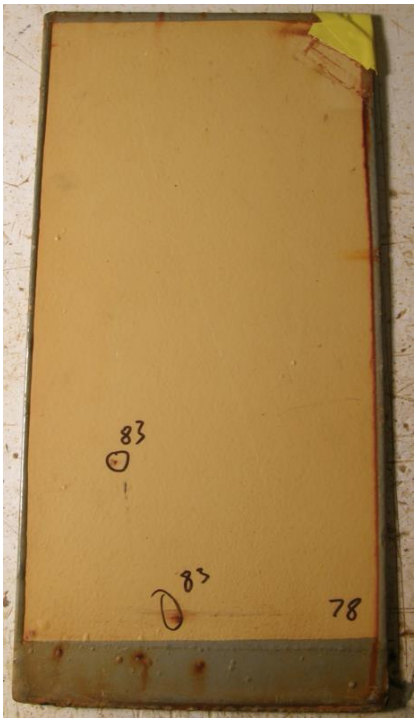

Coating *C* - Panel 78 - Back - Wk.101

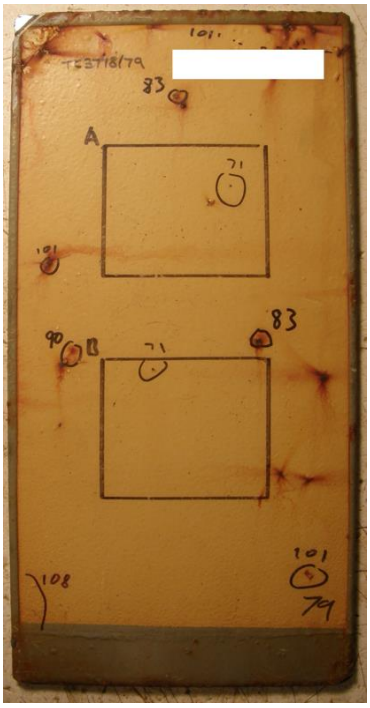

Coating *C* - Panel 79 - Front - Wk.127

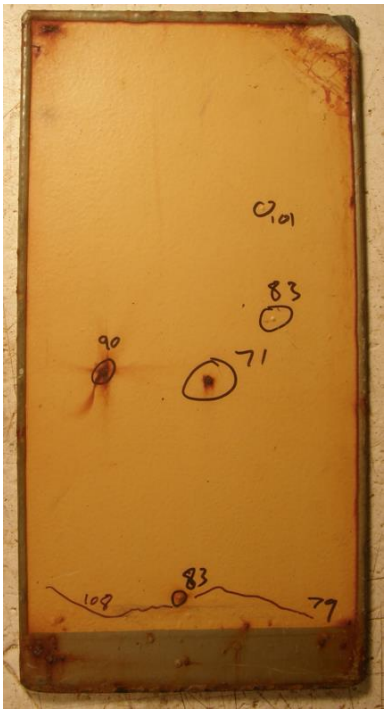

Coating *C* - Panel 79 - Back - Wk.127

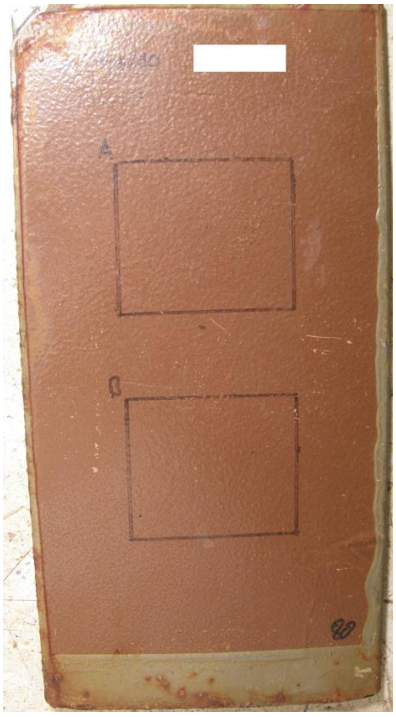

Coating *D* - Panel 80 - Front - Wk.145

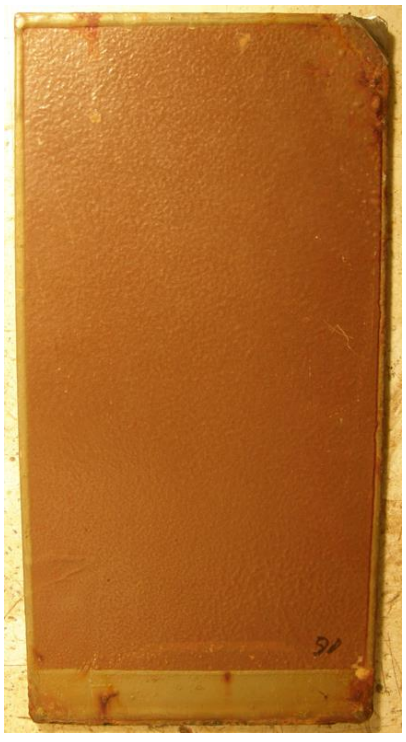

Coating *D* - Panel 80 - Back - Wk.145

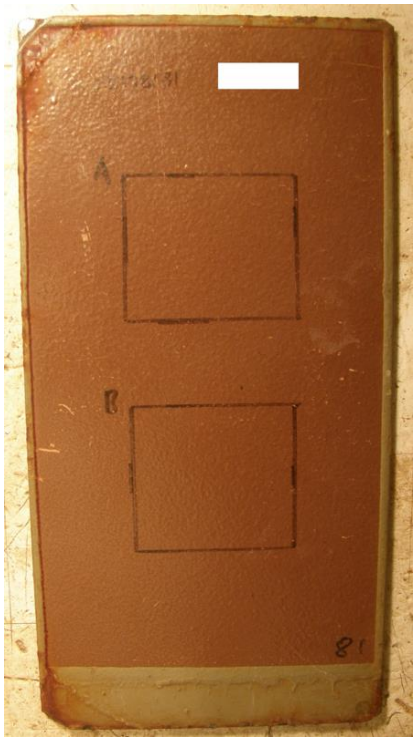

Coating *D* - Panel 81 - Front - Wk.145

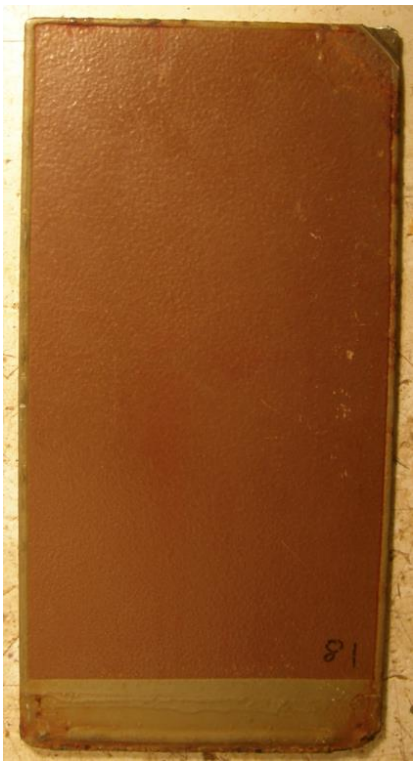

Coating *D* - Panel 81 - Back - Wk.145

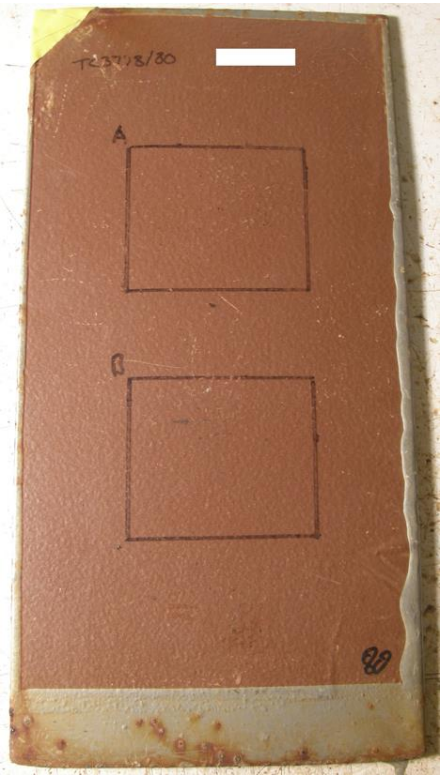

Coating *D* - Panel 82 - Front - Wk.101

Coating *D* - Panel 82 - Back - Wk.101

APPENDIX B – MODEL COATINGS AFTER ELECTROCHEMICAL TESTS

Note: for details about the model coatings, see Section 3.1.2.2.

MODEL COATING SAMPLES – STEEL

BEFORE COATING STRIPPING

TiCa model coating

AFTER COATING STRIPPING

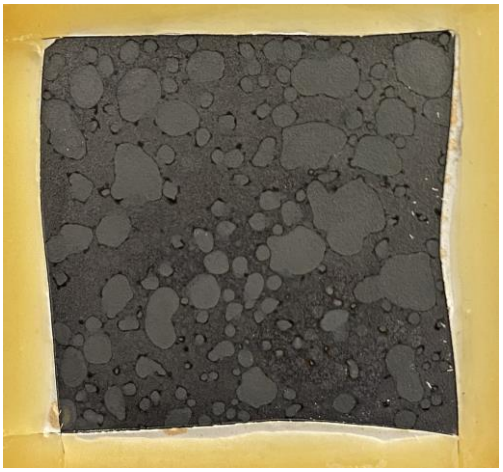

Substrate under *TiCa*

TiBaCa model coating

Substrate under *TiBaCa*

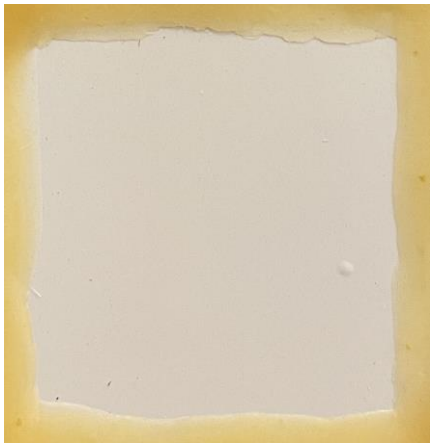

TiBaCaZn model coating

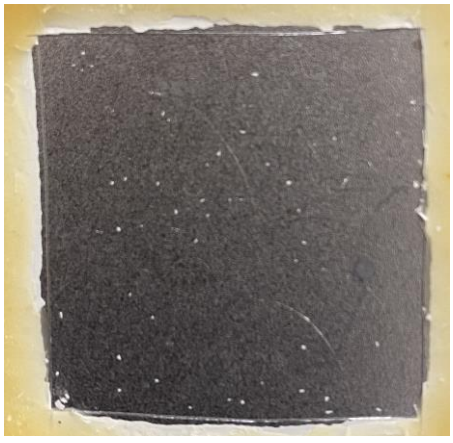

Substrate under *TiBaCaZn*

BEFORE COATING STRIPPING

AFTER COATING STRIPPING

TiBa model coating

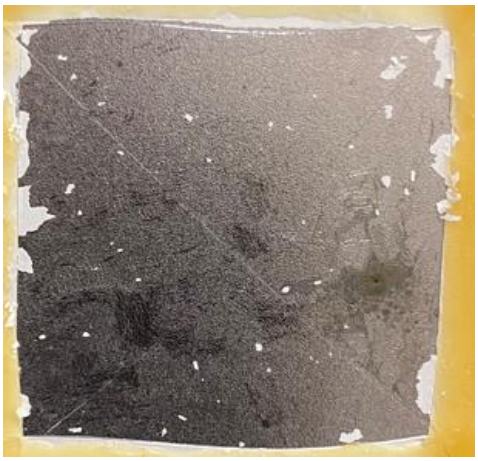

Substrate under *TiBa*

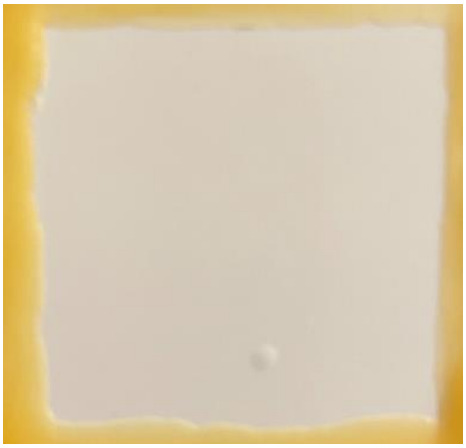

TiBaZn model coating

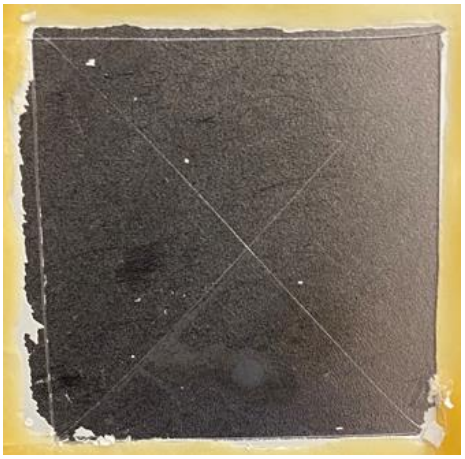

Substrate under *TiBaZn*

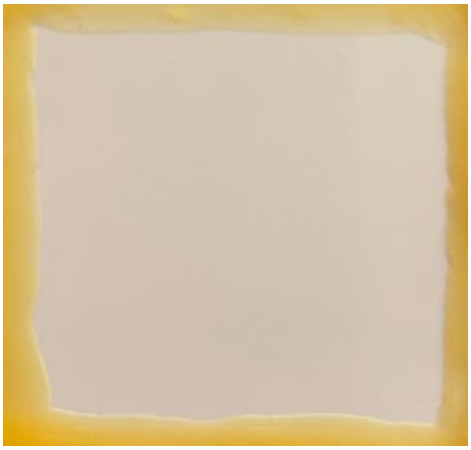

TiZn model coating

Substrate under *TiZn*

MODEL COATING SAMPLES – ALUMINIUM ALLOY

BEFORE COATING STRIPPING

AFTER COATING STRIPPING

TiCa model coating

Substrate under *TiCa*

TiBaCa model coating

Substrate under *TiBaCa*

TiBaCaZn model coating

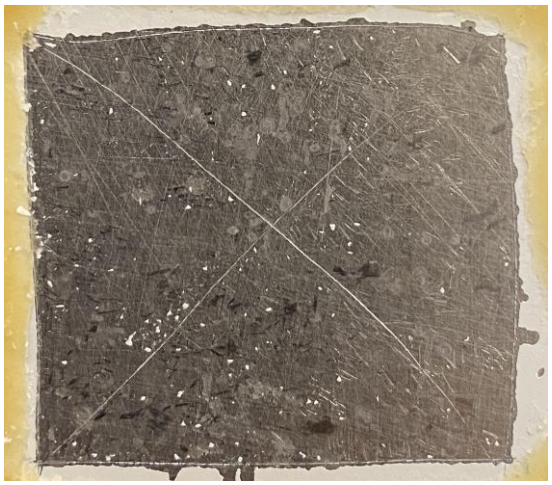

Substrate under *TiBaCaZn*

BEFORE COATING STRIPPING

AFTER COATING STRIPPING

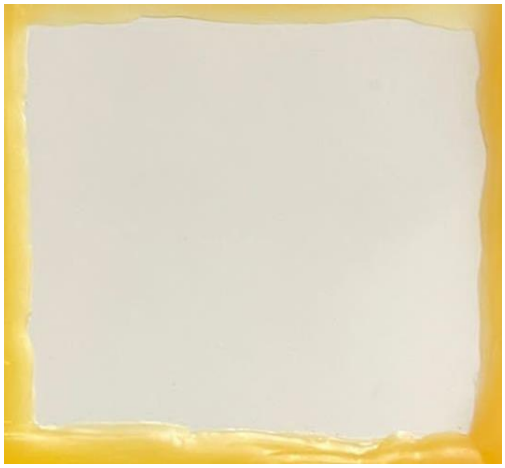

TiBa model coating

Substrate under *TiBa*

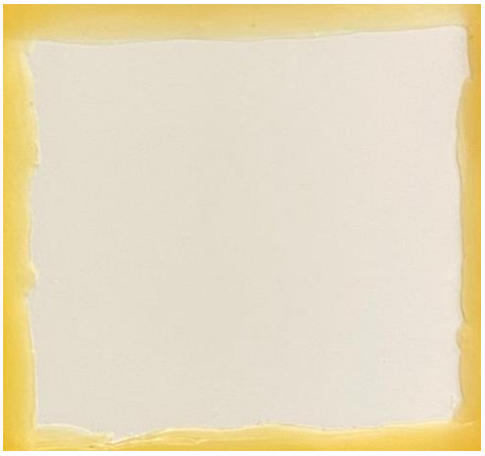

TiBaZn model coating

Substrate under *TiBaZn*

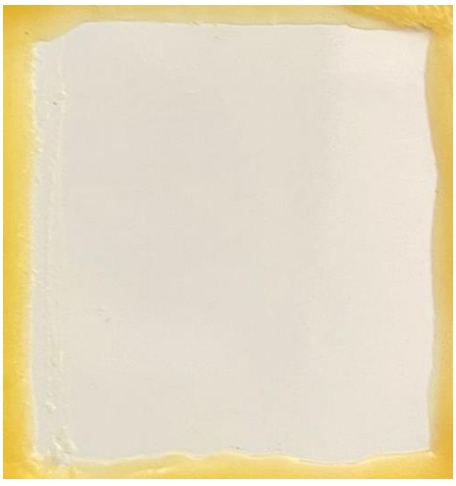

TiZn model coating

Substrate under *TiZn*